# Development of Carbon Fiber Reinforced Self-Consolidating Concrete Patch for Repair Applications

by

Mohamed Yakhlaf

A thesis
presented to the University of Waterloo
in fulfillment of the
thesis requirement for the degree of
Master of Applied Science
in
Civil Engineering

Waterloo, Ontario, Canada, 2013

## Declaration

I hereby declare that I am the sole author of this thesis. This is a true copy of the thesis, including any required final revisions, as accepted by my examiners.

I understand that my thesis may be made electronically available to the public.

## Abstract

Fiber-reinforced self-consolidating concrete is a relatively new material in civil engineering applications. The purpose of this study is to examine the effects of discrete Pitch-based carbon fibers on the fresh properties of self-consolidating concrete (SCC). Ten different carbon fiber-reinforced self-consolidating concrete (CFRSCC) mixtures were produced with two water/binder (W/B) ratios of 0.35 and 0.4, and 0%, 0.25%, 0.5%, 0.75%, 1% carbon fibers by concrete volume. Silica fume was used in all concrete mixtures to improve the dispersion of carbon fibers and the cohesiveness of the SCC. In addition, a high-range water reducer (HRWR) was used to enhance the workability of the concrete. The flow characteristics of the concrete mixtures were determined with respect to slump flow, J-ring slump, and $T_{50}$ slump flow time. The segregation resistance of the concrete mixtures was evaluated by using the sieve stability test. Visual stability index (VSI) was also used to assess the segregation resistance of concrete. Hardened properties such as compressive strength, splitting tensile strength, and fracture energy were evaluated. Test results revealed that the increased amount of carbon fibers decreased the flowing ability (filling ability and passing ability). Therefore, a greater HRWR dosage was required to achieve the targeted flow properties. The hardened test results showed that increasing the carbon fiber content decreased the compressive strength of the SCC, while the splitting tensile strength of the SCC was increased. Based on the fresh and hardened properties, two different mixes were chosen as optimum mixes in respect to the fresh and hardened properties as well as the cost of producing CFRSCC mixtures. These two mixes were mix M1 (SCC, 0% fibers) and mix M3 (CFRSCC, 0.50% fibers). Eleven RC beams were tested to investigate three different repair configurations: flexural-top patch, flexural bottom patch and shear span patch. Three different repair patch materials were used (Sikacrete-08 SCC, M1 SCC, and M3 CFRSCC). The structural load results showed that the patch repair was most effective (increasing ultimate load and

ductility) as a flexural-top patch and shear-span patch. Using a CFRSCC patch changed the mode of failure from shear to flexural failure in the shear-span patched beams.

## Acknowledgments

The author would like to acknowledge Professor Khaled Soudki for his supervision, advice, and support during my study and research work.

I would like to thank Dr. Safiuddin for his support and help in providing me with considerable amount of information on this topic. He has specifically instructed me on the proper protocol for using the laboratory equipment for material testing. I extend my thanks to all technicians: Richard Morrison, Doug Hirst, and Rob Sluban, and my colleagues in the concrete laboratory at the University of Waterloo for providing a great work environment. I would also like to extend my appreciation to Ann at the soil's laboratory for her support and help to finish the material tests properly.

I would like to express my gratitude to the High Education Ministry of Libya for giving me this opportunity to study abroad via their financial support. I am further thankful to Mr. Camron Monroe from BASF construction Chemicals Canada Ltd. for supplying chemical admixtures. Last but not least, I would like to thank Mitsubishi Company in USA for partially supplying the carbon fibers.

The author would like to send a special thanks to Zamiul Haque for his support and help.

## Dedication

I would like to dedicate this work to my parents especially my mother who passed away long time ago but she is still in my heart. I would also like to acknowledge my siblings for their continuous support and encouragement. And a special thanks to my fiancée, for her unconditional support and affection, which gave me the strength to finish my tenure. I am further inclined to dedicate my work to all the Libyan martyrs of 17$^{th}$ November revolution who brought freedom to my beloved homeland of Libya.

# Table of Contents

## List of Figures

## List of Tables

# Chapter 1 Introduction

## 1.1 Background

Self-consolidating or self-compacting concrete (SCC) is a relatively new and extremely cohesive concrete that flows under its own weight without the use of vibration. SCC has the ability to fill all the gaps completely in formwork and go around congested or heavy reinforcement without segregation and bleeding (El-Dieb et al. 2011). In order for the concrete to be classified as self-consolidating concrete, the concrete has to fulfill the fresh properties of SCC: which includes filling ability, passing ability, and segregation resistance. Self-consolidating concrete (SCC) has been described as "the most revolutionary development in concrete" construction over the last three decades. Advantages of SCC include the following: faster construction, reduction of site workers, better and easy finishing, easy placement, good durability, reduction of noise level, and reduction of pollution. SCC has been developed to compensate for the shortage of skilled labour in this industry. Thus, it has been rendered efficient and beneficial from both technological and economic standpoint. SCC can be used in all kinds of applications. Table 1.1 lists some SCC case projects. For example, SCC can be used in big or small structures, simple or complicated buildings, horizontal or vertical members, precast or cast-in-place. In the United States, approximately 40% of precast production uses SCC, while approximately 2-4% of cast-in-place uses SCC (Daczko 2012). Recently, SCC has been used as a repair material in Canada and Switzerland since SCC has the capability to flow and fill in the restricted areas (ACI 237R-07 2007, EFNARC 2002).

**Table 1.1 Case projects of SCC (Daczko 2012)**

| Location | Cast-in-place or Precast | Project | Project size ($m^3$) |
|---|---|---|---|
| Japan | Cast-in-place | LNG storage tank | 12,000 |
| Japan | Cast-in-place | Water purification plant | 200,000 |
| Japan | Cast-in-place | MMST tunneling | 8000 |
| USA | Cast-in-place | National Museum of the American Indian | 23,000 |
| Canada | Cast-in-place | Reaction Wall, University of Sherbrooke | |
| Korea | Cast-in-place | Diaphragm wall for inground LNG tank | 32,800 |
| Canada | Cast-in-place | Fill abandoned pump station in mine | |
| USA | Cast-in-place | LNG storage tank | 25,000 |
| Italy | Cast-in-place | Foundations and slabs for housing | 123,000 |
| USA | Precast | Double tee production | |
| New Zealand | Precast | Precast beams | |

Fibers including steel, polypropylene, glass and carbon fibers are being mixed with concrete to improve and enhance the hardened properties of concrete. The term "fiber reinforced concrete" is defined by the American Concrete Institute as a concrete containing dispersed, randomly oriented fibers (ACI 116R-00 2005). Adding fibers in self-consolidating concrete can reduce its workability and it becomes progressively difficult to achieve self-consolidation. On the other hand, adding fibers to the self-consolidating concrete may improve the strength and durability of this type of concrete. Generally, concrete is found to be a brittle material that fractures under tensile load. Therefore, its mechanical properties can be improved by adding randomly dispersed fibers. Fibers will reduce the crack opening at the loading stage and create a crack bridging, which can alter the behaviour of the concrete at failure. Therefore, if self-compacting concrete with fibers is achieved, then the fibers will play a very important role in the hardened properties. Carbon fibers have advantages over other fibers in terms of high corrosion resistance, high tensile strength, and high thermal conductivity. Carbon fiber reinforced concrete has been used

in producing different types of structural and non-structural elements. It can also be used to repair deteriorated concrete in different structures. Table 1.2 presents some examples where carbon fiber reinforced concrete was used in construction.

**Table 1.2 Applications of carbon fiber reinforced concrete (Safiuddin 2010)**

| Type of Application | Project | Project area ($m^2$) |
|---|---|---|
| Partition panel | Higashi – Murayama Purification | 80 |
| Curtain wall and parapet wall | Suidobashi Building of Tokyo Dental | 4,138 |
| Curtain wall | Nihonbashi – Honcho Building | 1,380 |
| Curtain wall and louver | Shinjuku District Heating Center | 5,650 |
| Curtain wall | Toshin 24 Omori Building | 3,000 |
| Curtain wall | Edo – Tokyo Museum | 12,000 |
| Curtain wall | Tokyo East 21 | 11,400 |
| Staircase | Kariha Atomic Power Plant | 108 |
| Formwork of walls | Hamaoka Atomic Power Plant | 2,900 |

Concrete technology always invents new concrete or hybrid concrete that has advantages over its conventional counterpart. Although concrete with steel, glass, and carbon fibers has been thoroughly studied, carbon fiber reinforced self-consolidating concrete has not received similar attention. There is limited information on the fresh and hardened properties of carbon fiber reinforced self-consolidating concrete and on its application as a repair patch material.

## 1.2 Research objectives and scope

It is important to note that carbon fiber reinforced concrete has been well researched (Ali 1972 & Waller 1974). Also, self-consolidating concrete (SCC) incorporating steel and polymer fibers has been significantly studied (Carlswärd et al. 2010, Yin et al. 2003 and Cunha et al. 2011).

However, the use of carbon fibers in SCC has not been studied. Incorporating carbon fibers in SCC can produce a high quality special concrete known as carbon fiber reinforced self-consolidating concrete (CFRSCC). CFRSCC offers the benefits of both carbon fibers and SCC. The objectives of this study are as follows:

- To examine the effects of pitch-based carbon fibers on the three key fresh properties (filling ability, passing ability, and segregation resistance) of SCC.
- To investigate the effect of pitch-based carbon fibers on the hardened properties (compressive strength, splitting tensile strength, and flexural strength) of SCC.
- To determine the optimum amount of carbon fibers for CFRSCC.
- To investigate the use of CFRSCC as a patch repair in reinforced concrete beams.

In total, ten concrete mixtures were batched. Two W/B ratios were used 0.35 and 0.40. The carbon fiber content (CF) ranged from 0 to 1%. The HRWR ranged from 1.5 to 8% for mixes 1 to 5 and from 1 to 7% for mixes 5 to 10. Each mix had 18 cylinders of 100mm by 200mm and 3 prisms of 100mm by 100mm by 300mm. A total of eleven beams were tested in two groups: The first group consisted of seven beams that were tested in flexure. The second group consisted of four beams that were tested in shear. The research outcome would be useful to produce and commercialize CFRSCC as a new repair material for use in concrete structures.

## 1.3 Thesis organization

There are six chapters in this thesis as follows:

**Chapter (1) Introduction:** This chapter introduces self-consolidating concrete, and fibers in concrete. It includes general information, and research objectives and scope of the study.

**Chapter (2) Literature review:** This chapter reviews the literature on self-consolidating concrete, fiber reinforced self-consolidating concrete, tests for self-consolidating concrete, and previous studies on fiber reinforced self-consolidating concrete (FRSCC).

**Chapter (3) Experimental investigation:** This chapter describes the experimental investigation on carbon fiber reinforced self-consolidating concrete (CFRSCC). It includes a description of constituent materials tests, design of carbon fiber reinforced self-consolidating concrete mixtures, preparation and mixing method, testing of fresh concrete, preparation of hardened concrete specimens, testing of hardened concrete properties, and the beam specimens fabrication, and their test setup and procedure.

**Chapter (4) Test results and discussion:** This chapter presents the test results and discussion of material fresh and hardened properties. It includes the material test results, the results of the fresh properties, hardened properties, and optimum mixture of CFRSSC.

**Chapter (5) Structural performance:** This chapter presents the test results and discussion of RC beams with patch repair. It includes failure modes, load-deflection, stiffness, ultimate strength, ultimate deflection, and ductility.

**Chapter (5) conclusions and recommendations:** This chapter presents the conclusion of this work, which includes concrete materials and structural beams, and the recommendation of future work.

# Chapter 2 Literature Review

This chapter reviews the literature on self-consolidating concrete, fiber reinforced self-consolidating concrete, tests for self-consolidating concrete, and previous studies on fiber reinforced self-consolidating concrete (FRSCC).

## 2.1 Self-consolidating concrete

Self-consolidating concrete (SCC) is a type of concrete that is able to flow under its own weight and requires no vibration. Advantages of SCC include: less labour, improved durability, ease in finishing and placement, economic, environmental and social benefits. SCC was first developed by Professor Okamura at the University of Tokyo in Japan in 1988 from an existing technology that was used for under water concrete to address the shortage of skilled labour. Ozawa and Maekawa carried out many studies to further develop self-consolidating concrete at the University of Tokyo (Okamura et al 2003). Figure 2.1 shows the timeline of developing self-consolidating concrete in the world.

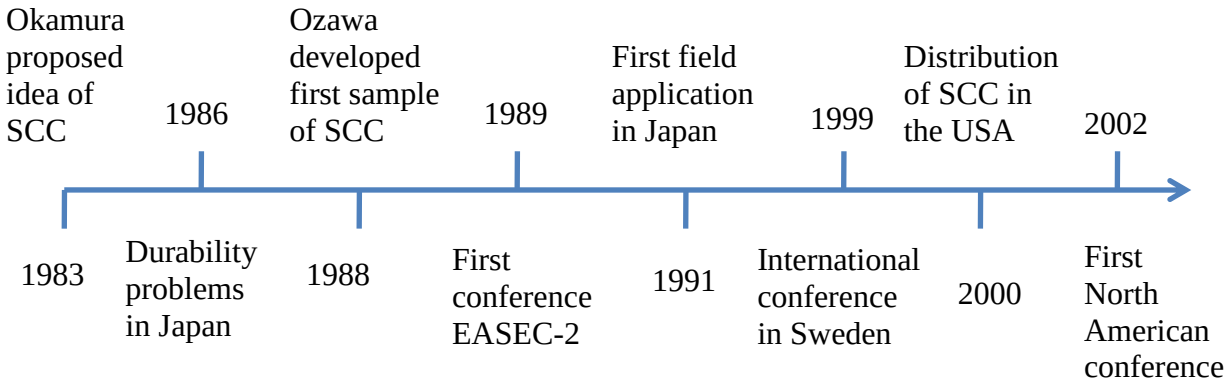


*Figure 2.1 Timeline of developing self-consolidating concrete (Douglas 2004)*

The three main fresh properties of SCC are filling ability, passing ability, and segregation, which have to be first obtained and must meet the specified SCC requirements. Filling ability is the ability of concrete to flow under its own weight and fill the spaces in the formwork. In 1940, Kennedy proposed the "excess paste theory" as a way to explain the mechanism of concrete workability as shown in figure 2.5. This theory states that a concrete mixture should have enough paste to surround the coarse aggregate. This excess paste minimizes the friction among the aggregates and thus provides better workability.

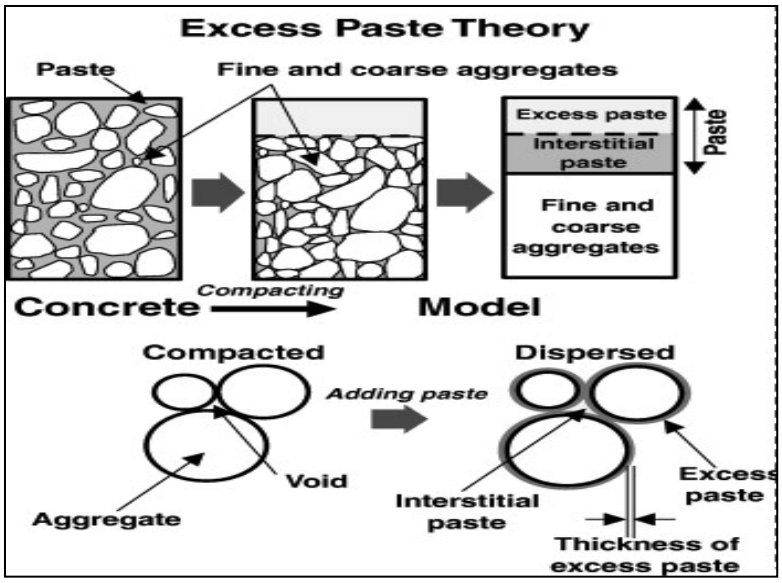


*Figure 2.2 The excess paste theory (Kismi et al. 2012)*

Passing ability is the ability of the concrete to pass through tight spaces (e.g. heavy reinforcement) with no blockage. The passing ability property is affected by the maximum aggregate size and coarse aggregate volume. Professor Hashimoto from his visualization experiments showed that the blockage occurred from the contact of the coarse aggregates (Okamura 1997). In order for the concrete to flow smoothly through narrow spaces the shear stress should be minimized. It was recommended that in order to reduce the blockage of the

concrete, the aggregate content should be reduced and Viscosity-Modifying Admixtures (VMA) should be added (Okamura 1997 & Okamura et al 1999).

Segregation resistance, or stability, is the ability of the concrete to remain homogeneous after flowing i.e. no bleeding (Douglas 2004). Bleeding is a special case of segregation in which water moves upwards and spreads into the concrete surface. Concrete should be stable and cohesive during the mixing, transporting, casting, and placing process. Concrete is allowed to have minimum bleeding and segregation. Stability depends on the cohesiveness and viscosity of the concrete. Reducing mixing water and increasing the amount of fine materials such as cement, fine aggregate, and powder admixtures will lead to better cohesiveness.

## 2.2 Fiber reinforced self-consolidating concrete

### 2.2.1 Fibers in concrete

Fibers are used to reinforce concrete to improve its tensile strength and toughness and reduce cracking. In the last thirty years, the use of fibers has increased in ready mixed concrete, pre-cast concrete, and shotcrete applications (Kosmatka et al 2008). Figure 2.1 shows the timeline of using fibers in concrete mixes.

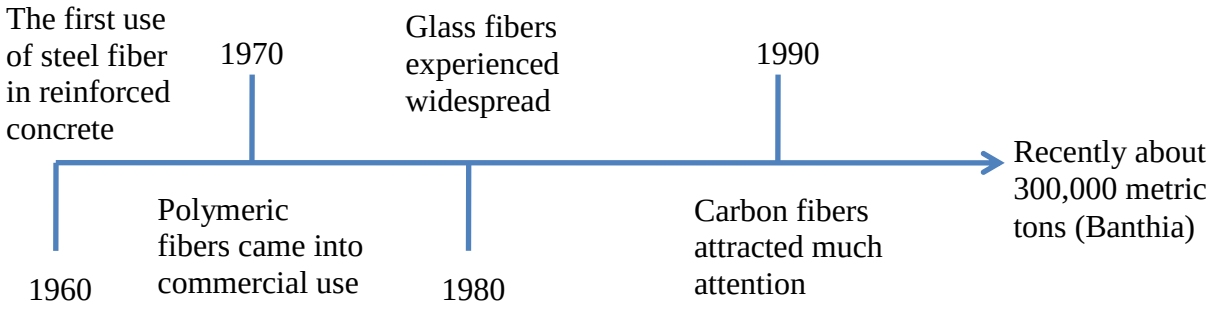


*Figure 2.3 Timeline of using fibers in the concrete mixes (ACI 544.1R 2002)*

About 300,000 metric tons of fibers are used in reinforced concrete industry every year. Steel fibers are the most common type of fibers (50% of the total used fibers), followed by polypropylene fibers (20% of total used fibers), then glass fibers (5% of the total used fibers) finally other types of fibers (25% of the total used fibers).

Extensive research work has been conducted on different type of fibers such as steel fibers, wood fibers, polypropylene fibers, glass fibers and carbon fibers mixed with concrete (Carlswärd et al. 2010, Yin et al. 2003, Cunha et al. 2010, Srinivasa et al. 2009, and Barluenga et al. 2007). Previous research indicated that fibers greatly affect the workability of normal and self-consolidating concrete due to the following factors: the shape of fibers, the stiffness of fibers, the surface characteristics of fibers, and the deformation of fibers. It was found that the addition of macro-synthetic fibers led to a decrease in the workability of concrete mixtures. For example, the addition of 40-50 mm macro-synthetic fibers decreased the slump flow and blockage in the L-Box test. Table 2.3 presents the properties of various fibers mixed with concrete.

**Table 2.1 Properties of various fibers (adopted from Kosmatka et al 2008)**

| Fiber type | Relative density (specific gravity) | Diameter (micro-meter) | Tensile strength (MPa) | Modulus of elasticity (MPa) | Strain at failure (%) |
|---|---|---|---|---|---|
| Steel | 7.80 | 100-1000 | 500-2600 | 210,000 | 0.5-3.5 |
| Glass | 2.54 | 8-15 | 2000-4000 | 72,000 | 3.0-4.8 |
| Polyethylene | 0.96 | 25-1000 | 80-600 | 5,000 | 12-100 |
| Aramid | 1.44 | 10-12 | 2000-3100 | 62,000-120,000 | 2-3.5 |
| Carbon | 1.90 | 8-9 | 1800-2600 | 230,000-380,000 | 0.5-1.5 |

#### 2.2.1.1 Steel fibers

ACI 544.1R defines steel fibers as short, discrete length steel bars having an aspect ratio (the length to diameter ratio) from 20 to 100 and diameters from 100 to 1000 μm. The Japanese Society of Civil Engineers (JSCE) has classified steel fibers based on their cross section: square cross section, circular section, and crescent section (ACI 544.1R 2002). Adding short steel fibers to a concrete mixture results in increasing the concrete toughness and controlling crack propagation. However, steel fibers accelerate the corrosion process, which is a disadvantage in comparison to other fibers (ACI 544.1R 2002). Self-consolidating concrete (SCC) containing steel fibers of 0.5% and 0.75% by volume exhibited a reduction in crack widths by around 50% and 25% compared to plain SCC (Carlswärd et al. 2010). Yin et al. (2003) found that the loads at crack initiation for specimens with different volume of steel fibers were almost the same. However, the peak load and the deflection at the peak load increased as the volume of steel fibers increased. Toughness was improved for the mixture that contained high steel fiber volume (1%) in comparison to mixtures that have lower dosage of steel fibers (0.25%) (Yin et al. 2003 and Cunha et al. 2011). The direct tensile strength of concrete with 1.5 percent steel fibers by volume can increase by about 30 to 40 percent. The shear and torsion strength of concrete with 1% steel fibers by volume can be increased from 0 to 30 percent. The flexural strength of concrete with sufficient amount of steel fibers can be improved by 50 to 75 percent. This improvement depends on length of fibers, specimen's size, and the test method. The steel fibers improve the ductility of the concrete, depending on the type and volume of steel fibers present. The pullout of steel fibers from concrete can be prevented or reduced by using wavy or crimped steel fibers.

#### 2.2.1.2 Glass fibers

The first research study on the use of glass fibers in concrete was conducted in early 1960s. The glass fibers suffered from alkali reactivity that occurs between the glass fibers and the cement paste. The alkali reactivity led to a reduction in concrete strength, which limited their use in concrete structures (ACI 544.1R 2002). To over come this issue, new alkali-resistant glass fibers (AR-glass fibers) were invented with improved long-term durability in concrete. AR-glass fibers were first introduced in the United Kingdom in 1967 and became the most widely used fibers in reinforced concrete. Glass fiber reinforced concrete (GFRC) is used in the fabrication of cladding panels, sandwich panels, integral rib panels, and steel-stud/flex-anchor panels (ACI 544.1R 2002).

Some studies have shown that the modulus of rupture (MOR) for AR-glass fibers decrease after 10 years under normal environmental conditions (ACI 544.1R 2002). The freeze-thaw resistance also decreases for the AR-glass fibers concrete. A study on polymer glass fiber reinforced concrete (P-GFRC) revealed that the freeze-thaw resistance was good due to the lower absorption of glass fibers (ACI 544.1R 2002).

#### 2.2.1.3 Carbon fibers

Since the 1970s many studies have been conducted to investigate the effectiveness of carbon fibers on the various properties of concrete (Ali 1972, Waller 1974 and Safiuddin 2010). The addition of carbon fibers to concrete offers significant improvements to the concrete mechanical properties such as flexural strength and toughness. In addition, impact resistance and fatigue resistance can be improved if the appropriate amount of carbon fibers is added to the concrete. Carbon fibers are attractive to engineers due to their low density and thermal conductivity.

Carbon fibers can be used to eliminate or reduce drying shrinkage problems as well as reduce cracking width. Carbon fiber reinforced concrete (CFRC) has been used in many projects because of its good thermal conductivity, lightweight, and high modulus of elasticity. It has been also used to produce curtain walls, partition panels, and formwork for walls (Safiuddin 2010).

Two types of carbon fibers are generally used in concrete are continuous high modulus polyacrylonitrile (PAN-based) carbon fibers and pitch-based carbon fibers. PAN-based carbon fibers have a very high modulus of elasticity and high tensile strength. They have been mostly used to produce aerospace and sport equipment. Although PAN-based fibers were the first type of chopped carbon fibers used in reinforced concrete; they are rarely used in civil engineering applications due to their high cost.

Pitch-based carbon fibers are used in civil engineering applications because of their lower cost even though they have a lower modulus of elasticity than PAN-based fibers. Pitch-based carbon fibers are used in many industrial fields due to their light weight, chemical stability, heat resistance and abrasion characteristics (JCMA 2010). The use of pitch-based carbon fibers in plain concrete leads to increases in flexural strength by about 85%, flexural toughness by about 205%, and compressive strength by about 22%. On the other hand, the drying shrinkage of concrete mixed with pitch-based carbon fibers was decreased by up to 90% and the electrical resistivity was decreased by up to 83% (Chung et al. 1992 and Chung 1992). These advantages make pitch-based carbon fibers more attractive for use in SCC. Although many studies were conducted on the use of pitch-based chopped carbon fibers in concrete, limited research has been carried out to evaluate SCC with carbon fibers. SCC containing carbon nano-fibers was studied to investigate its mechanical and electrical properties (Gao et al. 2010). In the present study, pitch-based chopped carbon fibers will be used to produce SCC. The optimum content of pitch-

based carbon fibers will be determined while meeting the performance requirements for the three key fresh properties of SCC.

### 2.2.2 Fiber reinforced self-consolidating concrete (FRSCC) mix design

Self-compacting concrete mixture design differs from conventional concrete mixture design. Development of SCC is basically conducted through trial and error batches, and to date there is no standard for SCC mix design in the world (Douglas 2004). SCC requires large amounts of fine materials and small amounts of coarse aggregates. This means more water is required to produce an SCC mixture. Consequently, dry shrinkage will occur which leads to concrete cracking. To solve the formation of dry shrinkage cracks in SCC, high range water reducer is added to the SCC mixture (Brown et al. 2011). Okamura (1993) and Ozawa (1989) applied limits on aggregate content, lower water binder ratio, and used superplasticizer in their mixture to produce self-consolidating concrete.

ACI 211.4R-08 (2008) outlines an approach based on the absolute volume method to design high strength concrete. Nielsson and Wallervik (2003) designed SCC mixture by changing the paste composition and keeping the aggregate composition the same. For fiber reinforced self-consolidating concrete (FR-SCC) design, a similar approach is followed. It is assumed that the fibers are replacing part of the coarse aggregate (ACI 211.4R-08 2008). Figure 2.4 presents the fiber reinforced self consolidating concrete (FRSCC) mix design outlined in ACI 211.R-08. Table 2.2 gives the maximum w/c ratio for high strength concrete. Table 2.3 gives estimates for the mixing water based on a fine aggrgetae content with 35% voids. If the void content is different from 35% then approach described in ACI 211.4R-08 (2008) should be followed.

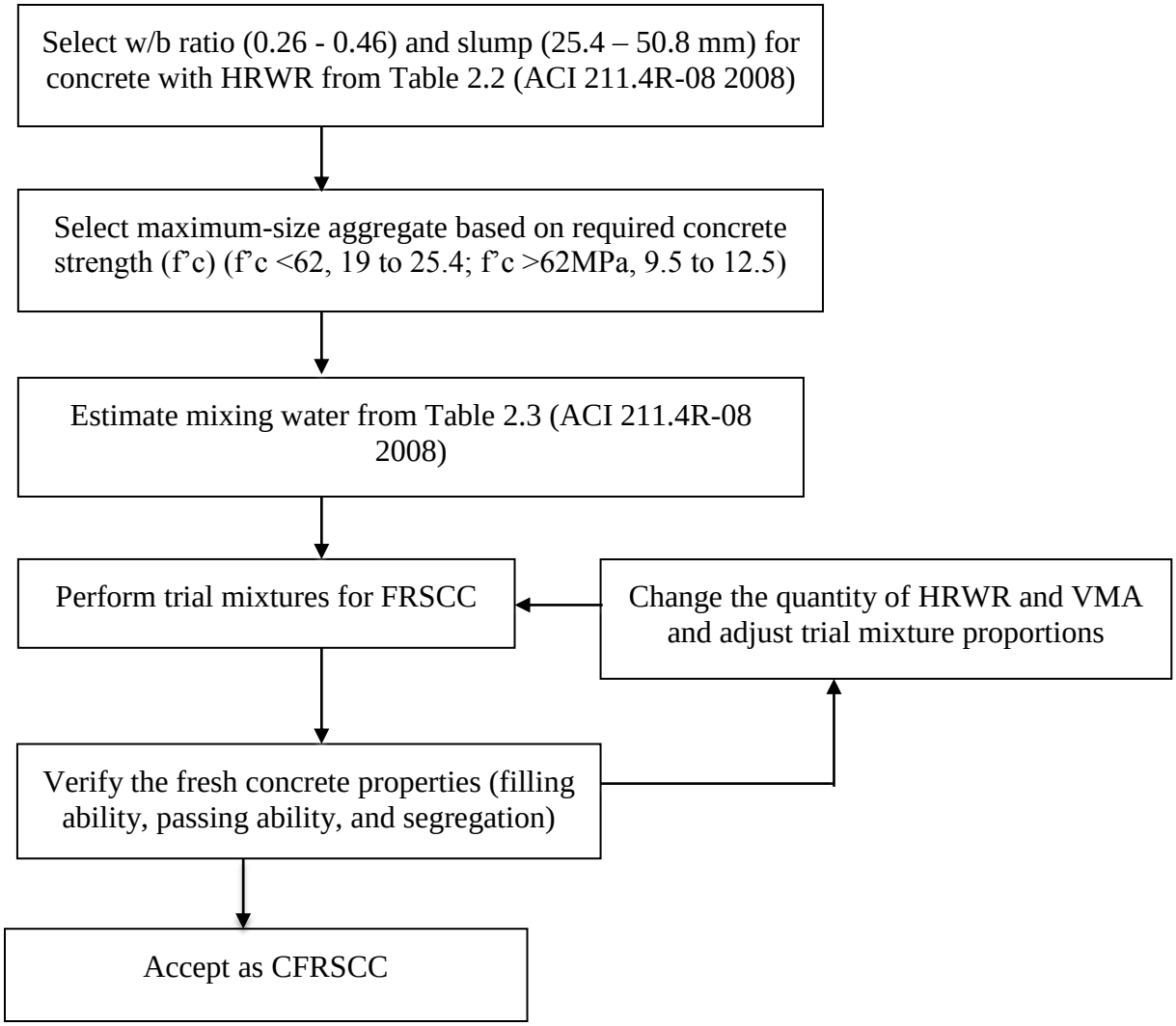


*Figure 2.4 Flow chart of fiber reinforced self consolidating concrete (FRSCC) mix design (adapted from ACI 211.4R-08 2008)*

**Table 2.2 Maximum w/c ratio for high strength concrete (ACI 211.4R-08 2008)**

| Required average compressive strength $f'_{cr}$ (MPa) | | w/c | | | | | | | |
|---|---|---|---|---|---|---|---|---|---|
| | | Maximum-size coarse aggregate (mm) | | | | | | | |
| | | 9.5 | | 12.5 | | 19 | | 25.4 | |
| | | with HRWR | without HRWR | with HRWR | without HRWR | with HRWR | without HRWR | with HRWR | without HRWR |
| 48 | 28-day | 0.50 | 0.42 | 0.48 | 0.41 | 0.45 | 0.40 | 0.43 | 0.39 |
| | 56-day | 0.55 | 0.46 | 0.52 | 0.45 | 0.48 | 0.44 | 0.46 | 0.43 |
| 55 | 28-day | 0.44 | 0.35 | 0.42 | 0.34 | 0.40 | 0.33 | 0.38 | 0.33 |
| | 56-day | 0.48 | 0.38 | 0.45 | 0.37 | 0.42 | 0.36 | 0.40 | 0.35 |
| 62 | 28-day | 0.38 | 0.30 | 0.36 | 0.29 | 0.35 | 0.29 | 0.34 | 0.28 |
| | 56-day | 0.42 | 0.33 | 0.39 | 0.32 | 0.37 | 0.31 | 0.36 | 0.30 |
| 69 | 28-day | 0.33 | 0.26 | 0.32 | 0.26 | 0.31 | 0.25 | 0.30 | 0.25 |
| | 56-day | 0.37 | 0.29 | 0.35 | 0.28 | 0.33 | 0.27 | 0.32 | 0.26 |
| 76 | 28-day | 0.3 | - | 0.29 | - | 0.27 | - | 0.27 | - |
| | 56-day | 0.33 | - | 0.31 | - | 0.29 | - | 0.29 | - |
| 83 | 28-day | 0.27 | - | 0.26 | - | 0.25 | - | 0.25 | - |
| | 56-day | 0.30 | - | 0.28 | - | 0.27 | - | 0.26 | - |

**Table 2.3 Estimation of mixing water based on using fine aggregate with 35% voids (ACI 211.4R-08 2008)**

| Slump (mm) | Mixing water ($kg/m^3$) | | | |
|---|---|---|---|---|
| | Maximum-size coarse aggregate (mm) | | | |
| | 9.5 | 12.5 | 19 | 25.4 |
| 25.4 to 50.8 | 184 | 175 | 169 | 166 |
| 50.8 to 76 | 190 | 184 | 175 | 172 |
| 76 to 101 | 196 | 190 | 181 | 178 |
| Entrapped air content | 2.5 | 2 | 1.5 | 1 |

### 2.2.3 Mechanics of crack formation and propagation for SCC and FRSCC

The failure of plain concrete in uniaxial tension is usually governed by a single crack formation. However, in fiber reinforced concrete (FRC), the fibers will work to resist crack propagation and provide crack bridging. This crack bridging depends on the effectiveness of the fibers and number of fibers that contributes to each crack. If the fibers break or pullout during crack initiation, concrete tension softening occurs and the FRC cannot carry load after the crack initiates and the load would decrease after the peak point load. However, multiple cracking occurs if the fibers can sustain load after the first crack initiates, more cracks will appear and more fibers will contribute to the load transfer for a more ductile behaviour (Vandewalle et al 2002). Figure 2.2 shows the behaviour of single and multiple cracking on a concrete specimen under uniaxial tensile loading.

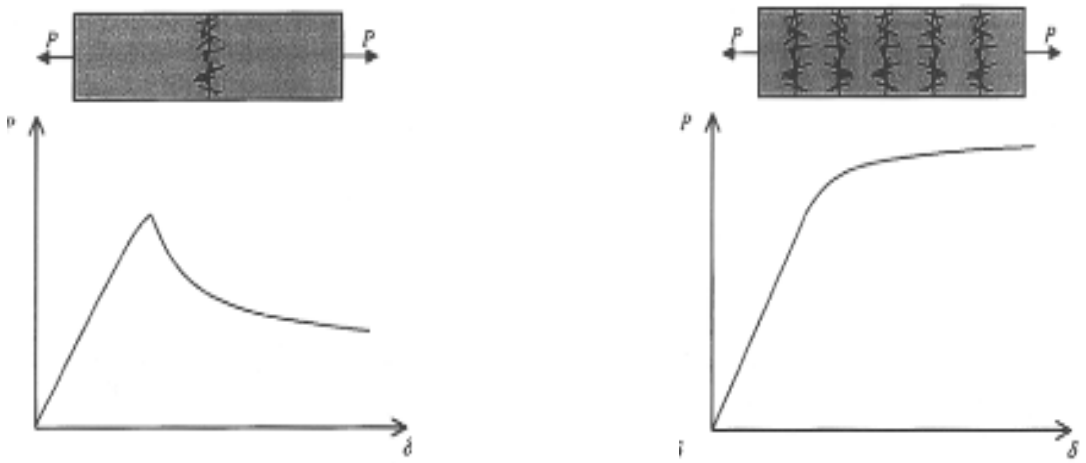


*a) Single cracking under uniaxial loading* *b) Multiple cracking under uniaxial loading*

*Figure 2.5 The behaviour of single and multiple cracking of the specimens under uniaxial loading (Vandewalle et al 2002)*

## 2.3 Tests for self-consolidating concrete

Different standard tests are given by the American Society for Testing and Materials (ASTM) and European Federation of Supplies of Specialist Construction Chemicals (EFNARC) to assess SCC fresh and hardened properties.

### 2.3.1 Tests used for fresh properties

Table 2.4 presents the different tests for SCC fresh properties and the range of the criteria values that should be satisfied for the fresh properties as set by different institutions.

**Table 2.4 Tests for SCC fresh properties and the criteria values set by different institutions**

| Test name | Property | Units | ASTM | ACI | EFNARC | European research project "Testing-SCC" |
|---|---|---|---|---|---|---|
| Slump flow | Filling ability | mm | 530-740 | 450-760 | 650-800 | 600-750 |
| T50 slump flow | Filling ability | Sec. | | 2-5 | 2-9 | 3.5-6 |
| Orimet | Filling ability | Sec. | | - | 0-5 | 3-12 |
| V-funnel | Filling ability | Sec. | | - | 6-12 | 3-12 |
| J-ring slump flow (blocking index) | Passing ability | mm | 0-50 | - | 0-10 | 0.20 |
| L-box | Passing ability | $h_2/h_1$ | | 0.8-1.0 | 0.8-1.0 | 0.7-1.0 |
| U-box | Passing ability | $(h_2-h_1)$ mm | | - | 0-30 | - |
| V-funnel at T5minutes | Stability | Sec. | | - | 0-3 | - |
| Column segregation | Stability | % | | <10 | - | - |
| VSI | Stability | | 0-3 | | - | - |
| Sieve resistance | Stability | % | | - | 0-15 | 0-20 |
| Penetration | Stability | mm | | | | 0-8 |

Tests for fresh properties of SCC are different from those used for conventional concrete. Three key fresh properties for SCC are filling ability, passing ability, and segregation resistance. To produce SCC mixtures the three key properties of fresh properties must fulfill the standard requirements (EFNARC 20002). However, there is no single test method that characterizes all the fresh properties of SCC (filling ability, passing ability, and stability) at one time. Each property therefore must be characterized using a different method. The following sections discuss these test methods.

#### 2.3.1.1 Test for filling ability

Filling ability is the ability of the SCC mixture to flow horizontally and vertically under its own weight. Filling ability can be measured or evaluated by using a slump flow, $T_{50}$ slump flow, Orimet and V-funnel tests (EFNARC 2002). There is a good correlation between the slump flow and the $T_{50}$ slump flow test with respect to repeatability and reproducibility. Slump flow test is the most common test used to measure the filling ability of SCC. The Slump flow and $T_{50}$ slump flow test equipment are commonly available. Historically, the slump flow test for SCC was first developed in Japan to evaluate the ability concrete to flow underwater. At that time, there was no standard to evaluate the filling ability; therefore, Shindoh and Tangermsirihul (2003) developed a test method to evaluate this property. Then the Japan Society of Civil Engineers (JSCE) adopted this method as a standard test. The Slump flow test was modified by the ASTM C 143/C 143M (ACI 237R-07 2007). Recently, ASTM C 1611C/C 1611M-09b was proposed to measure the filling ability.

#### 2.3.1.2 Test for passing ability

Passing ability is the ability of the SCC mixture to flow through the limited spaces between re-bars without blocking. Rebar blocking is defined as the concrete flow through the rebars, the rebars will restrict the coarse aggregate from flowing smoothly. Passing ability can be evaluated by using a J-ring slump flow (blocking index), L-box, U-box and V-funnel at $T_{5minutes}$ (EFNARC 2002 and TESTING-SCC 2005). The principle of the J-ring test method is Japanese, but the J-ring test was developed at the University of Paisley in UK (EFNARC 2002). The J-ring test indicates the deformability of SCC due to the reinforcement bars blocking (TESTING-SCC 2005). The J-ring can be used with the slump or Orimet test. This combination can bring the benefit of filling ability and passing ability as they have acceptable correlation.

#### 2.3.1.3 Test for segregation resistance

Segregation resistance or stability is a vital property of SCC. It is defined as the ability of the concrete to remain consistent and uniform during mixing, transport, and placement. Stability is determined under two conditions: static and dynamic (Daczko 2012). Dynamic segregation of concrete can occur during transportation, placing, and casting and it stops when static stability takes place. The static segregation occurs during the concrete consolidation. SCC mixtures must have sufficient viscosity, so that concrete can flow easily through restricted spaces and maintain uniformity without any compactions and have good cohesiveness (Khayat 1999). To improve the cohesiveness of SCC mixtures, we should reduce the coarse aggregate content, reduce maximum aggregate size, and increase the amount of carbon fibers. It is important to increase the cohesiveness to keep the bond between the aggregate and the mortar (Khayat 1999). Three tests are available to evaluate the stability of concrete “segregation resistance”: settlement column,

sieve stability, and penetration. All these tests are convenient for laboratory and site tests (TESTING-SCC 2005, EFNARC 2002).

### 2.3.2 Tests for hardened properties

When the SCC mixture was first introduced in North America, it was questioned whether the hardened properties were affected by the fresh properties or not. Since the SCC mixture is a highly flowable concrete; hardened properties such as shrinkage and creep are very important properties after the consolidation process. Hardened properties of SCC have been investigated and compared with those of conventional concrete (Daczko 2012). It was found that the hardened properties such as compressive strength, tensile strength, fracture energy, elastic modulus, creep, and shrinkage for SCC are slightly different from those of normal concrete. Figure 2.6 shows that in the last 12 years there has been a growth of publications on the hardened properties of SCC versus conventional concrete.

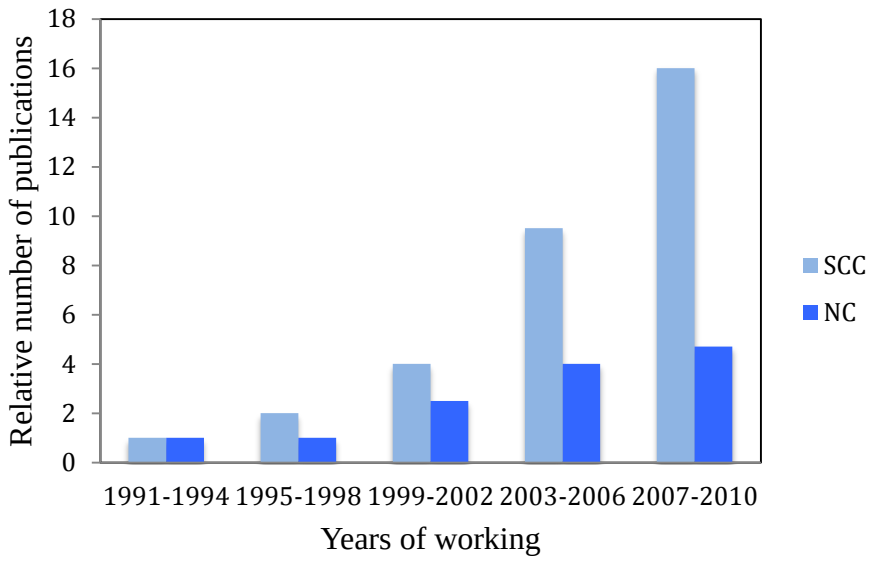


*Figure 2.6 Growth of publication on hardened properties for self-consolidating concrete (SCC) and normal concrete (NC) (adopted from Daczko 2012)*

#### 2.3.2.1 Test for compressive strength

Compressive strength is one of the most important properties for concrete. The compressive strength is defined as "the measured maximum resistance of a concrete specimen to axial loading" (Kerkhoff et al. 2002). Compressive strength mainly depends on the water/binder ratio (w/b), type of cement, cementitious materials, aggregates, the degree of compaction, the age of the concrete and curing type. Usually, the compressive strength of SCC is higher than 50MPa (Hela et al 2005). However, adding fibers whether carbon fibers or steel fibers to the concrete are known to reduce the compressive strength (Aydin 2007). Compressive strength ($f'_c$) is obtained by dividing the ultimate axial load (P) by the cross sectional area of specimen (A). The $f'_c$ can be calculated for a cylinder as given in the equation below (Douglas 2004):

#### 2.3.2.2 Test for tensile strength

Concrete is weak in tension; therefore, the tensile strength of the concrete is usually ignored in concrete design. When fibers made from steel, glass, or synthetic materials are added to the concrete, the tensile strength of the concrete is improved. Fibers typically work as internal reinforcement in concrete, and can eliminate or reduce a crack from growing (VTRC 10-R8). Usually, tensile strength ranges from 2 to 5 MPa for normal concrete. The tensile strength can be calculated by a splitting cylinder test using the formula below:

$$T = \frac{2 \times P}{\pi l d} \qquad \text{Equation 2.1}$$

Where:

$T$= Splitting tensile strength, MPa,

*P*= maximum applied load indicated by the testing machine, N,

*l*= Length, mm,

*d*= diameter, mm.

#### 2.3.2.3 Test for flexural strength

The flexural strength of plain or fiber reinforced concrete can be determined using a third point bending test of a concrete prism to determine the modulus of rupture, $f_r$ according to CSA A23.2-8C ASTM C1609/C1609M – 10, as follows:

$$f_r = \frac{PL}{bh^2} \qquad \text{Equation 2.2}$$

Where:

*P*= maximum applied load, N,

*L*= specimen length, mm,

*b*= width of section, mm,

*h*= height of section, mm.

## 2.4 Fiber reinforced self-consolidating concrete (FRSCC)

### 2.4.1 Fresh properties of FRSCC

#### 2.4.1.1 Filling ability

The filling ability is affected by the increase of fiber amount and fiber length. The workability decreases when the fiber amount and length are increased. Forgeron and Omer (2010) found that when the filling capacity, V-funnel, and L-box tests were performed on different SCC mixtures with 38mm and 50mm fiber lengths, the fiber length played a very important role in SCC filling

ability characteristics. It was clear that fiber lengths affected the SCC during concrete moving around obstacles. Brown et al. (2010) reported that steel fibers with concentrations of 0.4% and 0.6% by volume in the SCC mixtures met the minimum target of slump flow requirement. In the same study, sufficient stability was not attained in the mixtures with 0.4% and 0.6% by volume of synthetic fibers and these mixtures were considered as normal fiber reinforced concrete FRC (not SCC). Nehdi and Ladanchuk (2004) found that in the slump flow of SCC mixtures containing higher fiber volume were lower than the SCC mixture containing lower fibers volume. Liao et al. (2010) found that the flowability of normal SCC mixtures was achieved and the flow diameter was 600mm for all the cases. However, the flowability of self-consilidating high performance fiber reinforced concrete (SC-HPFRCCs) was not as high as that for the SCC mixtures; these mixes required slight vibration. El-Dieb and Taha (2012) studied the flow characteristics and acceptance criteria of fiber-reinforced self-consolidating concrete (FR-SCC). They found that the maximum polypropylene fiber content that could be added to the SCC mixtures without affecting the SCC characteristics should be between 1 and 1.3 kg/m$^3$ according to the V-funel and filling box tests. These ranges were different from those found using a slump flow test because this test was less affected by inclusion of fibers. In case of SCC mixtures with steel fibers, the maximum steel fiber factor ($V_f \times L/D$) ranged between 50-100.

#### 2.4.1.2 Passing ability

Grünewald and Walraven (2010) found that the presence of fibers in SCC increased the bar spacing for non-blocking compared to SCC mixtures with no fibers. The type and content of fibers affected the bar spacing for non-blocking. Aydin (2007) found that the J-ring test results did not exhibit any effect of fiber inclusion when the steel fiber content was below 1%. Ding et al. (2011) and Gencel (2011) found that as the fibers content increased, the J-ring value, which

indicates the blocking index, increased. Sahmaran (2004) studied the effect of steel fibers on the passing ability by using the J-ring slump flow test. He found from that the fiber inclusion did not affect the blocking index value. Fiber reinforced self-consolidating concrete results from the L-box test showed that the concrete mixtures can flow in a narrow spacing with out blockage (Corinaldesi 2004).

#### 2.4.1.3 Segregation resistance (Stability)

Khayat and Roussel (2000) showed that a viscosity-enhancing admixture (VEA) can improve the stability of self-consolidating concrete with fibers. They compared two different FRSCC mixtures: The first series of FRSCC mixtures with VEA and less HRWR and the second series of FRSCC mixtures with no VEA and more HRWR. It was found that FRSCC mixtures with VEA showed good stability and no segregation. Unlike FRSCC mixtures with VEA, FRSCC mixtures without VEA exhibited segregation of the aggregates at the edges of the mixtures. El-Chabib and Nehdi (2006) found that the segregation resistance significantly increased with increasing the w/c ratio and HRWRA dosage. They also found that the coarse/total aggregate ratio did not affect the segregation, whereas increasing of the cementitious materials content caused the segregation to increase for SCC mixtures with high w/c ratio and the segregation slightly decreased for SCC with low w/c ratio.

### 2.4.2 Hardened properties of FRSCC

#### 2.4.2.1 Compressive strength

The effect of fibers on the compressive strength of SCC mixtures varies in the published literature. It was found that fibers do not always decrease the compressive strength of SCC mixture. Gencel et al. (2011) found that as polypropylene fiber content increased the

compressive strength of SCC mixtures increased. Forgeron and Omer (2010) observed that the fibers had no effect on the compressive strength. As it was observed from their test results, the compressive strength for SCC with 0% maro-synthetic fibers was 44MPa and SCC with 0.40% maro-synthetic fibers was 45MPa. Akcay and Tasdemir (2012) found that the fibers did not significantly affect the compressive strength. The compressive strength was 115MPa for concrete mixture with 0.75% steel fibers by volume and 118MPa for concrete mixture with 0.75% steel fibers by volume and 1.5% by volume of steel fibers.

#### 2.4.2.2 Splitting tensile strength

Gencel et al. (2011) found that the splitting tensile strength values increased with increasing fiber content. However, Sahmaran and Yaman (2005) found that the splitting tensile strength reduced from 3.4MPa to 3.08MPa due to the reduction of longer hooked ends of steel fibers. Akcay and Tasdemir (2012) studied the effect of hybrid fibers on the hardened properties of SCC. They found that the splitting tensile strength did not change when the fiber content was increased. Mazaheripour et al. (2011) found that the splitting tensile strength increased as the polypropylene fiber volume increased.

#### 2.4.2.3 Flexural strength

The flexural strength generally increases as the fiber and cement content increase. At 0% fibers the flexural strength was 3MPa, but at 12kg/m$^3$ the flexural strength increased to about 8MPa (Gencel et al. 2011). Akcay and Tasdemir (2012) found that the fracture energy increased as the fiber content increased. The fracture energy ($G_F$) was significantly increased with the increase of fiber content. In their study, the fracture energy for the reference concrete mixture was 94N/m while the fracture energy for the concrete mixture with 0.75% of steel fibers was 2248N/m.

Mazaheripour et al (2011) studied the effect of fibers on the lightweight SCC and found the flexural strength increased by about 9% when the polypropylene fiber volume increased.

## 2.5 Research needs

Based on the current state-of-the art about fiber reinforced self-consolidating concrete, the following points can be drawn and gaps can be identified:

- A considerable amount of research has been undertaken on different fibers such as steel fibers, glass fibers, and synthetic fibers in concrete. However, use of carbon fibers in concrete has not been intensively studied.
- Carbon fibers have been studied in conjunction with steel fibers and synthetic fibers in self-consolidating concrete.
- The effect of carbon fibers on the fresh properties of self-consolidating concrete (filling ability, passing ability, and segregation) has not been intensively studied.
- Very limited studies have investigated the effect of carbon fibers on the compressive strength and splitting tensile strength.
- The fracture energy of carbon fiber reinforced self-consolidating concrete has not been studied.
- There is no standard or guidelines for mixture proportioning of carbon fiber reinforced self-consolidating concrete (CFRSCC).
- There are no standards to evaluate fresh properties of CFRSCC as it is available for SCC.

Therefore, this research study aims to address the gaps in the state of the art and investigate the fresh and hardened properties of CFRSCC.

# Chapter 3 Experimental Investigation

This chapter describes the experimental investigation to assess carbon fiber reinforced self-consolidating concrete (CFRSCC). It includes a description of constituent material tests, design of carbon fiber reinforced self-consolidating concrete mixtures, preparation and mixing method, testing of fresh concrete, preparation of hardened concrete specimens, testing for hardened concrete properties, the beam specimens fabrication, and their test setup and procedure.

## 3.1 Testing of constituent materials

Carbon fiber reinforced self-consolidating concrete (CFRSCC) used here was made up of limestone crushed concrete aggregate, manufactured concrete sand according to OPPS 1002 specification, normal Portland cement (Type I), silica fume, tap water, high-range water reducer and carbon fibers were used as the components for producing the. This section discusses the selection and testing of the constituent materials.

Normal Portland cement according to ASTM type I (CSA type 10) was used in this study. The relative density of the cement was taken from the material supplier sheets. No cement tests were conducted in this project. Also, silica fume was used in this project as a supplementary material to replace some of the cement and increase the compressive strength of the concrete. Silica fume of 10% by binder weight was used in all SCC mixtures.

Locally available limestone crushed concrete aggregates were used. 10mm maximum aggregate size was chosen based on recommendations in the literature in producing self-consolidating concrete. The aggregates were tested to obtain the saturated surface dry based relative density, absorption, and moisture content according to ASTM C127 (2007) and ASTM C566 (2004).

These properties are important in the mix design proportion. Also, gradation of the aggregates was performed by using sieve analysis according to ASTM C136 (2006). Locally manufactured sand from crushed concrete stone was used. The sand was tested for relative density, absorption, and moisture content according to ASTM C128 (2007) and ASTM C566 (2004). The gradation of the concrete sand was evaluated according to ASTM C136 (2006).

The optimum sand/aggregate (S/A) ratio was obtained from the compacted bulk density of the aggregate blends. The test procedure was according to ASTM C29/C29M (2009). A metal container was filled with aggregate blends in three layers and each layer was compacted 21 times. The measurement was reported for different S/A ratios. The optimum S/A ratio was chosen based on the maximum compacted relative density. The S/A ratio is important for the absolute volume concrete mix design of the self-compacting concrete.

Ten (10) mm pitched based carbon fibers were used in the CFRSCC mixture. The properties of the carbon fibers were taken from the data material sheets as specified by the supplier.

High range water reducer (HRWR) was used as superplastesizer. It is very important to improve the workability of self-consolidating concrete. The properties of the HRWR such as relative density and solid content were adopted from the supplier data material sheets. Tap water was used in different dosages to obtain the best workability. Tap water was not tested, but its properties such as total solids and density were adopted from the tap water analysis conducted by the Regional Municipality of Waterloo (2003). Viscosity modifying admixtures (VMA) were not used in this project.

## 3.2 Design of carbon fiber reinforced self-consolidating concrete mixtures

### 3.2.1 Design approach

Carbon fiber reinforced self-consolidating concrete (CFRSCC) mixtures were designed according to ACI 211.4R-08 (2008). The CFRSCC mixture designs were for non-air-entrained concrete. The absolute volume method was used to calculate the absolute volume of each SCC component to occupy one cubic meter of concrete.

A total of ten non-air-entrained self-consolidating concrete mixtures incorporating different contents of pitch-based carbon fibers were developed in this study. Two mixtures were control mixes with no fibers and eight mixtures had different percentages of carbon fibers.Two different water binder ratios of 0.35 and 0.4 were used. These water binder ratios were chosen to achieve compressive strengths of the CFRSCC mixtures in the range of 50 to 70 MPa and minimum slumps of 50 to 75 mm with HRWR (ACI 211.4R-08 2008). The maximum coarse aggregate size was 10 mm. The silica fume content was kept constant at 10% by weight of binder. HRWR was added to the CFRSCC mixtures to enhance their workability; the HRWR dosages for the group of 0.35 and 0.4 W/B ratios were 1.5–8.0% and 1.0–7.0%, respectively. Carbon fibers were added to the self-consolidating concrete to improve its hardened properties. Carbon fibers were added in different dosages ranging between 0 to 1% by concrete volume. The optimum S/A ratio of 0.55 was used to design the self-consolidating concrete. This value was obtained from the compacted bulk density of aggregate blends in section 4.1.5. The water in the mixtures was adjusted twice: First based on the fine aggregate void content (ACI 211.4R-08, 2008) and later based on the moisture content and absorption of the aggregates.

### 3.2.2 Trial CFRSCC mixtures

Twenty (20) trial mixtures were done to achieve the optimum fresh properties of CFRSCC mixtures. The HRWR dosages varied until the CFRSCC fresh properties fulfilled the limits of SCC set by ASTM standards. In total, ten concrete mixtures were batched using the steps outlined below. Two W/B ratios were used 0.35 and 0.40. The carbon fiber content (CF) ranged from 0 to 1%. The HRWR ranged from 1.5 to 8% for mixes 1 to 5 and from 1 to 7% for mixes 5 to 10. The details of the primary mixtures proportions for the CFRSCC mixtures are presented in Table 3.1. The steps for the primary mixture design are as follows (ACI 211.4R-08 2008):

- Select the W/B ratio (0.35 and 0.40).
- Select the maximum aggregate size based on compressive strength of 62MPa.
- Estimate the mixing water for a slump between 50mm to 75mm.
- Calculate the void content of fine aggregate and adjust the mixing water if the void content is different from 35% (ACI 211.4R-08 2008).
- Determine the relative proportions of the coarse and fine aggregate based on the sand aggregate ratio.
- Calculate the quantities of cementitious material (cement and silica fume), carbon fibers, HRWR, sand, and coarse aggregate.

**Table 3.1 Details of the primary mixture proportions of the carbon fiber reinforced self-consolidating concrete**

| Concrete Mix | W/B ratio | CF (% vol.) | CA (kg) | FA (kg) | Binder (B) | | W (kg) | CF (kg) | HRWR | |
|---|---|---|---|---|---|---|---|---|---|---|
| | | | | | C (kg) | SF (kg) | | | (% b) | (kg) |
| M1 | 0.35 | 0.00 | 784.2 | 958.5 | 432.7 | 48.1 | 189.8 | 0.0 | 1.50 | 7.2 |
| M2 | 0.35 | 0.25 | 778.4 | 951.4 | 432.7 | 48.1 | 189.8 | 4.7 | 2.00 | 9.6 |
| M3 | 0.35 | 0.50 | 767.1 | 937.6 | 432.7 | 48.1 | 189.8 | 9.5 | 3.50 | 16.8 |
| M4 | 0.35 | 0.75 | 746.4 | 912.3 | 432.7 | 48.1 | 189.8 | 14.2 | 6.70 | 32.2 |
| M5 | 0.35 | 1.00 | 736.2 | 899.8 | 432.7 | 48.1 | 189.8 | 18.9 | 8.00 | 38.5 |
| M6 | 0.40 | 0.00 | 811.9 | 992.3 | 378.6 | 42.1 | 189.8 | 0.0 | 1.00 | 4.2 |
| M7 | 0.40 | 0.25 | 806.7 | 985.9 | 378.6 | 42.1 | 189.8 | 4.7 | 1.45 | 6.1 |
| M8 | 0.40 | 0.50 | 796.2 | 973.1 | 378.6 | 42.1 | 189.8 | 9.5 | 3.00 | 12.6 |
| M9 | 0.40 | 0.75 | 783.5 | 957.6 | 378.6 | 42.1 | 189.8 | 14.2 | 5.00 | 21.0 |
| M10 | 0.40 | 1.00 | 741.7 | 906.7 | 378.6 | 42.1 | 189.8 | 18.9 | 7.00 | 33.7 |

*CF= Carbon fibers, CA= Coarse aggregate, FA= fine aggregate, C=Cement, SF= Silica fume, W= Water, HRWR= High range water reducer.*

### 3.2.3 Adjustment of the CFRSCC mixtures

After the trial mixtures were finished for all batches, the optimum dosages for the constituent materials were adopted as the final CFRSCC mixture. The primary mixture proportions for the CFRSCC were determined based on the surface-dry saturated relative density of the coarse aggregates and sand. However, in producing the CFRSCC mixtures, the aggregates were saturated under laboratory condition; thus, the mixing water used need to be adjusted. The mixing water was adjusted according to the actual aggregate moisture content and absorption. Table 3.2 gives the adjusted mixture proportions of the CFRSCC mixtures. Therefore, ten batches were prepared to cast cylinders and prisms for the hardened properties tests.

**Table 3.2 Details of adjusted mixture proportions of the carbon fiber reinforced self-consolidating concrete.**

| Concrete Mix | W/B ratio | CF (% vol.) | CA (kg) | FA (kg) | Binder (B) | | W (kg) | CF (kg) | HRWR | |
|---|---|---|---|---|---|---|---|---|---|---|
| | | | | | C (kg) | SF (kg) | | | (% b) | (kg) |
| M1 | 0.35 | 0.00 | 777.4 | 948.9 | 432.7 | 48.1 | 179.8 | 0.0 | 1.50 | 7.2 |
| M2 | 0.35 | 0.25 | 771.7 | 941.9 | 432.7 | 48.1 | 178.0 | 4.7 | 2.00 | 9.6 |
| M3 | 0.35 | 0.50 | 760.5 | 928.2 | 432.7 | 48.1 | 172.9 | 9.5 | 3.50 | 16.8 |
| M4 | 0.35 | 0.75 | 740.0 | 903.2 | 432.7 | 48.1 | 162.2 | 14.2 | 6.70 | 32.2 |
| M5 | 0.35 | 1.00 | 729.8 | 890.8 | 432.7 | 48.1 | 157.8 | 18.9 | 8.00 | 38.5 |
| M6 | 0.40 | 0.00 | 804.9 | 982.5 | 378.6 | 42.1 | 182.4 | 0.0 | 1.00 | 4.2 |
| M7 | 0.40 | 0.25 | 799.7 | 976.2 | 378.6 | 42.1 | 181.0 | 4.7 | 1.45 | 6.1 |
| M8 | 0.40 | 0.50 | 789.3 | 963.4 | 378.6 | 42.1 | 176.4 | 9.5 | 3.00 | 12.6 |
| M9 | 0.40 | 0.75 | 776.7 | 948.1 | 378.6 | 42.1 | 170.5 | 14.2 | 5.00 | 21.0 |
| M10 | 0.40 | 1.00 | 735.3 | 897.5 | 378.6 | 42.1 | 161.2 | 18.9 | 7.00 | 33.7 |

*CF= Carbon fibers, CA= Coarse aggregate, FA= fine aggregate, C=Cement, SF= Silica fume, W= Water, HRWR= High range water reducer.*

## 3.3 Preparation and mixing method

The volume of the concrete mixtures was calculated before starting the mixing process. The batched amount was calculated based on the amount of concrete required to cast cylinders and prisms while considering the capacity of the pan mixer. The amount of concrete was increased by 15% to account for losses that might occur during mixing and testing.

The concrete mixtures were prepared using a pan-type revolving mixer of 50L maximum capacity as shown in Figure 3.1. The coarse and fine aggregates were first charged and mixed together with a ¼ of the total mixing water for about 60 seconds. Then, the binders, cement and silica fume, were added with a ¼ of the total mixing water and mixed for about 120 seconds. After that, the mixing operation was stopped for about 180 seconds and the mixture was covered

with wet burlap to prevent loss of water due to evaporation. This was done to ensure that the aggregates are fully saturated. After the rest time of 180 seconds, for the control mix with no fibers, the remainder of the mixing water (½ of the total mixing water) with the HRWR dosage was added into the mixer and the mixture was mixed further for about 180 seconds. The same sequence was followed for the mixture with fibers, except that the fibers were added before adding the rest of the mixing water including HRWR dosage. The concrete mixtures were mixed for a total time of 6 minutes excluding the rest time. Various trial concrete batches were prepared to obtain the optimum dosage of HRWR for use in the CFRSCC mixtures. The mixture quantity was 25L for all concrete batches.

*Figure 3.1 The pan-type revolving mixer*

## 3.4 Testing of fresh concrete properties

Immediately after the completion of mixing, the concrete mixtures were tested for filling ability, passing ability, segregation resistance, air content, and unit weight or wet density. The test procedures are discussed below.

### 3.4.1 Filling ability test

Filling ability is the ability of SCC to flow horizontally and vertically under its self-weight. The slump flow and $T_{50}$ slump flow time tests were followed in accordance with ASTM C 1611/C 1611M-09b (2009) to measure the filling ability of SCC.

The slump flow was determined by measuring the diameter of the concrete spread in two perpendicular directions (D1, D2), where D1 is the largest diameter of the flow patty. The steel tray was placed on a leveled floor. The mold was lifted upward and the concrete was allowed to flow. The slump flow measurement was taken after the spread of the concrete completely stopped. Slump flow values should be in a range between 550 to 800 mm.

$T_{50}$ slump flow time was also measured for all concretes from the same test; it is the time that the concrete took to reach a diameter of 50 cm. A stopwatch was used to measure $T_{50}$. The stopwatch was started as the mold was lifted upward and the concrete was allowed to flow. Once the concrete touched the 50-cm diameter circle marked on the base plate, the stopwatch was stopped and the $T_{50}$ slump flow time was recorded. $T_{50}$ slump flow time should be in the range from 2 to 7 seconds. The apparatus and test measurement of slump flow test are shown in Figure 3.2.

(a) Slump flow apparatus (b) Measurement of slump flow

*Figure 3.2 Slump flow apparatus and measurement*

### 3.4.2 Passing ability test

Passing ability is the ability of SCC to flow through the limited spaces between rebars with no blocking. It mainly depends on the maximum size and volume of the aggregates. The J-ring slump flow test was used in this study according to ASTM C 1621/C 1621M-09b (2009) to measure the passing ability. This test is similar to the slump flow test, except that it is carried out in the presence of a J-ring around the slump cone. The steel tray was placed in a leveled floor. The mold was lifted upward and the concrete was allowed to flow. The J-ring slump flow measurement was taken after the spread of the concrete completely stopped. The two perpendicular diameters (D1, D2; D1 > D2) of the concrete spread in the presence of a J-ring were measured to determine the J-ring slump flow. Blocking index was calculated by subtracting slump flow from J-ring slump flow. The blocking index should range from 0 to 50 mm. The apparatus and measurement of J-ring slump flow are presented in Figure 3.3.

*(a) J-ring slump flow apparatus* *(b) Measurement of J-ring slump flow*

*Figure 3.3 J-ring slump flow apparatus*

### 3.4.3 Segregation resistance test

Segregation resistance or stability is a vital property of SCC. It is defined as the ability of the concrete to remain consistent and uniform during mixing, transport, and placing. Stability affects the hardened properties such as strength and durability. There are several techniques to measure the segregation resistance of SCC including column segregation, penetration, and sieve stability tests. The segregation resistance can also be qualitatively assessed based on visual observations. In this study, the sieve stability test, which was proposed by Nagataki and Fujiwara (1995) and given in Safiuddin et al. (2008), was used to quantify the segregation resistance of SCC. In addition, the segregation resistance of SCC was visually assessed with respect to the visual stability index (VSI).

#### 3.5.3.1 Sieve stability test

The sieve stability apparatus consisted of a bucket (two liters volume), a sieve (4.75 mm opening size) attached to a pan, and a stopwatch as shown in Figure 3.4. The test procedure was as follows: the sieve and pan were weighed separately, the bucket was filled with SCC and the

concrete was poured onto the sieve and rested for about 5 minutes to allow some mortar to pass through the sieve, the sieve/pan with the concrete were weighed, the sieve with the concrete retained was separated, the pan including the mortar was weighed, the concrete retained on the sieve was washed to obtain the coarse aggregates in saturated surface dried (SSD) condition; then the SSD coarse aggregates were weighed, finally the segregation index was determined using the following equation:

$$SI = \frac{M_p}{M_c} \times 100\% \qquad \text{Equation 3.1}$$

Where:

*SI*= Segregation index (%)

$M_p$= Mass of the mortar that passed the sieve (kg)

$M_c$= Mass of the mortar contained in concrete (kg) = Concrete mass – Aggregate mass in SSD condition

A desirable segregation index (SI) for SCC and CFRSCC should be between 0 to 18 % as proposed by Nagataki and Fujiwara (1995).

*Figure 3.4 Sieve analysis apparatus for aggregate segregation*

### 3.4.3.2 Visual stability index (VSI)

Visual stability index (VSI) indicates the bleeding condition and stability (segregation level) of freshly mixed SCC. ASTM C 1611/C 1611M – 09b (2009) categorizes the visual stability index for SCC into four groups; these groups are defined below [19]:

a) VSI = 0 refers to highly stable SCC
b) VSI = 1 indicates stable SCC
c) VSI = 2 implies unstable SCC
d) VSI = 3 infers highly unstable SCC

In this study, the VSI of SCC was determined by observing the visual quality of the concrete mix in the slump flow test. Each concrete mix was given a VSI value, which indicated the stability of the CFRSCC. The index value varied from 0 to 3 to describe the degree of concrete stability.

### 3.5.5 Test for air content and unit weight

The procedure in ASTM C 231/C 231M-09b (2009) standard was followed to determine the air content of fresh concrete by using type B air meter. The apparatus of the air content was prepared before the concrete was ready. The bowl was placed in a level base and filled up to the

top with the concrete. Then, the bowl was covered and water was pumped into the bowl to substitute the air with water. Finally, the main air valve was pushed and the air content was read from the pressure gauge. However, to determine the unit weight a bowl was used to measure the volume of concrete. The procedure in ASTM C 138/C 138M - 10b (2010) was followed to obtain the unit weight of each mix. Some exceptions were applied to reflect that the concrete was SCC. The bowl was weighted with no concrete. Then, it was filled with the concrete and weighted, then the unit weight was obtained. Figure 3.5 shows the apparatus used for the air content and unit weight.

*Figure 3.5 Air content apparatus*

## 3.5 Testing of hardened concrete properties

This section describes the tests that were carried out to evaluate the hardened concrete properties of the CFRSCC mixtures. In particular, the compressive strength, splitting tensile strength, and

fracture energy tests. The preparation of the hardened concrete specimens and the various tests that were done are discussed below in details.

### 3.5.1 Hardened concrete specimens

Twelve concrete cylinders (200 mm diameter × 100 mm length) were used for the compression strength test, six concrete cylinders (200 mm diameter × 100 mm length) were used for the splitting tensile strength test, and 3 prisms (100 mm wide × 100 mm deep × 350 mm long) were used for the fracture energy test. Figure 3.6 (a) and 3.6 (b) shows forms for the cylinders and the prisms. Once the mold for the cylinders and prisms were prepared and oiled, the concrete was poured into the mold and filled to the top without any compaction. The concrete in the cylinders and prisms were screeded to level the top surface and remove any extra concrete. Figure 3.6c shows the casting of concrete prisms.

*(a) The cylinders (100mm × 200mm)* *(b) The prisms (100mm × 100mm × 350mm)*

*Figure 3.6 Forms of the cylinders and the prisms*

*(c) Casting of prisms*

*Figure 3.6 Forms of the cylinders and the prisms (cont'd)*

After casting, all the cylinders and prisms were stored in the laboratory. The ASTM C 192/C 192M – 07 (2007) standard was followed for the curing process. Two protocols for curing were used. The cylinders were cured in a humid room, and the prisms were cured for about one week by covering them with wet burlap. Figure 4.7 shows the curing processes.

*(a) Wet burlap for curing.*

*(b) The humid room for curing*

*Figure 3.7 The curing process for cylinders, prisms, and beams*

### 3.5.2 Test for compressive strength

Compressive strength of the hardened concrete was determined according to ASTM C39/C39M – 09a (2009). The compressive strength of the concrete cylinders was tested at 3, 7, 14, 28 days. The concrete cylinders were removed from the molds after two days and placed in a humidity room. The concrete cylinders were cured until a day before testing. The ends of the cylinders were ground using a surface grinder to achieve good surface. The cylinders were tested using a hydraulic compression test machine with a 1500 kN capacity. Figure 3.8 shows the hydraulic compression tester and the grinder machine. The load was applied onto the concrete cylinders at a rate of 0.35 to 0.7 mm/min. The maximum load (kN) and the compressive strength (MPa) were recorded. The average of three test cylinders results was calculated to determine the compression strength.

*(a) The hydraulic compression tester* *(b) The grinder machine*

*Figure 3.8 The hydraulic compression tester and the grinder machine*

### 3.5.3 Test for splitting tensile strength

The splitting tensile strength of the hardened concrete was measured in accordance to ASTM C496/C496M – 04 (2004). The cylinders were removed from the molds and cured until day before testing. The splitting tensile strength was determined at 14 and 28 days. Figure 3.9 shows the splitting tensile strength test set-up.

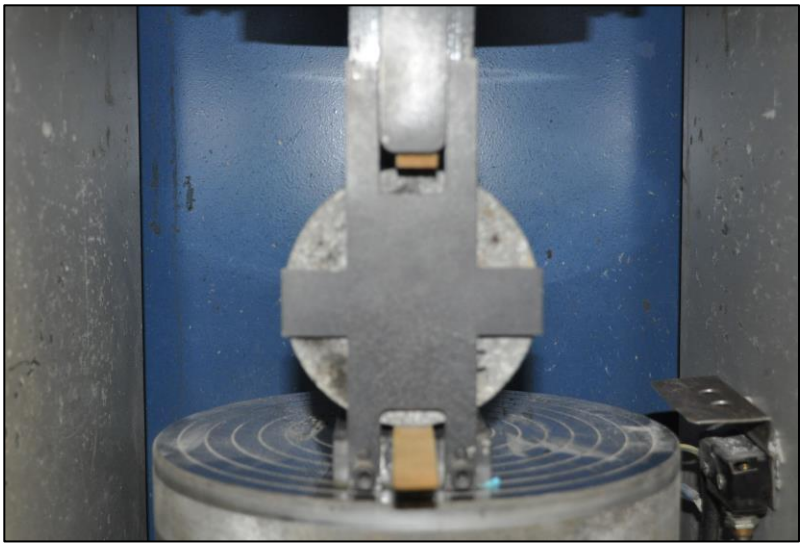

*Figure 3.9 The splitting tensile strength test set-up.*

The length and diameter of the specimens were measured using electronic digital calipers. Bearing strips were placed at the top and bottom of the specimens to ensure proper straight line loading as shown in Figure 3.9. Load was applied using the same machine used in the compressive strength test. The splitting tensile strength was calculated at the ultimate load capacity using Equation 3.2.

$$T = \frac{2 \times P}{\pi l d}$$ Equation 3.2

Where,

*T*= Splitting tensile strength, MPa,

*P*= Maximum applied load indicated by the testing machine, N,

*l*= Length, mm,

*d*= Diameter, mm.

### 3.5.4 Test for fracture energy

Fracture energy of the CFRSCC mixtures was determined using prisms tested in flexural under third-point loading according to ASTM C1609/C1609M – 10 (2010). Three prisms (100 mm wide × 100 mm deep × 350 mm long) were cast, cured using wet burlap and tested at 28 days. A closed-loop servo-hydraulic testing system with 100kN capacity was used to perform this test. The load was applied at a rate of 0.075mm/minute. Two linear variable differential transducers (LVDTs) were mounted, one on each side of the prism, onto a jig that was clamped to the specimens. The LVDTs were used to measure the mid-span deflection of the specimens. Figure 3.10 shows flexural strength test set up.

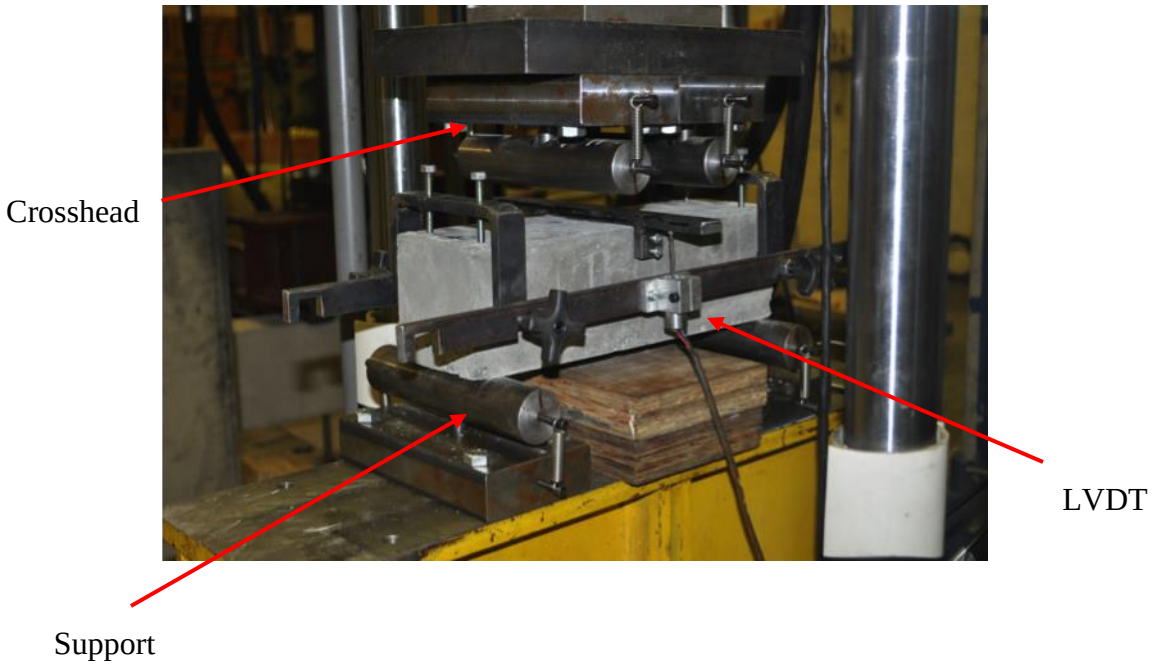


*Figure 3.10 The flexural strength test set up*

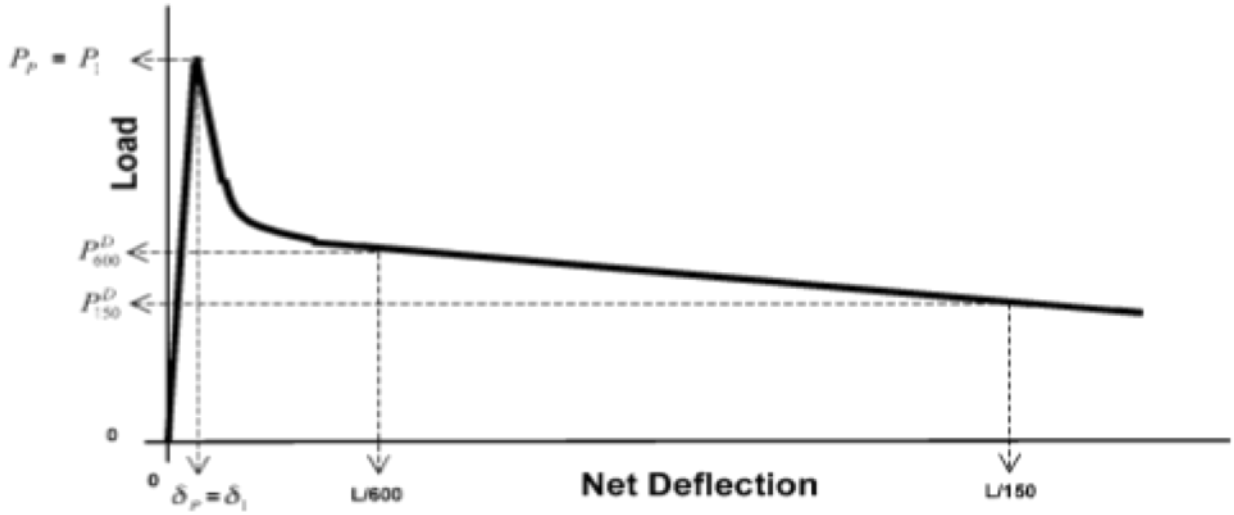


*Figure 3.11 The average net deflection measurements (ASTM C1609/C1609M – 10 (2010))*

Typical data collected included the applied load and mid-span deflection from the two LVDTs as shown in Figure 3.11. The fracture energy or toughness $T^{D}_{150}$ is determined by calculating the

area under the load-deflection curve up to a net deflection of L/150. The first-peak strength or "modulus of rupture" is determined from peak load as given in Equation 3.3. The equivalent flexural strength ratio ($R^{D}_{T,150}$) is determined using Equation 3.4.

$$f_1 = \frac{P_1 \times L}{bd^2} \qquad \text{Equation 3.3}$$

Where,

$f_1$= The first peak strength, MPa,

$P_1$= The peak load, N,

$L$= The span length, mm,

$b$= The average width of the specimen, mm,

$d$= The average depth of the specimen, mm.

$$R^{D}_{T,150} = \frac{150 \times T^{D}_{150}}{f_1 \times b \times d^2} \times 100\% \qquad \text{Equation 3.4}$$

Where,

$R^{D}_{T,150}$= The equivalent flexural strength ratio, %,

$T^{D}_{150}$= Area under the load vs. net deflection curve 0 to L/150, toughness,

$f_1$= First peak strength, MPa,

$b$= The average width of the specimen, mm,

$d$= The average depth of the specimen, mm.

### 3.5.5 Scanning electron micrograph (SEM)

Figure 3.12a shows the scanning electron microscope device. Samples for all mixtures were prepared from the tested specimens in the fracture energy tests. The samples were cut into 20mm by 20mm size using a concrete saw. The samples were cleaned and dried. The samples should be dried in order for the samples to be conductive. The samples were coated using a golden coating as shown in Figure 3.12b. The samples were then placed inside the scanning microscope. The SEM images were taken at magnification of 100 micrometer.

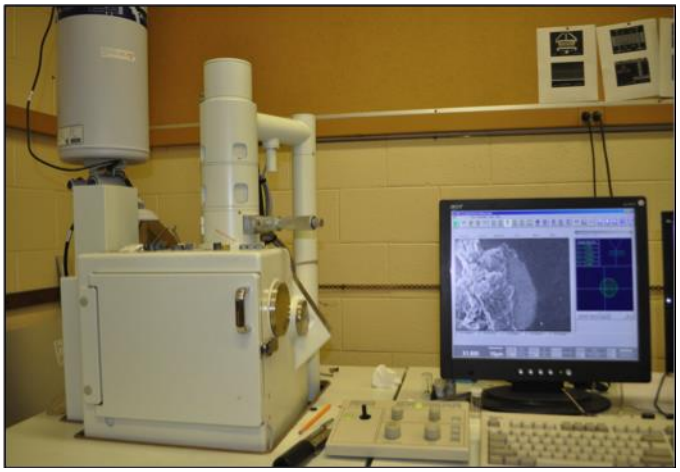

*a) Scanning electronic microscope*

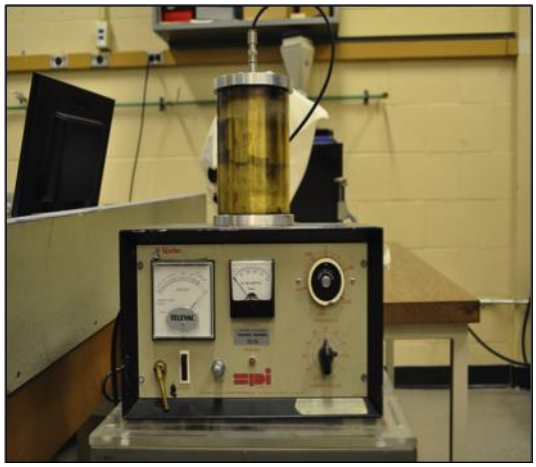

*b) Golden coating device*

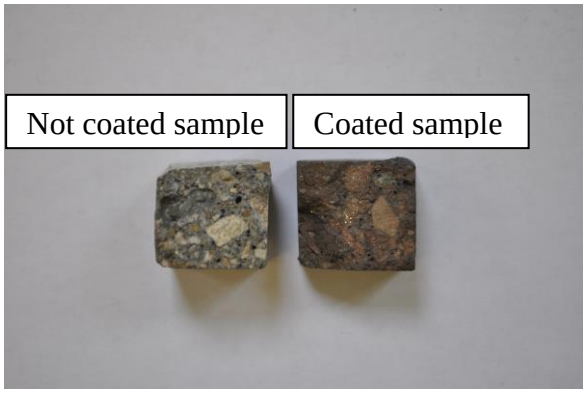


*c) Samples with and without coating*

*Figure 3.12 Scanning electronic micrographs (SEM) set up*

## 3.6 Beam tests

A total of eleven reinforced concrete beams were designed in accordance to CSA Standard A23.3-04. Group (1) consisted of four beams designed to study the shear behaviour of reinforced concrete beams under shear loading; group (2) consisted of seven beams designed to study the flexural behaviour of reinforced concrete beams under flexural load. The test variables consisted of the repair materials (SCC (M1), CFRSCC (M3), and Sikacrete-08 SCC), location of repair (shear, tension, and compression), and loading configuration (flexure, shear) as presented in Table 3.6.

**Table 3.3 Details of the beam specimens**

| Failure configuration | Location of repair | Number of specimen | Repair material |
|---|---|---|---|
| Shear | Shear | 4 | Control<br>M1*<br>M3*<br>Sikacrete-08 SCC |
| Flexure | Tension | 4 | Control<br>M1<br>M3<br>Sikacrete-08 SCC |
| | Compression | 3 | M1<br>M3<br>Sikacrete-08 SCC |

*M1=Self-consolidating concrete, M3=Self-consolidating concrete with 0.5% by vol. carbon fibers, Sikacrete-08 SCC, * Mixture M1 and M3 was chosen based on the fresh and hardened results.*

### 3.6.1 Design and construction of beams

The beams in group (1) shear were 150mm wide × 350mm deep × 2400mm long and the beams in group (2) flexure were 150mm wide × 300mm deep × 2400mm long. Group (1) beams had 4-20M longitudinal bars in the tension zone and 2-15M longitudinal bars in the compression zone. The shear reinforcement consisted of 6 mm diameter closed stirrups spaced at 180 mm in the repair zone (500mm) and 6mm diameter closed stirrups spaced at 150 mm in the rest of the beam. This stirrup layout ensures that failure will occur in the repair zone. Group (2) beams had 2-15M longitudinal bars in the tension zone, 2-10M bars in the compression zone and 6 mm diameter closed stirrups at a spacing of 130 mm. Figure 3.13 shows the beam geometry and reinforcement layout. Figure 3.14 shows the location of the patch repair in the flexure beams (tension and compression) and shear beams (shear zone).

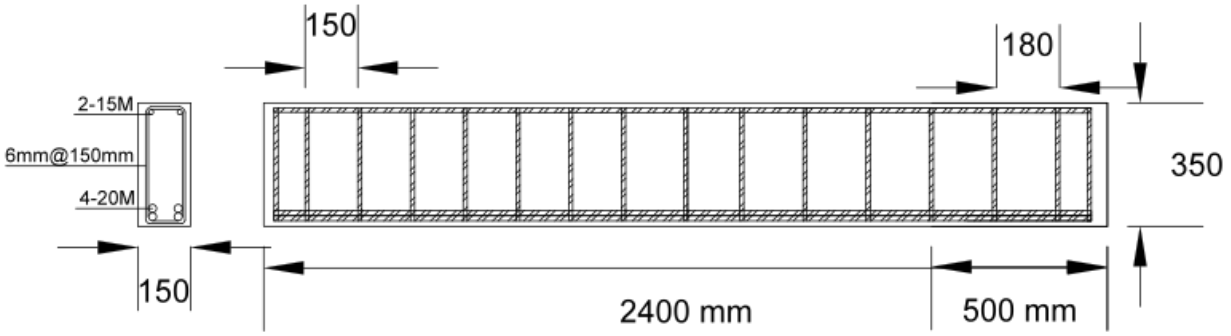


*Figure 3.13 (a) Specimen geometry and reinforcement details – shear beams (dimensions in mm)*

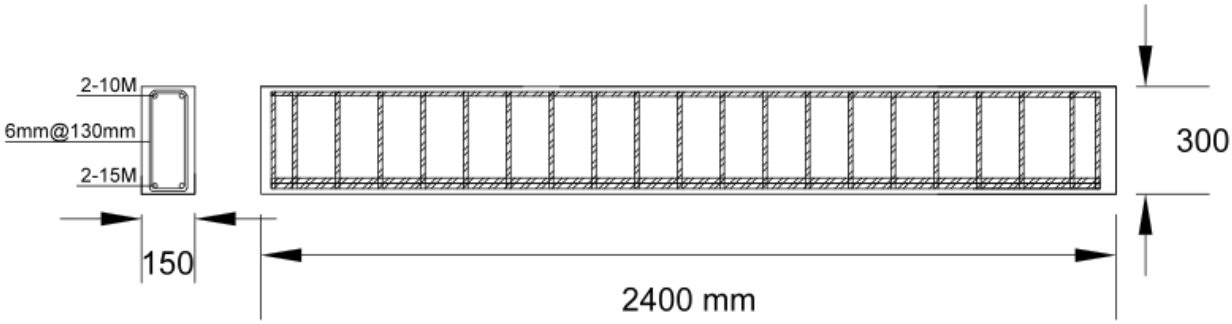


*Figure 3.13 (b) Specimen geometry and reinforcement details – flexural beams (dimensions in mm)*

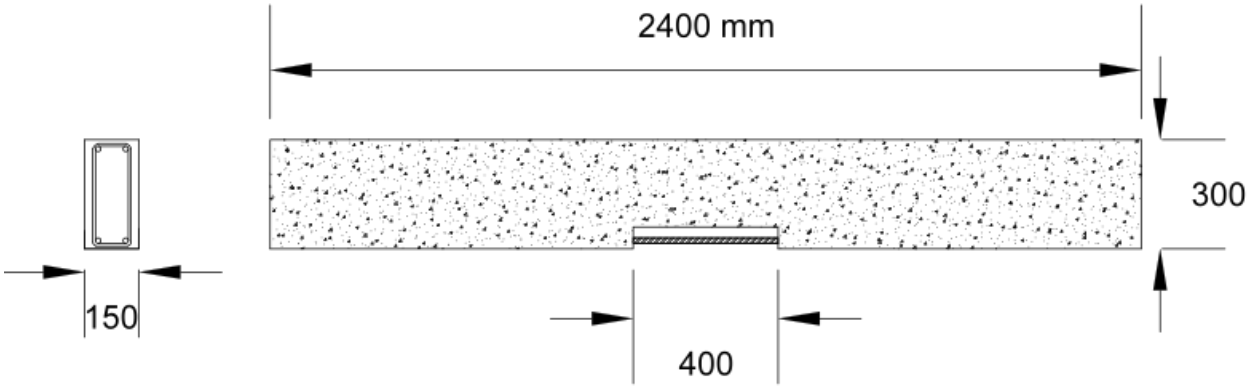


*(a) Flexural beam (tension region patch)*

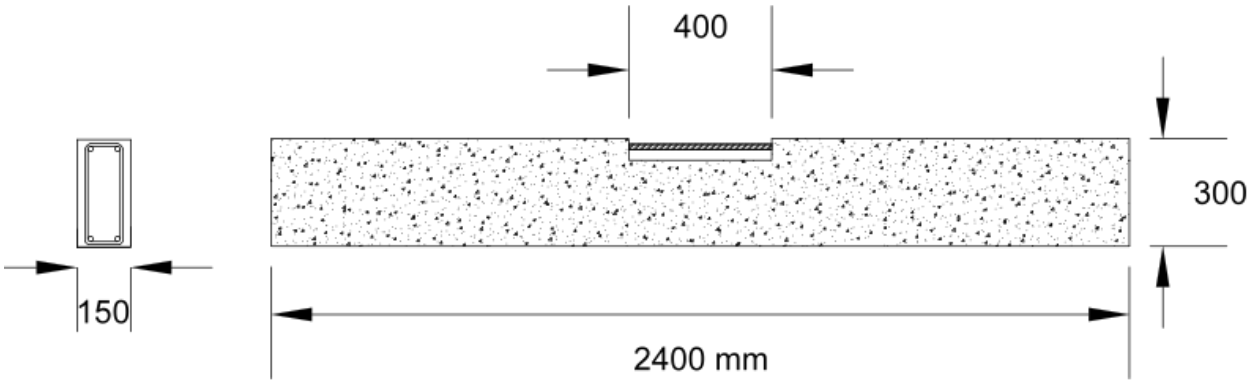


*(b) Flexural beam (compression region patch)*

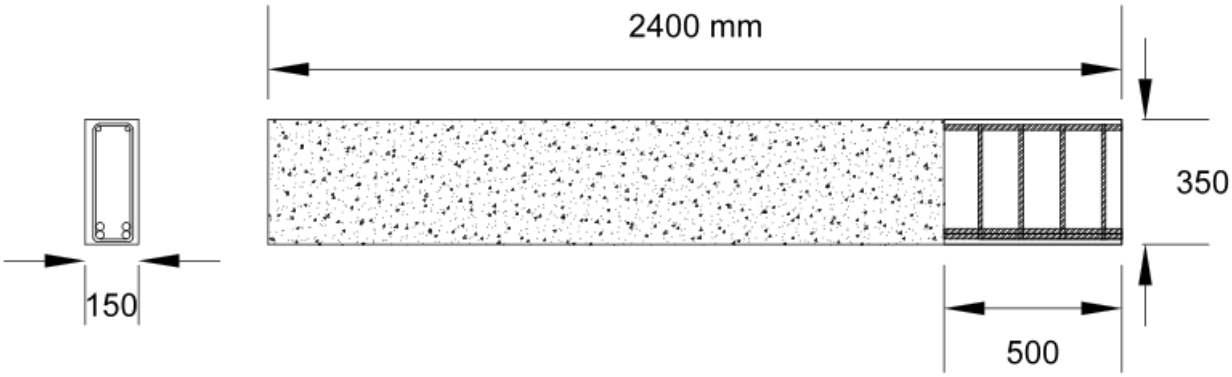


*(c) Shear beam (shear region patch)*

*Figure 3.14 Location of patch repair: a) bottom patch, b) top patch, c) shear span patch*

Table 3.5 presents the steel reinforcement properties, which were provided by Harris certificate (reinforcing bar supplier). Normal vibrated concrete supplied by Hogg Ready mix was used to fabricate the beam specimens. The concrete had maximum aggregate size of 19 mm and no admixtures were used. The specified compressive strength at 28-days was 40MPa.

**Table 3.4 Materials properties for all reinforcing bars (obtained from Harris certificate reinforcing bar supplier)**

| Material property | Φ6mm | 10 M | 15 M | 20 M |
|---|---|---|---|---|
| Yield strength (MPa) | 380 | 431 | 487 | 412 |
| Ultimate strength (MPa) | - | 574 | 602 | 637 |
| Maximum Elongation (%) | - | 19.5 | 17.5 | 15 |

The formwork was prepared in the laboratory as shown in Figure 3.15a. The formwork was built in such a way that was convenient to cast and remove the beams. Caging of the reinforcing steel was done prior to placing them in the formwork.

*(a) Beam formwork* *(b) Strain gauge installation*

*Figure 3.15 Beams formwork and strain gauges installation*

The forms were oiled to ease the removal of the beams after casting. The cages were placed inside the forms and the concrete cover was fixed using chairs on the bottom and both sides. Foam was used to make the voids in the beam section where the different repair materials will be

applied. Normal vibrated concrete was used to fabricate the beams. The top of each beam was screeded to remove any extra concrete and ensure good level. The beams were cured for about two weeks using wet burlap. Then the beams were stripped from the formwork. Figure 3.16 shows the reinforced concrete beams with the repair zone.

*Figure 3.16 Beams configuration before repair*

### 3.6.2 Repair procedure

After the beams were cast and cured, the beams were sandblasted to ensure adequate bond between the existing normal concrete and the repair materials. The beams were repaired using Sikacrete-08 SCC as a commercial product, mix M1 (SCC), and mix M3 (CFRSCC with 0.5% by vol. carbon fibers). Mixes M1 and M3 were chosen based on the hardened properties results and the cost perspective for each mix. Sikacrete-08 SCC comes in a bag of 25 kg. It was mixed at the concrete laboratory using a handheld mixer. The water was weighed and the Sikacrete-08 SCC was gradually added to the water at the same time the handheld mixer was mixing the concrete. The mixing process was in accordance to the manufactured specifications. On the other hand, Mixtures M1 and M3 were developed at the concrete laboratory. Mixtures M1 and M3 were prepared using a pan mixer in the concrete laboratory, for more information refer to section

3.3. Figure 3.17 shows the constituent materials for mix M1 and mix M3. The formwork used for repairing the beams is shown in Figure 3.18.

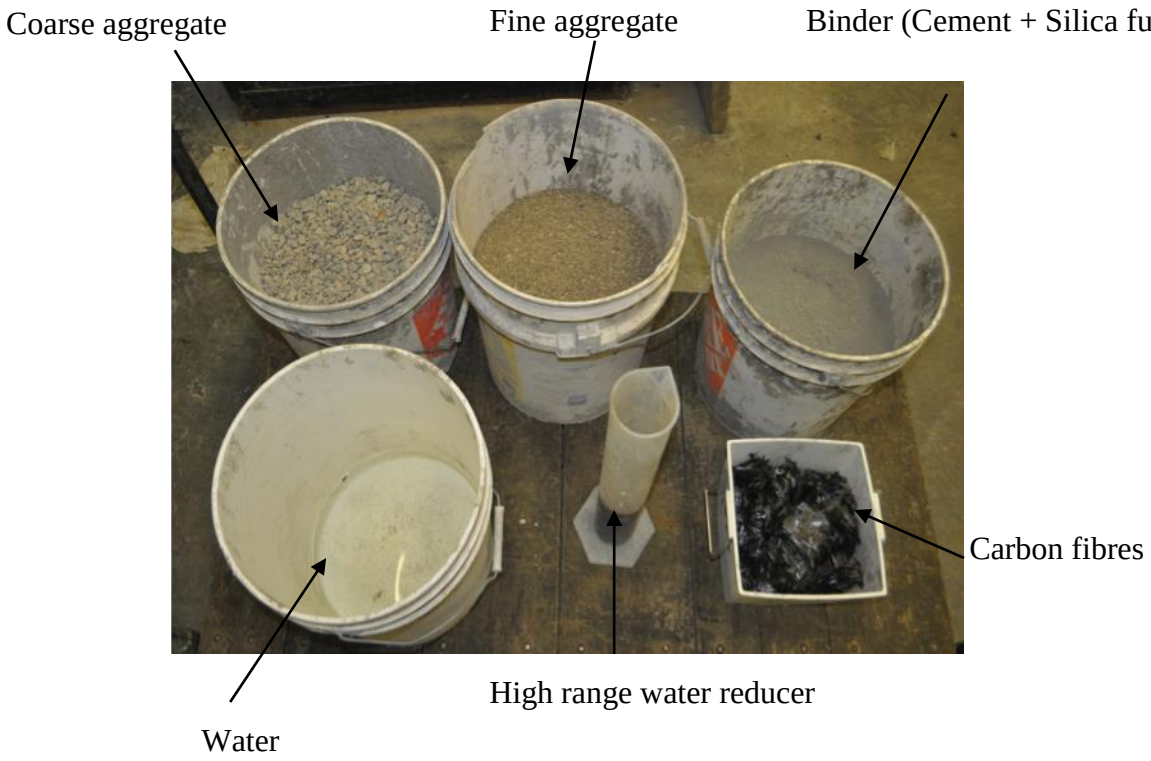


*Figure 3.17 Constituent materials for CFRSCC mixtures M1 and M3*

*Figure 3.18 The formwork for repairing the beams*

Once the formwork was finished, water was spread on the old concrete to ensure that the old concrete will not absorb any water from the repair materials. The concrete patch was mixed and poured in the repaired zones. The repaired zones were cured for about a week using wet burlap. Figure 3.19 shows the beams after patch repair vs. the control beam.

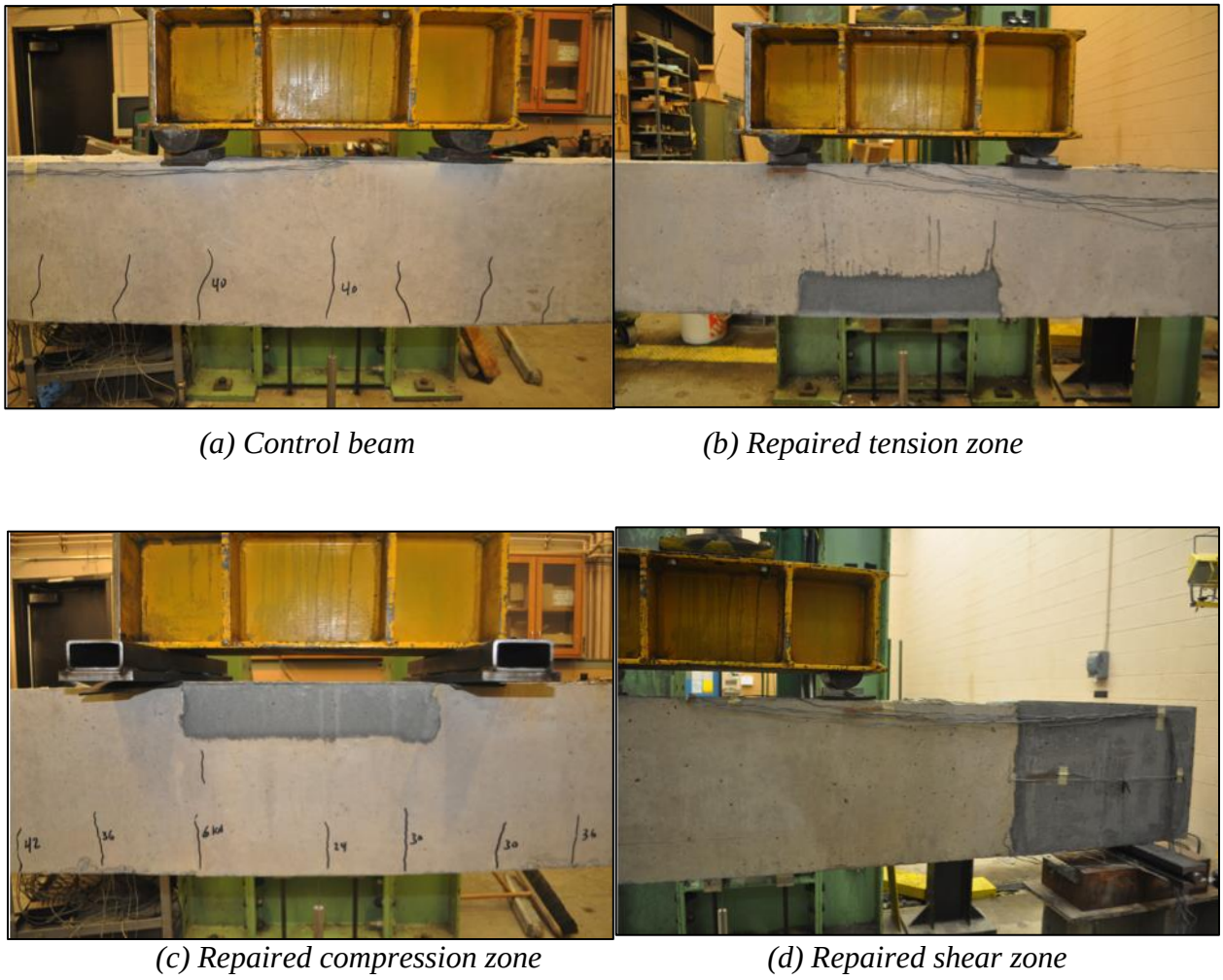


*(a) Control beam* *(b) Repaired tension zone*

*(c) Repaired compression zone* *(d) Repaired shear zone*

*Figure 3.19 Patch repair configuration*

### 3.6.3 Instrumentation

The load was measured using a load cell mounted on the actuator. A linear variable differential transformer (LVDT) with a range of 75 mm was mounted in the center of the beam to measure

the mid-span deflection. Strain gauges were used to measure the strain in the reinforcement and concrete. Two concrete strain gauges were placed: one in the repair material and another in the old concrete. The strain gauges for steel were 5 mm and for concrete were 60 mm. The steel strain gauges were placed in the middle of the reinforcing steel bars and on the stirrups. The locations of the strain gauges on the steel rebars were ground then cleaned using a conditioner and alcoholic isopropylene, and then the strain gauges were mounted using glue. The strain gauges were calibrated to ensure that they were working before testing. A schematic of instrumentation is shown in Figure 3.20.

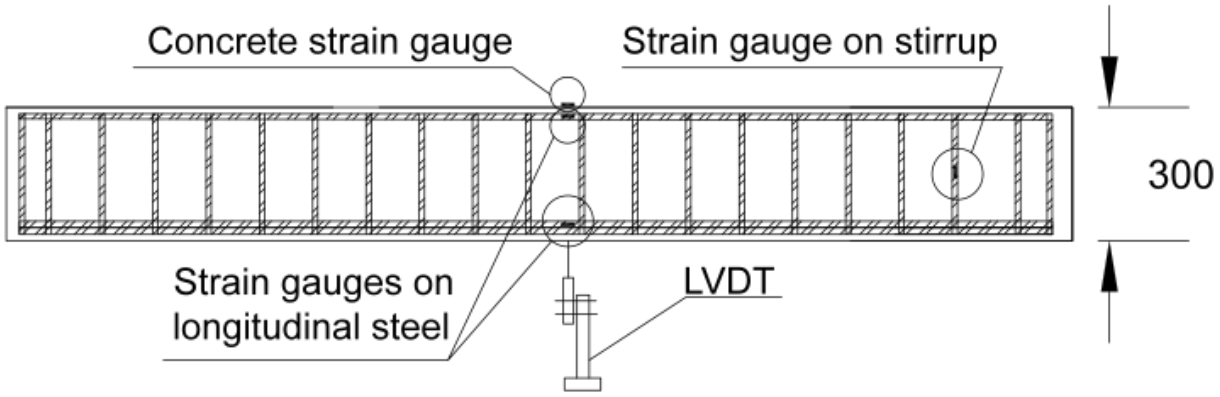


*Figure 3.20 (a) Schematic of instrumentation - flexural beams*

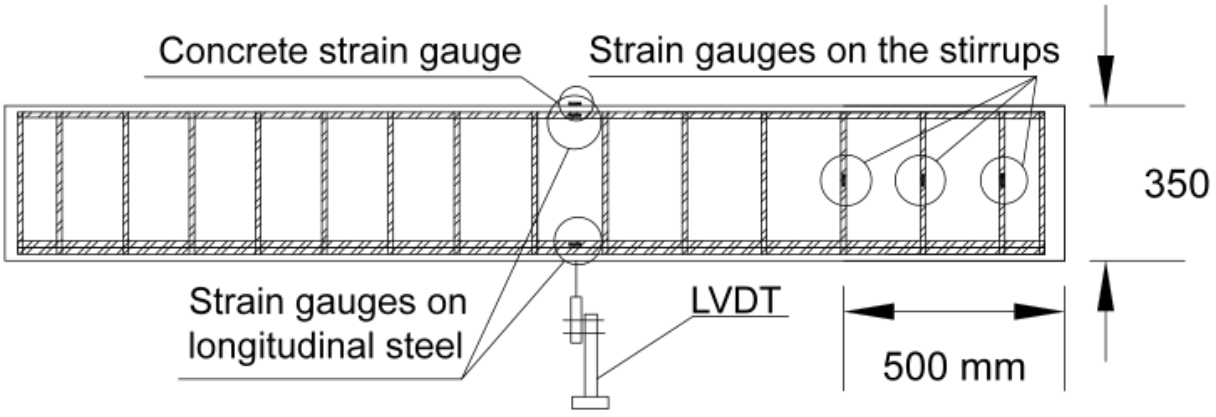


*Figure 3.20 (b) Schematic of instrumentation - shear beams*

### 3.6.4 Test setup and procedure

A servo-hydraulic actuator with a capacity of 500 kN was used for the loading test. Figure 3.21 shows the testing frame set-up. Four point loading scenario was chosen to test all the beams. The beams had a 2100 mm clear span and a constant moment region of 500 mm. The loading points and support points were marked to ensure that the beam was the right place. Then the beam was placed in the test frame over the supports. The actuator was controlled by MTS407 controller in stroke control at a displacement rate of 1.2 mm/min for the flexural test and 0.15 mm/min for the shear test. All beams were loaded up to failure or when the load dropped by 20% of the maximum load then the test was stopped. During the test, crack mapping and photos of failure modes were taken. The strain and LVDTs were measured using an SCXI National Instrument sat acquisition system and stored on a computer.

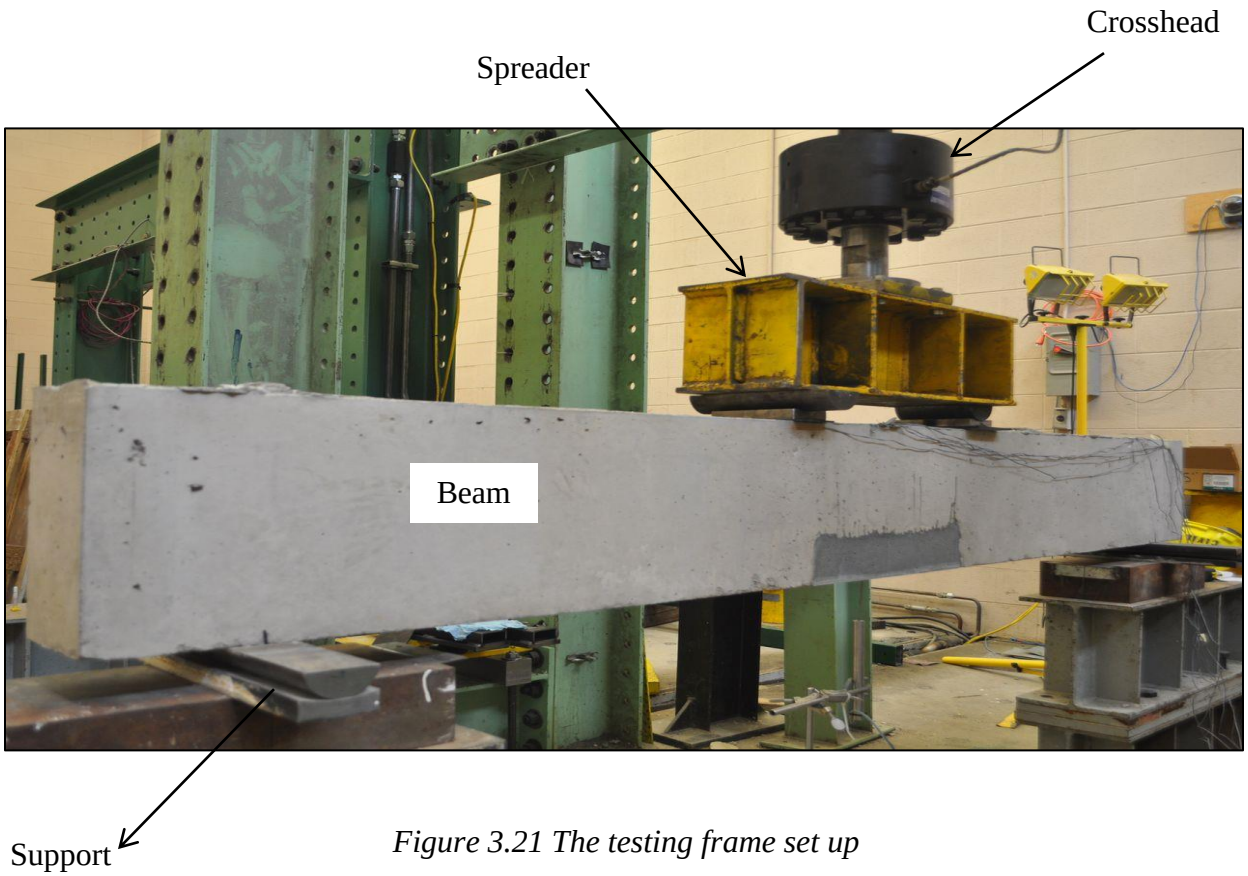


*Figure 3.21 The testing frame set up*

# Chapter 4 Fresh and Hardened CFRSCC Properties

In this chapter, the test results for the CFRSCC are presented and discussed.

## 4.1 Materials

Normal (Type I) portland cement, crushed limestone (coarse aggregate, CA), manufactured sand (fine aggregate, FA), silica fume (SF), HRWR, and tap water (w) were used in this study. The manufactured sand conformed with the specification OPSS 1002 [18]. Table 1 shows the physical properties of these materials.

**Table 4.1: Physical properties of constituent materials**

| Material | Properties |
|---|---|
| Normal Portland cement (C) | Relative density: 3.15 |
| Crushed limestone coarse aggregate (CA) | Maximum aggregate size: 10 mm |
| | Saturated surface-dry based relative density: 2.74 |
| | Absorption: 1.13% |
| | Moisture content: 0.393% |
| Manufactured concrete sand (FA) | Relative density : 2.68 |
| | Absorption: 1.15% |
| | Moisture content: 0.144% |
| Pitch-based carbon fibers (CF) | Relative density: 1.85 |
| | Tensile strength: 1770 MPa |
| | Tensile modulus: 180 MPa |
| | Length: 10 mm |
| | Diameter: 17 μm |
| High-range water reducer (HRWR) | Relative density: 1.064 |
| | Solid content: 33% |
| Silica fume (SF) | Relative density: 2.2 |
| Normal tap water (W) | Total solids: 430 mg/L |
| | Density at 24 °C: 997.28 kg/m$^3$ |

### 4.1.1 Physical properties of coarse aggregates (stone)

Table 4.1 shows the test results of the physical properties of the coarse aggregates. The relative density of the coarse aggregate was determined based on the saturated surface dry condition as 2.74. The relative density for the natural stones should be in the range of 2.4 to 2.9. The absorption of the stone was 1.13% which is in the acceptable range of 0.5 to 4.5 %. Therefore, the stone has met the relative density and absorption requirements, so the stone can be used in the concrete mixture. The absorption of the stone is close to the minimum limits that mean less water would be added to the concrete.

### 4.1.2 Grading of coarse aggregate

Figure 4.1 shows the coarse aggregate grading. The sieve analysis was used to determine the grading. 10 mm was the maximum aggregate size as obtained from Figure 5.1. The coarse aggregate grading was located in between the ASTM upper and lower limits. The figure shows that the coarse aggregate is very well graded which leads to fewer voids in the concrete mixture.

### 4.1.3 Physical properties of fine aggregate (sand)

The sand relative density was 2.68 as seen from Table 4.1. The most natural aggregates relative density is usually in the range of 2.4 to 2.9. The relative density of the sand is less than the relative density of the stone, which means that the stone is heavier than the sand. In addition, the absorption of the sand was 1.15% which is within the acceptable range of 0.2 to 3 %. The value of 1.15 % is close to the minimum value of the sand which means less water would be absorbed by the sand during mixing. Evaporable moisture content also was obtained under the lab condition environment as 0.144 %.

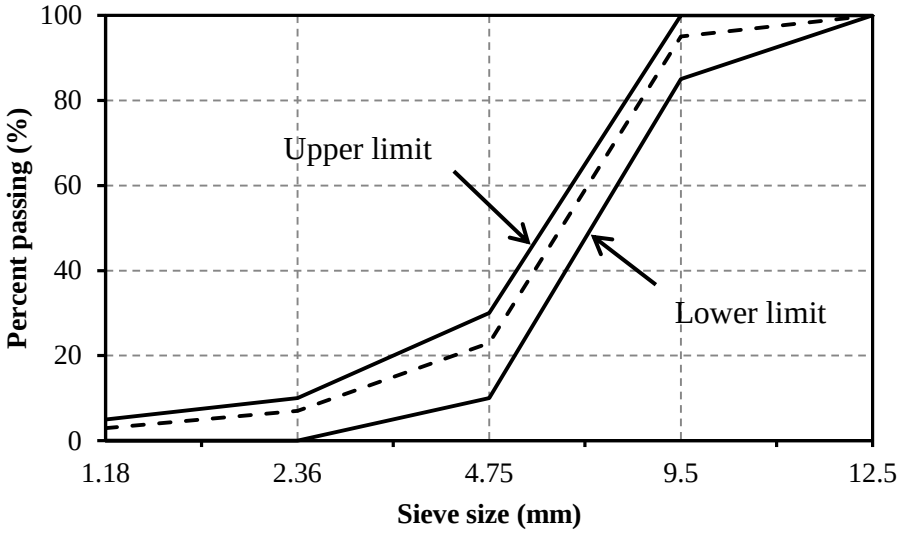


*Figure 4.1 Coarse aggregate gradation (ASTM C33/C33M-08 2009)*

### 4.1.4 Grading of fine aggregate

Figure 4.2 shows the fine aggregate grading. The sieve analysis was used to determine the grading of fine aggregate. The fine aggregate grading was within the limits of ASTM and the sand was very well graded which leads to fewer voids. As it is stated in the design and control of concrete mixture "the amount of fine aggregate passing the 300 μm (No.50) and the 150 μm (No. 100) sieves affect the workability, and bleeding of concrete; therefore, most of the specifications suggest that the passing aggregate through No.300 sieve should be between 5 to 30%". As it can be seen from Figure 4.2 that the amounts of fine aggregates that passed through the No. 300 sieve was 20% which is within the acceptable range.

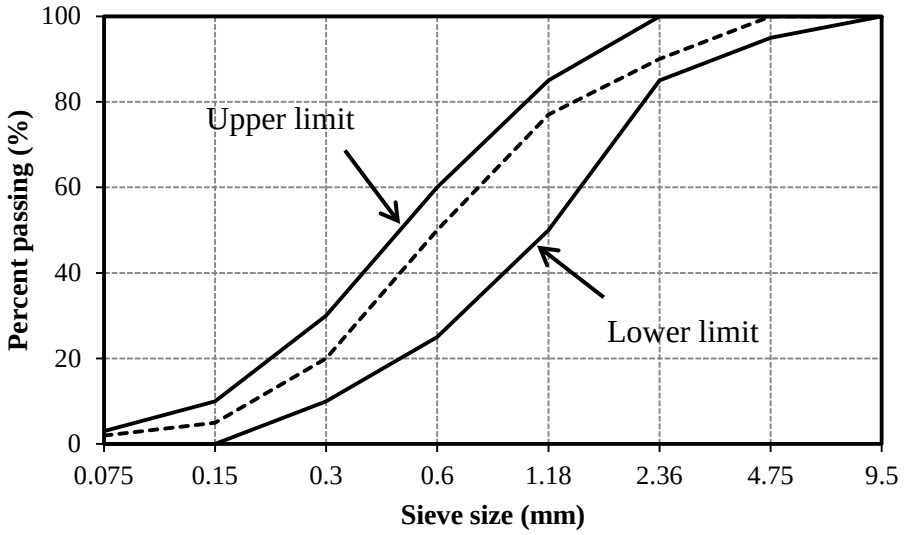


*Figure 4.2 Fine aggregate gradation (OPSS 1002)*

### 4.1.5 Sand / aggregate ratio

As can be seen from the Figure 4.3, the bulk density of the aggregate blends increased as the fine aggregate / coarse + fine aggregate (FA / (CA+FA)) ratio was increased up to 0.55. After this point the curve started to drop. The bulk density started from 1960 Kg/m$^3$ at 0.35 FA / (CA+FA) ratio, and it increased to the maximum bulk density of 2050 Kg/m$^3$ at 0.55 FA / (CA+FA) ratio. After the bulk density reached the maximum value, the curve started to drop until it reached 2030 kg/m$^3$ at 0.65 FA / (CA+FA) ratio. From the curve, it is clear that the optimum sand to aggregate ratio is 0.55 within the highest bulk density of 2050kg/m$^3$. This means that the maximum bulk density of 0.55 for the sand to aggregate ratio had less voids than the other bulk density of blends of aggregate.

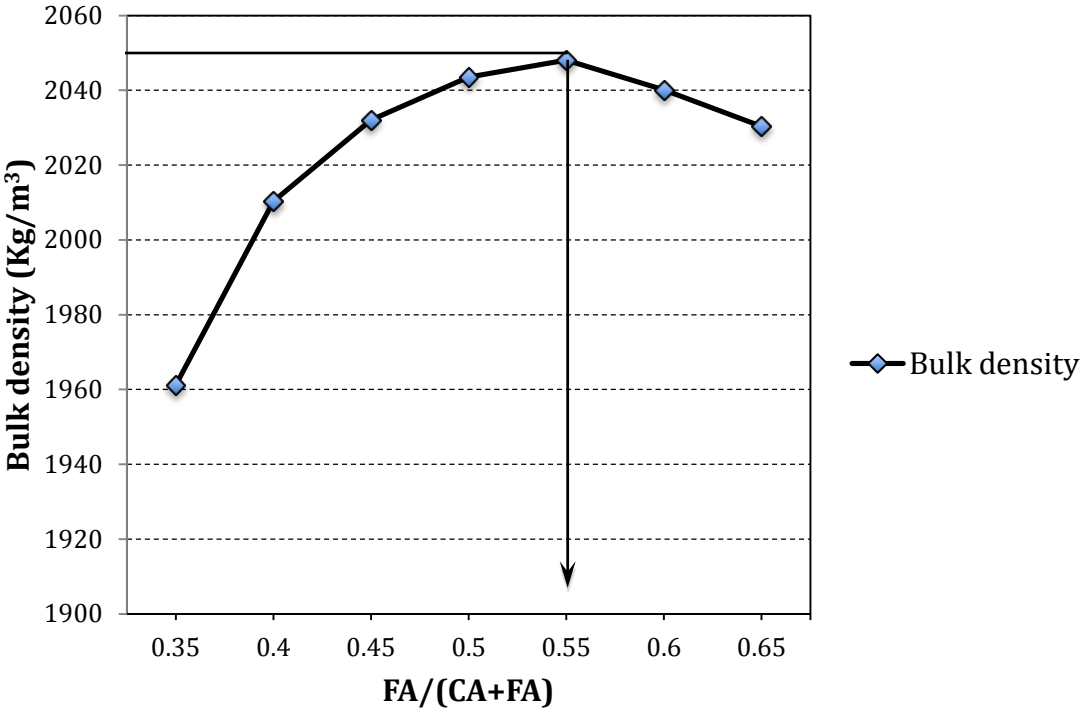


*Figure 4.3 Relationship between bulk density and sand to aggregates ratio (FA/(CA+FA)).*

## 4.2 Fresh properties of CFRSCC mixtures

The slump flow, the J-ring slump, and the segregation index were measured simultaneously for each mixture to determine the filling ability, passing ability, and segregation of the SCC. In addition, air content and unit weight were determined. The following sections present these results.

### 4.2.1 Filling ability

The filling ability was measured with respect to slump flow and $T_{50}$ slump flow time. The effect of carbon fibers on the slump, slump flow and $T_{50}$ slump flow are plotted in Figures 4.4, 4.5, and 4.6 respectively. The slump for the CFRSCC mixtures was between 250 and 280 mm as shown in Figure 4.4. These values of the slump are in the range of SCC required values (Ferraris et al. 2000).

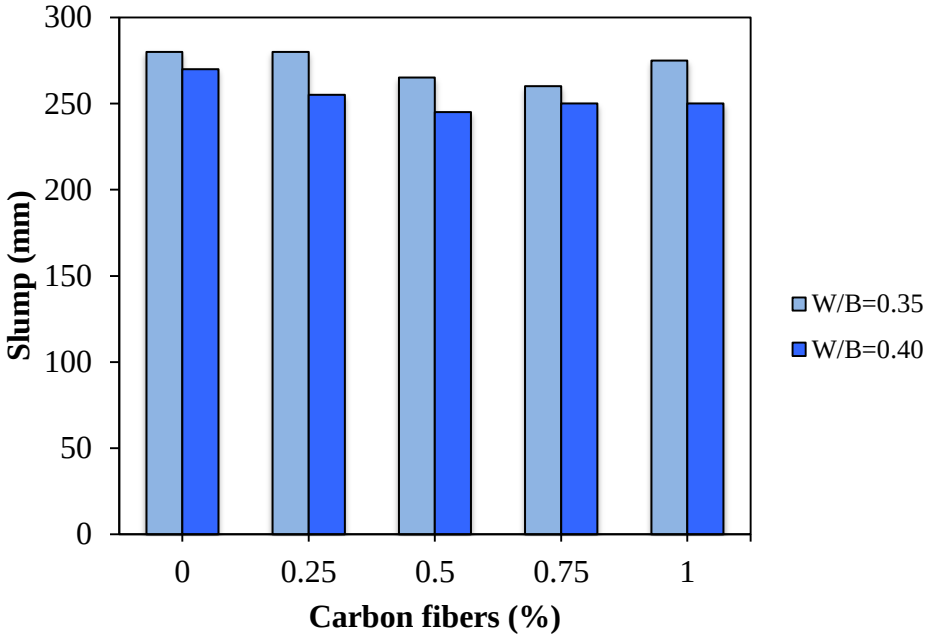


*Figure 4.4 Effect of carbon fibers content on the slump of CFRSCC*

Carbon fibers greatly affected the slump flow for CFRSCC. This is because, as the fiber volume increases, the interaction between carbon fibers can restrict the flowing ability in SCC (Nehdi et al. 2004). As shown in Figure 4.5, the slump flow values for the mixtures varied from 550 mm to 745 mm. The slump flow for SCC ranges from 550 mm to 850 mm (Ferraris et al. 2000, Grünewald et al. 2004 and Schutter 2005). Mixtures M5 and M10 had 1% carbon fibers by

volume which is the highest amount of fibers used in the present study; these two mixtures successfully fulfilled the slump flow requirements of SCC. However, mixtures M5 and M10 required a higher HRWR dosage than the rest of the mixtures to achieve the target slump flow of SCC. This is because the flowing ability of the concrete was significantly reduced in these two mixtures due to the higher volume of carbon fibers. A higher HRWR dosage was needed to improve the flowing ability of CFRSCC mixtures. Increased HRWR dosage increases the deformability of concrete to achieve the target flowing ability (EFNARC 2002).

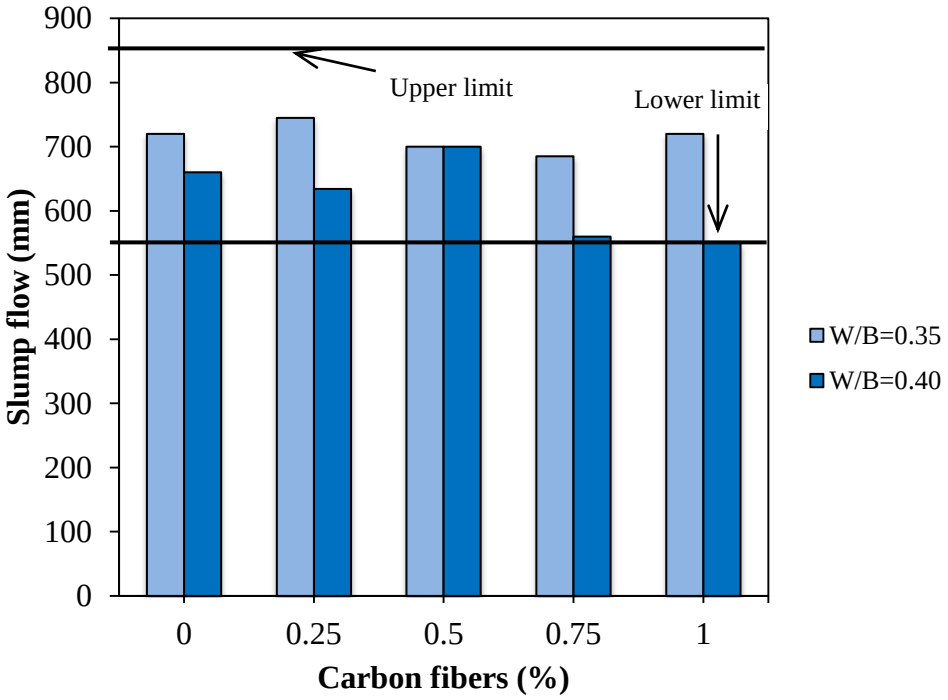


*Figure 4.5 Effect of carbon fibers content on the slump flow of CFRSCC*

Mixtures M1 and M6 (0% carbon fibers) showed higher deformability than the other CFRSCC mixes with respect to $T_{50}$ slump flow time. Figure 4.6 shows the effect of carbon fibers on the $T_{50}$ slump flow time. $T_{50}$ slump flow time increased with higher volume of carbon fibers because the inclusion of fibers makes CFRSCC mixture more viscous, and thus slows the flow of concrete. $T_{50}$ slump flow time for the mixtures without and with carbon fibers varied from 2.4 to 30 seconds. The $T_{50}$ slump flow time of SCC is typically 2-7 seconds (EFNARC 2002 and Khayat 2000). Hence, the $T_{50}$ slump flow time results for M9 and M10 mixtures did not meet the requirements for SCC. HRWR played a very significant role in improving the workability SCC mixture whereas carbon fibers decreased concrete workability. Therefore, finding the optimum balance between the amount of carbon fibers and the dosage of HRWR is important for mixtures to be successful in meeting the requirements for SCC fresh properties.

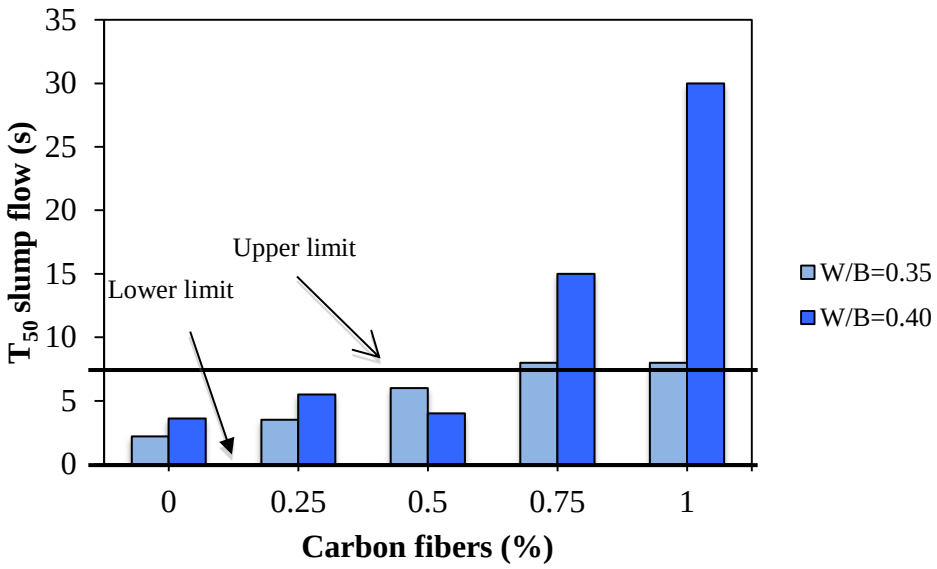


*Figure 4.6 Effect of carbon fibers content on the $T_{50}$ slump flow time of CFRSCC*

### 4.2.2 Passing ability

The J-ring slump flow test was used to measure the passing ability of the mixtures. As shown in Figure 4.7, the J-ring slump for CFRSCC varied between 250 to 275 mm. These values of J-ring slump are similar to the slump values reported by Ferraris et al. (2000). The limits of J-ring slump for SCC are between 250 and 280 mm.

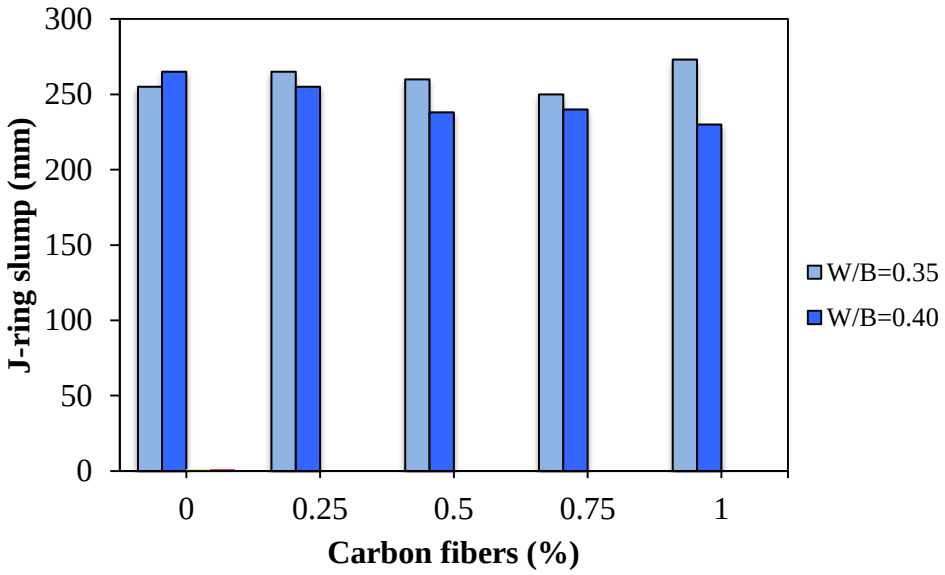


*Figure 4.7 Effect of carbon fibers content on the J-ring slump of CFRSCC*

As shown in Figure 4.8, the J-ring slump flow of different CFRSCC mixtures varied from 477.5 to 730 mm. It was generally lower than the slump flow.

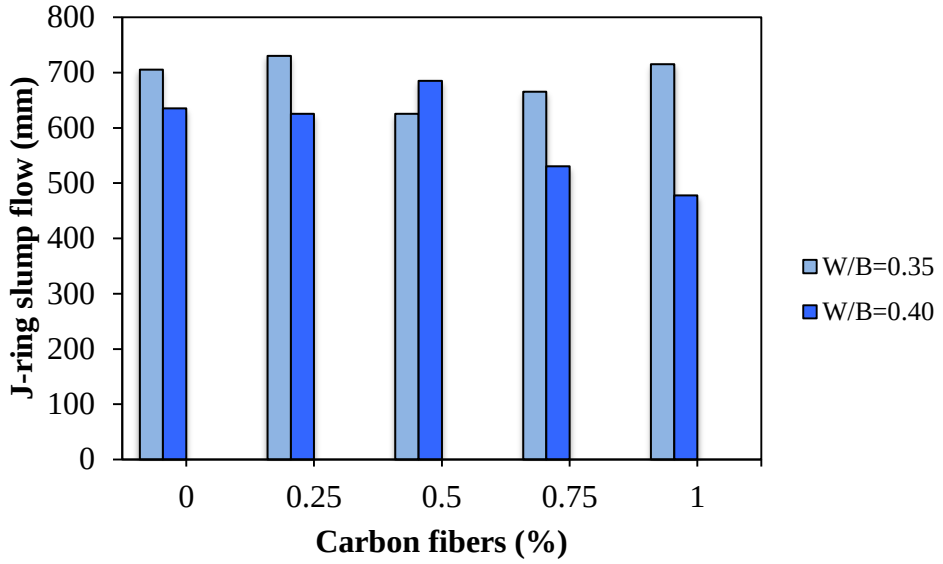


*Figure 4.8 Effect of carbon fibers content on the J-ring slump flow of CFRSCC*

The J-ring slump flow was used to calculate the blocking index. Subtracting the J-ring slump flow from the slump flow provides the blocking index. As shown in Figure 4.9, the blocking index for different CFRSCC mixtures produced in the present study was in the range of 0-50 mm; this is within the range specified in ASTM C1621/C1621M-09b (ASTM C1621 2009). The incorporation of carbon fibers generally increases the blocking index for a given workability if the HRWR is constant. This is because the presence of fibers restricts the concrete mixture from moving through space between obstacles (rebar). However, it greatly depends on HRWR. An adequate HRWR can significantly decrease the blocking index. For example, M4 had a 20 mm blocking index, whereas M5 had a 5 mm blocking index although it had the highest amount of carbon fibers. This is because a substantially high HRWR dosage was used in M5 mixture. At a greater HRWR dosage, the slump flow was substantially increased; therefore, the blocking index was decreased. This made the M5 concrete mixture move easily around the rebars during flow.

Furthermore, Mix M1 (control mixture without fiber) had a blocking index of 15 mm whereas Mix M5 had a blocking index of 5 mm. This indicates that HRWR had a greater influence on the blocking index of the concrete mixture. Thus, it is clear that the HRWR played a vital role to improve the passing ability of CFRSCC.

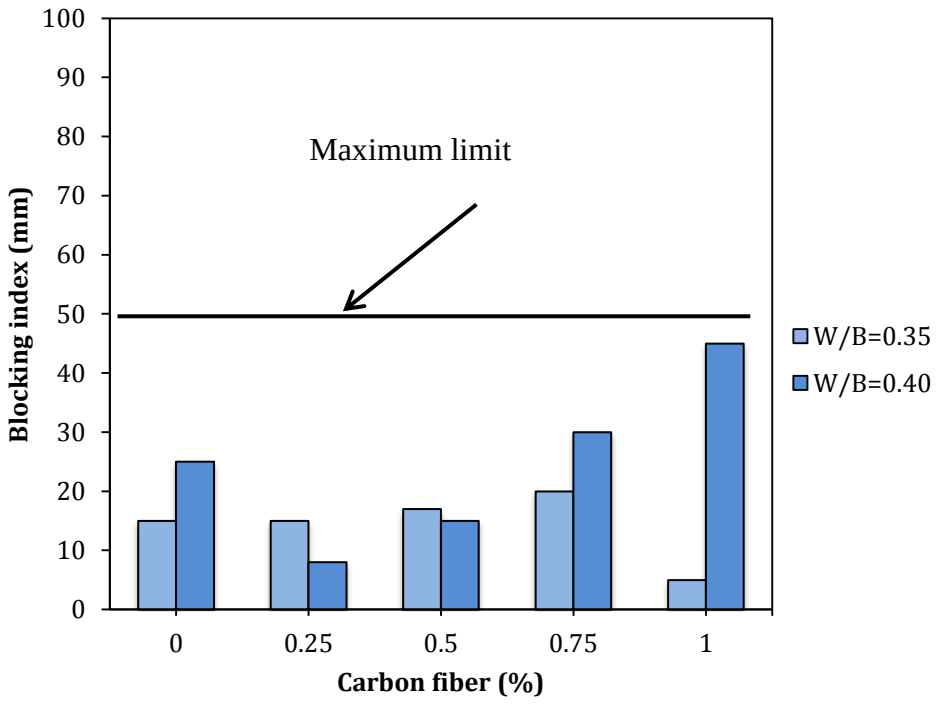


*Figure 4.9 Effect of carbon fibers content on the blocking index of CFRSCC*

### 4.2.3 Segregation index (SI)

The sieve stability test was adopted to investigate the segregation resistance with respect to segregation index. The segregation index varied from 9% to 12% for mixtures with the W/B ratio of 0.35. On the other hand, the segregation index was between 3% and 7.8% for mixtures with

the W/B ratio of 0.4. The effect of carbon fibers on segregation index is presented in Figure 4.10. All CFRSCC mixtures had their segregation index below the maximum limit of 18% reported by Perez et al. (2002). Mixture M1 had the highest segregation index (12%) whereas mixture M3 had the lowest segregation index (9%) among the mixtures produced with the W/B ratio of 0.35. Moreover, mixture M7 had the highest segregation index (7.8%) and mixture M9 had the lowest segregation index (3%) among the mixtures produced with the W/B ratio of 0.40 as can be seen from Figure 4.10.

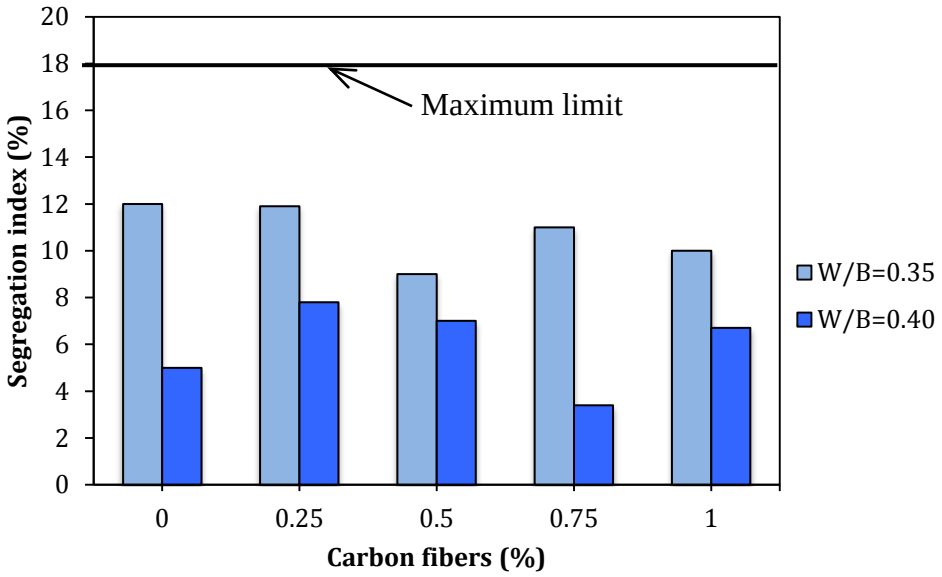


*Figure 4.10 Effect of carbon fibers content on the segregation index of CFRSCC*

In general, the segregation index decreased when the carbon fibers content increased. This is because the increased volume of carbon fibers decreased the fluidity of the concrete mixture. SCC is more prone to segregation due to higher fluidity (EFNARC 2002). This segregation tendency is reduced in the presence of fibers (EFNARC 2002). Thus, the increased volume of carbon fibers greatly decreased the segregation in CFRSCC mixture. Nevertheless, it should be

mentioned that HRWR also affected the segregation index of concretes produced in the present study. HRWR significantly improves the flowing ability of CFRSCC by enhancing its fluidity, which affects the segregation index. For example, M4 and M5 required a very high dosage of HRWR, which is 6.7% and 8%, respectively. These high dosages of HRWR increased the segregation index for these two mixtures. Therefore, the effect of carbon fibers in reducing segregation index was counter balanced in these two cases in the presence of a higher HRWR dosage.

### 4.2.4 Visual stability

Visual stability index (VSI) of CFRSCC mixtures was obtained from the slump flow test. The photos of slump flow patty for all concrete mixtures are shown in Figures 4.11 to 4.15. The concrete mixtures were in the highly stable state (VSI = 0) to stable state (VSI = 1). As it can be seen from Figure 11, mixtures M1 and M6 were homogenous and showed no evidence of segregation or bleeding; hence, they were highly stable (VSI = 0). Similarly, mixture M5 was highly stable (VSI = 0), as shown in Figure 15. Also, it can be seen from Figure 12 that mixture M2 showed very slight bleeding and mixture M7 showed negligible coarse aggregate concentration at the middle of the flow; therefore, they were designated as the moderately stable concrete mixtures (VSI = 0.5). Mixtures M8 and M4 were moderately stable with no evidence of bleeding but with negligible coarse aggregate concentration or a very small mortar halo (VSI = 0.5) whereas mixtures M3, M9, and M10 were stable with slight bleeding as sheen on the surface and a small mortar halo (VSI = 1), as shown in Figures 13 to 15. In summary, the observation of the photos of slump flow patty revealed that all mixtures passed the VSI requirements of SCC.


*a) Mix M1: VSI = 0 (highly stable); no evidence of bleeding, mortar halo, and aggregate piling.*


*b) Mix M6: VSI = 0 (highly stable); negligible coarse aggregate concentration at the middle of the flow patty but no evidence of bleeding and mortar halo.*

*Figure 4.11 Visual stability index (VSI) of M1 and M6 concrete mixtures*


*a) Mix M2: VSI = 0.5 (moderately stable); very slight bleeding and a very small mortar halo < 5 mm.*


*b) Mix M7: VSI = 0.5 (moderately stable); negligible coarse aggregate concentration at the middle of the flow patty and a very small mortar halo < 5 mm.*

*Figure 4.12 Visual stability index (VSI) for M2 and M7 mixtures*


*a) Mix M3: VSI = 1 (stable); concrete shows slight bleeding as a sheen on the surface and a small mortar halo < 10 mm.*


*b) Mix M8: VSI = 0.5 (moderately stable); no evidence of bleeding and mortar halo mortar but negligible coarse aggregate concentration at the middle of the flow patty.*

*Figure 4.13 Visual stability index (VSI) for M3 and M8 mixtures*


*a) Mix M4: VSI = 0.5 (moderately stable); no evidence of bleeding but negligible coarse aggregate concentration at the middle of the flow patty and a very small mortar halo < 5 mm.*


*b) Mix M9: VSI = 0.5 (moderately stable); concrete shows very slight bleeding as a sheen on the surface and a very small mortar halo < 5 mm.*

*Figure 4.14 Visual stability index (VSI) for M4 and M9 mixtures*


*a) Mix M5: VSI = 0 (highly stable); no evidence of bleeding, mortar halo, and aggregate piling.*


*b) Mix M10: VSI = 1 (stable); concrete shows very slight bleeding as a sheen on the surface and a very small mortar halo < 10 mm.*

*Figure 4.15 Visual stability index (VSI) for M5 and M10 mixtures*

### 4.2.5 Air content and unit weight

The air content of the CFRSCC mixtures was 1.4 to 3.5%, as shown in Figure 4.16. The concrete mixtures were designed to be non-air entrained with an entrapped air content of 2% [25]. The air content results indicate that carbon fibers did not cause any significant air entrapment. This is attributed to the high flowing ability of the concrete. However, the overall entrapped air content of the concretes produced with the W/B ratio of 0.35 was relatively low, as compared to the concretes fabricated with the W/B ratio of 0.40. This is because the concretes with the W/B ratio of 0.35 possessed a higher flowing ability, as can be seen from Figure 4.5. The increased flowing ability facilitated the release of entrapped air-voids from concrete.

The unit weights of the CFRSCC mixtures are shown Figure 4.17. The unit weight varied in the range of 2360 to 2460 kg/m$^3$. The unit weight decreased as the carbon fibers increased; the reason is that carbon fibers were the lightest component in the concrete mixtures.

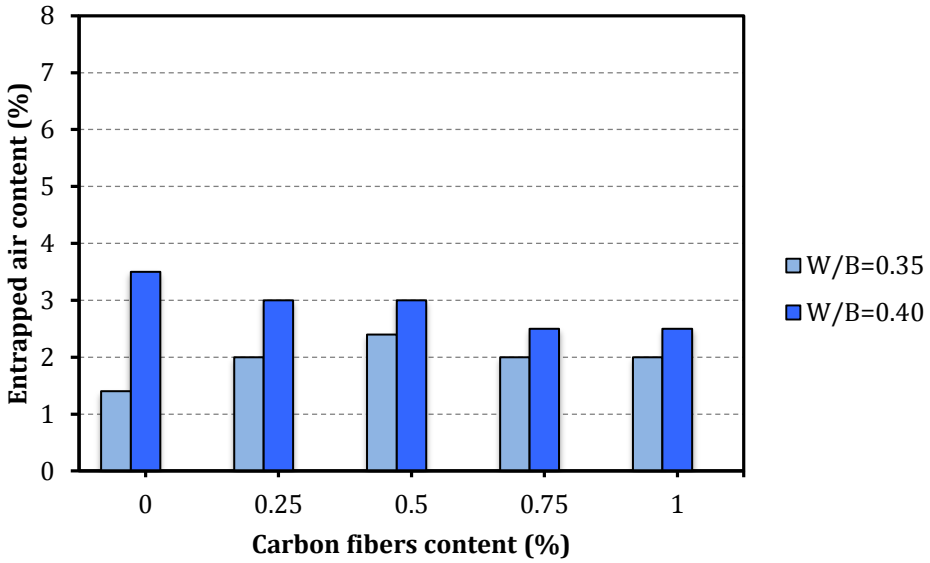


*Figure 4.16 Effect of carbon fibers content on the entrapped air content of CFRSCC*

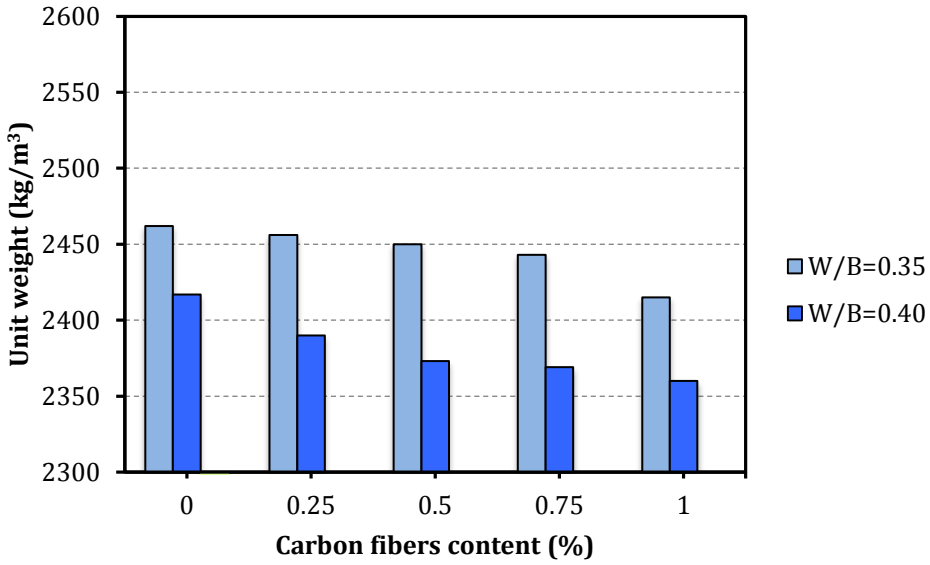


*Figure 4.17 Effect of carbon fibers content on the unit weight of CFRSCC*

## 4.3 Hardened properties of CFRSCC mixtures

Compressive strength, tensile strength, and flexural strength were evaluated in this research study. The following sections present the test results.

### 4.3.1 Compressive strength results

The compressive strength test results for the CFRSCC mixtures after 3, 7, 14, and 28 days are summarized in Figures 4.18 and 4.19. The compressive strength values are the average results of three cylinders (dimension 100 mm by 200 mm) and were tested in accordance with ASTM C39/C39M – 09a. As it can be seen from Figure 4.18, the compressive strength for all mixes with 0.35 W/B ratio decreased as the carbon fibers increased. This is because the carbon fibers replaced some of the coarse and fine aggregates. Mix M1 achieved a compressive strength of 95MPa after 28 days, which was the highest compressive strength value while mix M4 had a compressive strength of 60.2MPa after 28 days, which is the lowest compressive strength as it can be seen from Figure 4.18. Also, the compressive strength of all mixes with 0.40 W/B ratio decreased as the carbon fibers increased. The reason behind this reduction was the replacement between aggregates and carbon fibers. However, the higher W/B ratio led to a reduced compressive strength of all mixes at 28 days. The highest compressive strength was for mix M6 at 80MPa and the lowest compressive strength was for mix M9 at 39MPa.

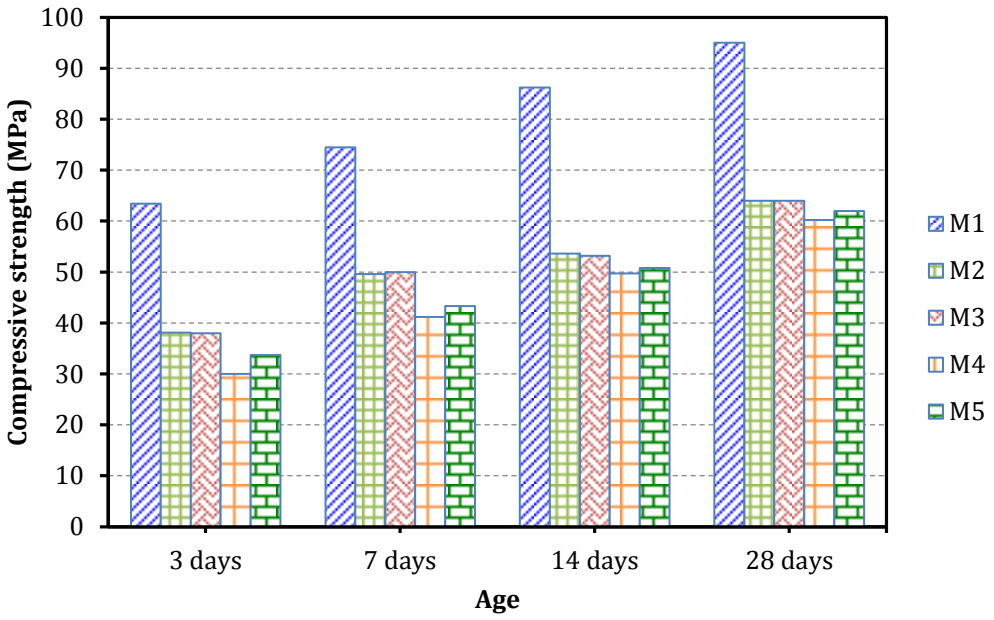


*Figure 4.18 Effect of carbon fiber content on the compressive strength for mixes with 0.35 W/B ratio*

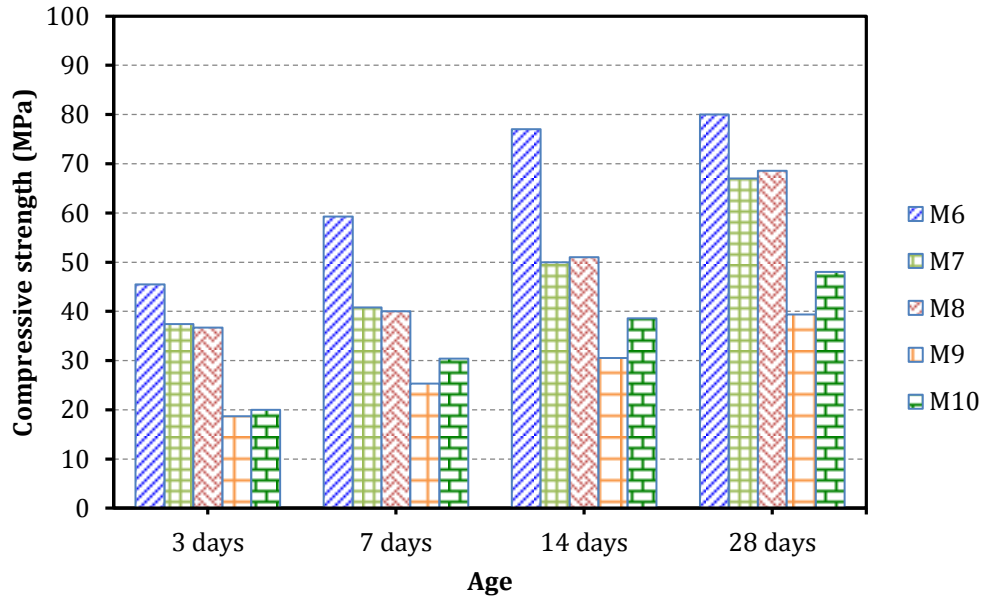


*Figure 4.19 Effect of carbon fiber content on the compressive strength for mixes with 0.40 W/B ratio*

#### 4.3.1.1 Effect of carbon fiber content on compressive strength

As can be seen from Figures 4.18 and 4.19 the compressive strength decreased as the carbon fiber content increased. The compressive strength dropped from 90MPa for mix M1 (0% fibers content) to 64MPa for mix M2 (0.25% fiber content). However, the compressive strength slightly decreased as the fiber content increased. For instance, mix M2 (0.25% fibers content) had a compressive strength of 64MPa while mix M5 (1% fibers content) had a compressive strength of 62MPa, which is a negligible reduction in compressive strength. It seems that for the lower W/B ratio of 0.35 the fiber content had no significant effect on the compressive strength as shown in Figure 4.18. On the other hand, for mixes M6 to M10, the fiber content had a significant effect on compressive strength as can be seen from Figure 4.19. The compressive strength decreased as the fibers content increased. The compressive strength for M6 (0% fibers content) was 80MPa while the compressive strength for mix M10 (1% fibers content) was 48MPa as it can be seen from Figure 4.19.

#### 4.3.1.2 Effect of water binder ratio (W/B) on compressive strength

W/B ratio significantly affected the compressive strength. It is clear from Figure 4.20 that as the W/B ratio decreased the compressive strength increased. The maximum compressive strength of mixes with W/B ratio of 0.35 with 0% fiber contnet was 95MPa while the maximum compressive strength of mixes W/B ratio of 0.40 with 0% fiber content was 80MPa. The compressive strength dropped by 15% as W/B ratio increased from 0.35 to 0.40. The compressive strength is related to the reduction in porosity of the concrete. The porosity of CFRSCC mixtures was reduced as the W/B ratio decreased. As evident from Figure 4.16 the entrapped air for mixes 1 to 5, which had a W/B ratio of 0.35 was lower than that for mixes M6

to M10, which had a W/B ratio of 0.40. At the lower W/B ratio, the cement content was lower as given in Table 3.2. As Safiuddin (2010) stated that the cement content enhanced the bundles of aggregates and increased the amount of calcium silicate hydrate (C–S–H) that led to a higher compressive strength.

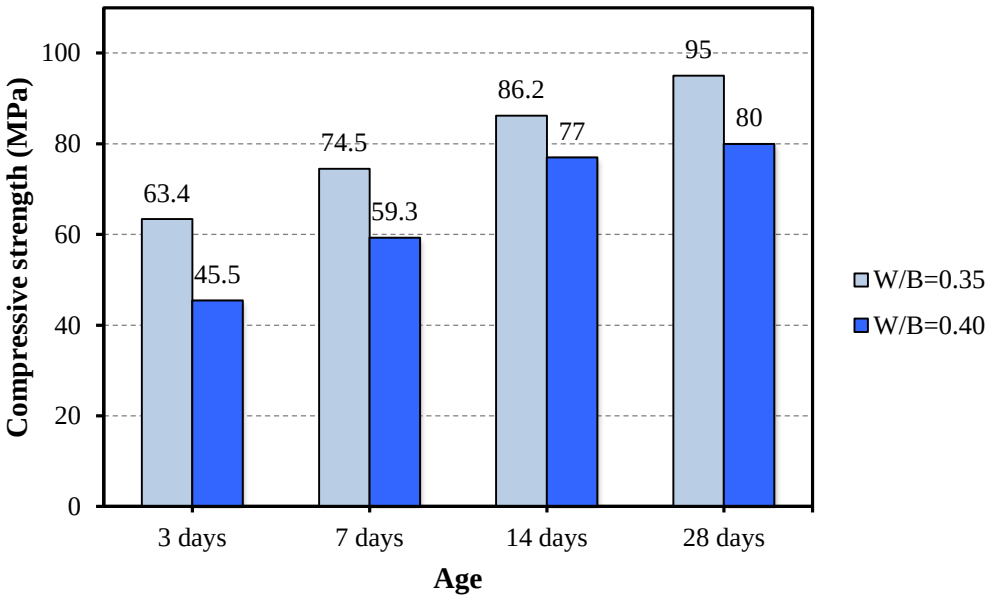


*Figure 4.20 Effect of water binder ratio (W/B) on compressive strength (0% fiber content)*

### 4.3.2 Splitting tensile strength results

The splitting tensile strength for the CFRSCC mixtures is presented in Figures 4.21 and 4.22. The splitting tensile strength was tested after 14 and 28 days in accordance with ASTM C496/C496M – 04 standard. The test procedure was explained in section 3.6.3. Figure 4.21 shows that the splitting tensile strength increased as the carbon fibers content increased for CFRSCC mixes with W/B = 0.35. Mix M1 (0% fibers content) had a tensile strength of 4.20MPa while Mix M5 (1% fibers content) had a tensile strength of 4.80MPa. The splitting tensile strength for mix M6 (0% fibers content) was 4.10MPa and the splitting tensile strength for mix

M10 (1% fibers content) was 4.70MPa as presented in Figure 4.22 for CFRSCC mixes with W/B = 0.40. The splitting tensile strength increased up to about 12% at 1% of carbon fibers content.

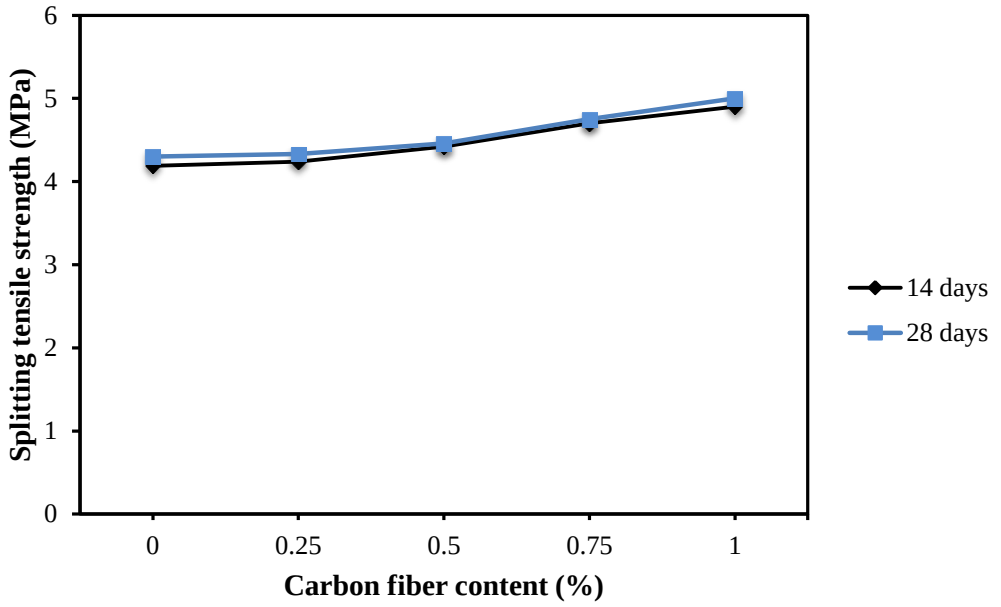


*Figure 4.21 Effect of carbon fibers content on the splitting tensile strength for mixes with 0.35 W/B ratio*

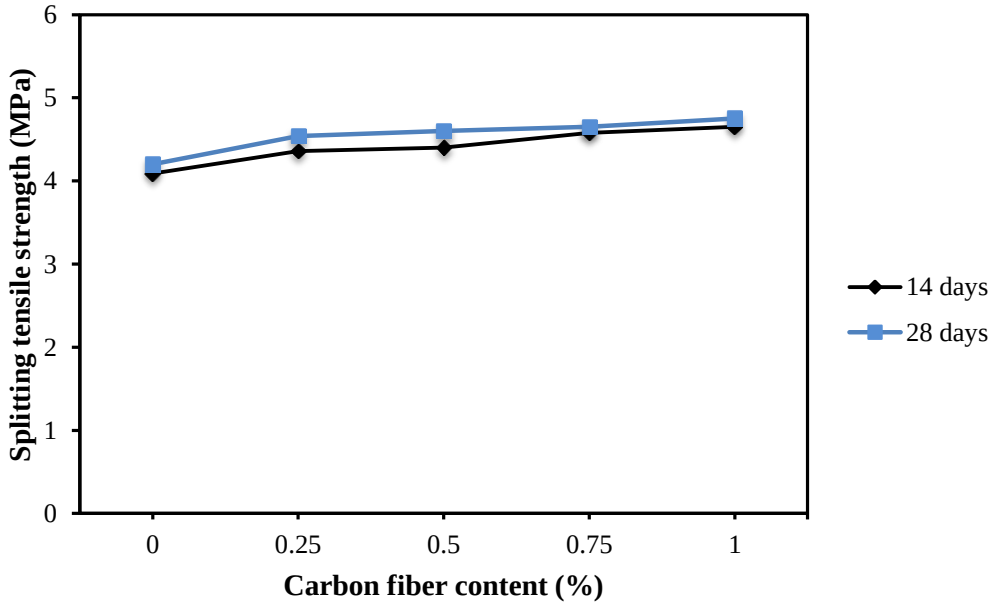


*Figure 4.22 Effect of carbon fibers content on the splitting tensile strength for mixes with 0.40 W/B ratio*

#### 4.3.2.1 Effect of carbon fiber content on splitting tensile strength

Figures 4.21 and Figure 4.22 show the effect of carbon fibers on the splitting tensile strength. It can be seen from Figures 4.21 and 4.22 that as the carbon fibers increased the splitting tensile strength increased. For example, the splitting tensile strength for mixes M1, M2, and M5 was 4.40MPa, 4.45MPa, and 4.80MPa, respectively. It is discussed that increase in splitting tensile strength was because the percentage of carbon fibers reduced the crack growing and led to higher failure loads. Once the load was applied, the cracks started to appear and the concrete cylinder started to split in two parts. The fibers created a bridge through the split portions of the cylinder and delayed the splitting of the two parts. The stresses were transferred from the concrete to the fibers through the fiber bridging.

#### 4.3.2.2 Effect of water binder ratio (W/B) on splitting tensile strength

W/B ratio had no significant effect on the splitting tensile strength as shown in Figure 4.23. The splitting tensile strength for mix M1 (0% fibers content) was 4.30MPa while the splitting tensile strength for mix M6 (0% fibers content) was 4.20MPa. Also, the splitting tensile strength for mix M5 (1% fibers content) was 4.80MPa while the splitting tensile strength for mix M10 (1% fibers content) was 4.70MPa. The differences in tensile strength between the mixes with W/B ratio = 0.35 and the mixes with W/B ratio = 0.40 was between 0.20 and 0.10MPa. It is clear from Figure 4.23 that the W/B ratio did not significantly affect the splitting tensile strength of CFRSCC mixes. Since the splitting tensile strength is related to compressive strength; as the W/B ratio increased the splitting tensile strength decreased.

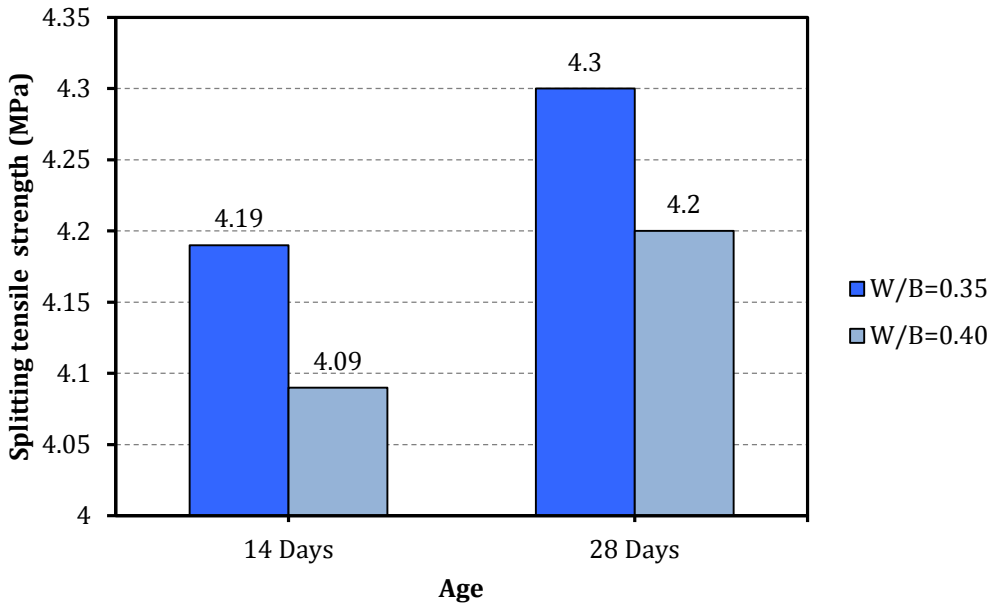


*Figure 4.23 Effect of water binder ratio (W/B) on splitting tensile strength*

### 4.3.3 Modulus of rupture

The flexural strength test (modulus of rupture) results for prisms made from the CFRSCC mixtures are summarized in Figure 4.24 and Figure 4.25. As it can be seen from Figure 4.24, the modulus of rupture for all mixes with 0.35 W/B ratio ranged between 7.60MPa and 8.05MPa. Mix M5 (1% fibers content) had the highest modulus of rupture, while mix M3 (0.5% fibers content) had the lowest modulus of rupture. Carbon fibers increased the modulus of rupture of the CFRSCC mixtures because they were able to reduce the crack opening. The number of fibers that crossed the crack or failure surface also affected the modulus of rupture. However, for CFRSCC mixes with 0.40 W/B ratio, the modulus of rupture ranged between 6.68MPa and 8.40MPa as it can be seen from Figure 4.25. Mix M7 (0.25% fibers content) had the highest modulus of rupture, while mix M8 (0.5% fibers content) had the lowest modulus of rupture. It is evident that a carbon fiber content of 0.25% or 0.75% gave the optimum modulus of rupture for

the CFRSCC mixtures with W/B = 0.35 and 0.40. These results are unexpected results; thus, more specimens and tests are required to justify the results. No trend is absorbed from the test results.

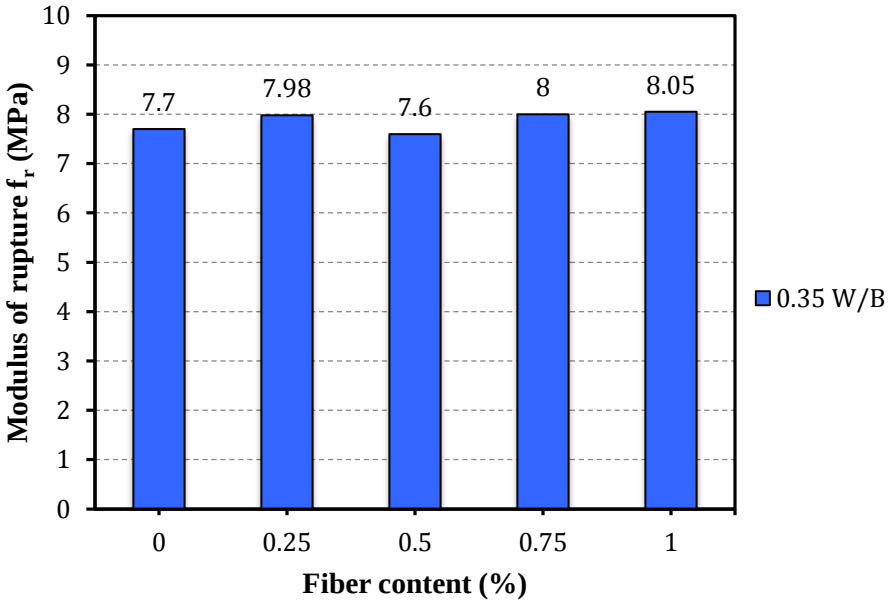


*Figure 4.24 Modulus of rupture for CFRSCC mixtures with 0.35 W/B ratio*

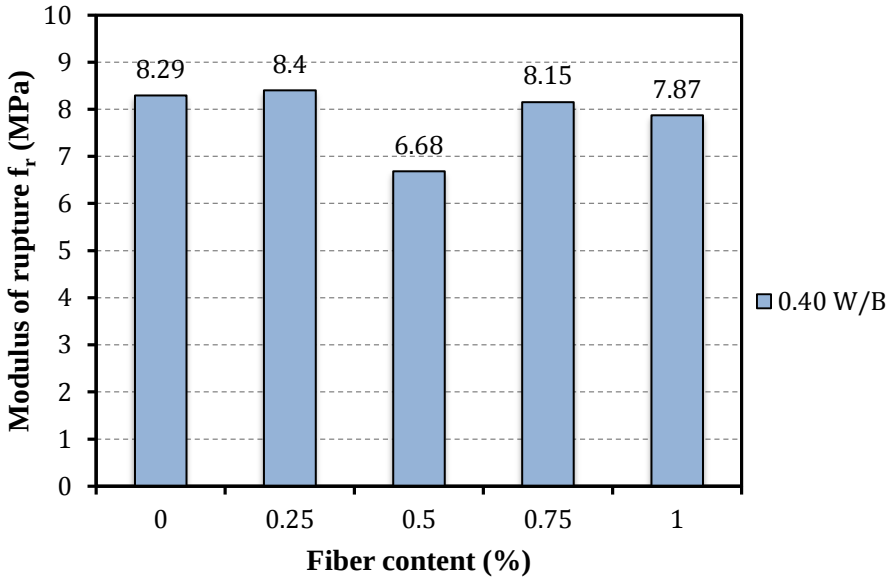


*Figure 4.25 Modulus of rupture of CFRSCC mixtures with 0.40 W/B ratio*

### 4.3.4 Load deflection response of CFRSCC mixtures

Figure 4.26 and Figure 4.27 show the load deflection response for each fracture toughness specimen. The deflection data were calculated from the average of two LVDTs. The load deflection curves consisted of a linear curve up to the peak load and then the curve dropped gradually until the load reached zero. Mix M1 (0% fibers content) had a brittle post-peak response with maximum mid-span deflection less than 0.4 mm. Mixes M2 to M5 had a slightly better post-peak response with maximum mid-span deflection less than 0.7 mm. However, the post-peak response for each mixture with 0.40 W/B ratio was identical with maximum mid-span deflection of 0.7mm. Most of the mixes did not reach a deflection of 1/150 in accordance to ASTM C1609 possibly because of the short fibers used. The displacement at the peak load was identical with mid-span deflections of 0.06mm for all mixes with 0.35 and 0.40 W/B ratio.

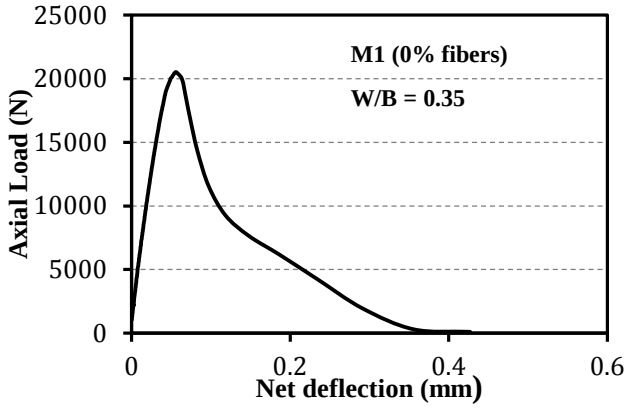


*a) Load vs. net deflection of Mix M1*

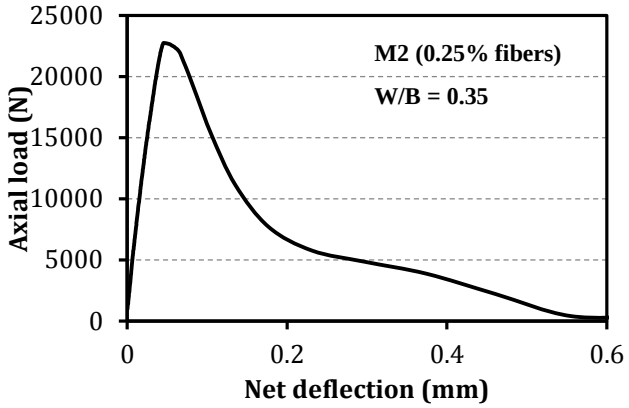


*b) Load vs. deflection of Mix M2*

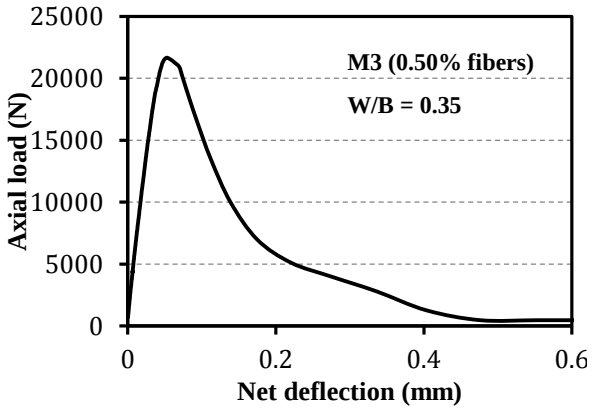


*c) Load vs. net deflection of Mix M3*

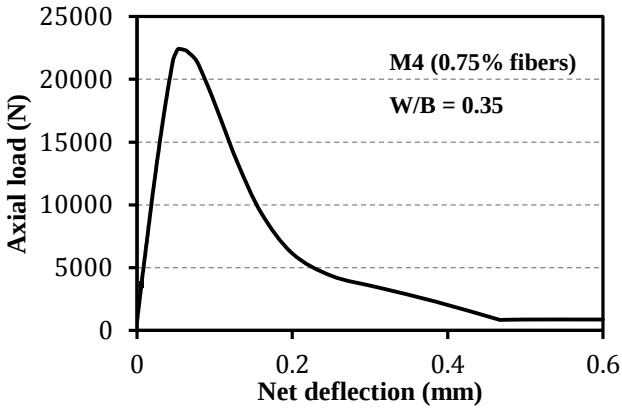


*d) Load vs. net deflection of mix M4*

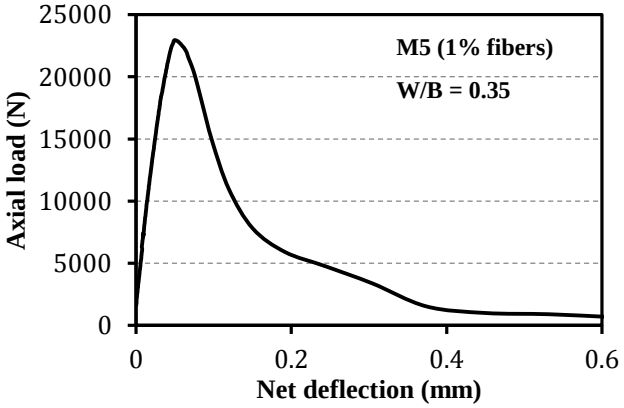


*e) Load vs. net deflection of Mix M5*

*Figure 4.26 Load vs. deflection of concrete mixtures of 0.35 W/B ratio*

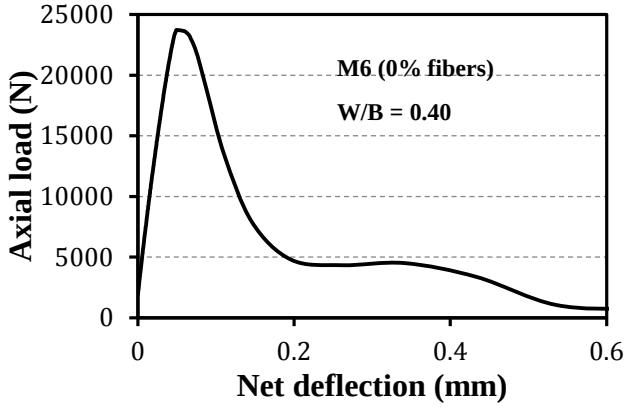


*a) Load vs. net deflection of Mix M6*

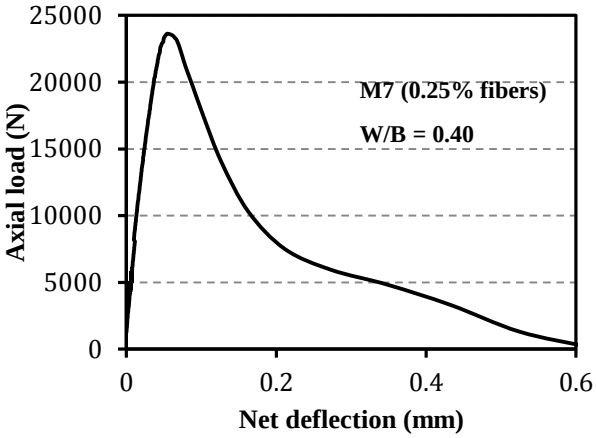


*b) Load vs. net deflection of Mix M7*

*c)*

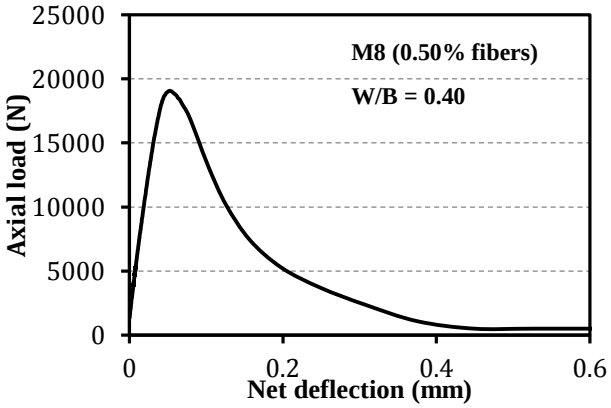


*Load vs. net deflection of mix M8*

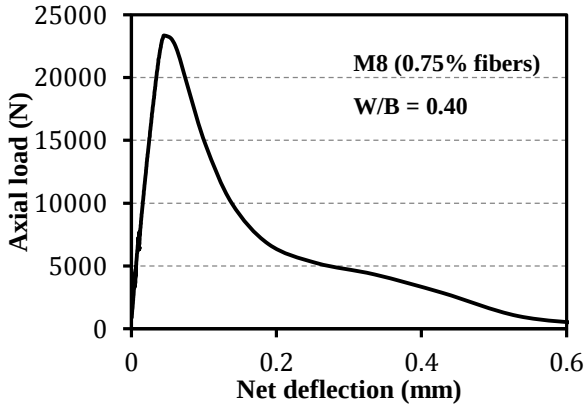


*d) Load vs. net deflection of M9*

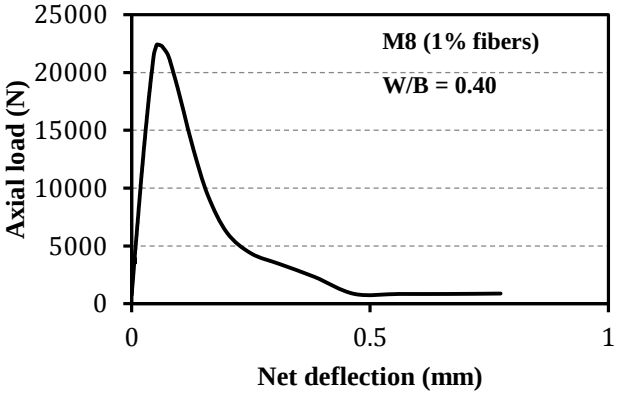


*e) Load vs. net deflection of Mix M10*

*Figure 4.27 Load vs. deflection of concrete mixtures of 0.40 W/B ratio*

### 4.3.5 Toughness (fracture energy) and the effect of carbon fibers

Figure 4.28 and Figure 4.29 show the toughness for each CFRSCC mixture. The toughness is calculated as the area under the load-deflection curves presented in section 4.3.4. The toughness of mixes with 0.35 W/B ratio ranged between 3895 N-mm and 2475 N-mm. The carbon fibers increased the toughness of fracture energy. The carbon fibers helped the concrete mixtures to absorb more energy as it can be seen from Figure 4.28 and as such mixes with carbon fibers had improved toughness. Mix M2 (0.25% fibers content) had the highest toughness of 3895 N-mm, while mix M1 (0%fibers content) had the lowest toughness of 2475 N-mm. Mixes M3 to M5 with carbon fiber content of 0.5% to 1% had similar toughness regardless of the fiber content. The toughness achieved by these mixes was 31% higher than the control mix (with no fibers), but 20% lower than the mix with 0.25% fibers. These results suggest that the optimum fiber content has been reached.

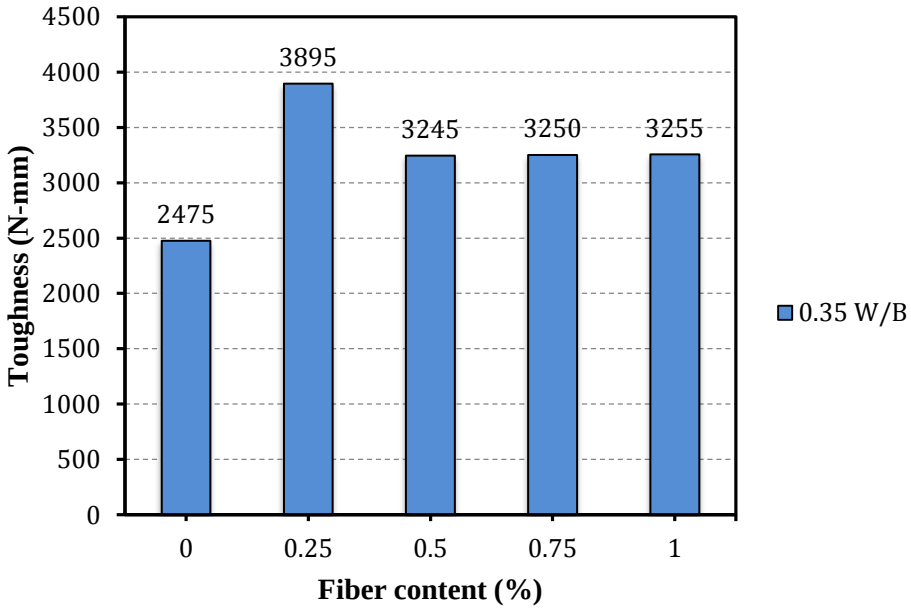


*Figure 4.28 Toughness of mixtures with 0.35 W/B ratio*

The toughness values for CFRSCC mixes with 0.40 W/B ratio ranged between 3670 N-mm and 2710 N-mm as seen from Figure 4.29. However, an opposite trend was observed in comparison to mixes with W/B of 0.35. Mix M6 (0% fibers content) had the highest toughness, while mix M10 (1%fibers content) had the lowest toughness. It was very hard to achieve the fresh properties of mix M10; thus, the toughness was affected. However, mix M9 (0.75% fiber content) had 3400 N-mm. This value was close to the toughness value of mix M6. Therefore, at higher W/B ratios 0f 0.40, the presence of carbon fibers did not improve the toughness of the CFRSCC mixtures.

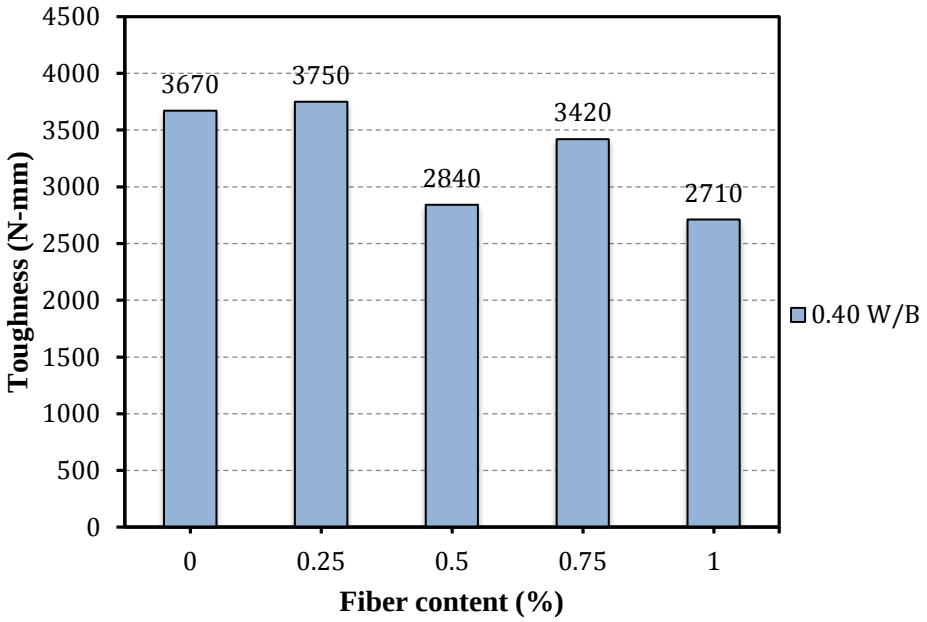


*Figure 4.29 Toughness of mixtures with 0.40 W/B ratio*

### 4.3.6 Scanning electron microscope (SEM)

The scanning electron micrographs (SEMs) of the fracture surface for the different CFRSCC fracture energy specimens are shown in Figures 4.30 to 4.34. In these figures, the magnification used was mostly ×100. Figures 4.30 to 4.34 show the fracture surface of each CFRSCC mixture. The micrographs exhibited that the carbon fibres were well distributed in each concrete mixture.

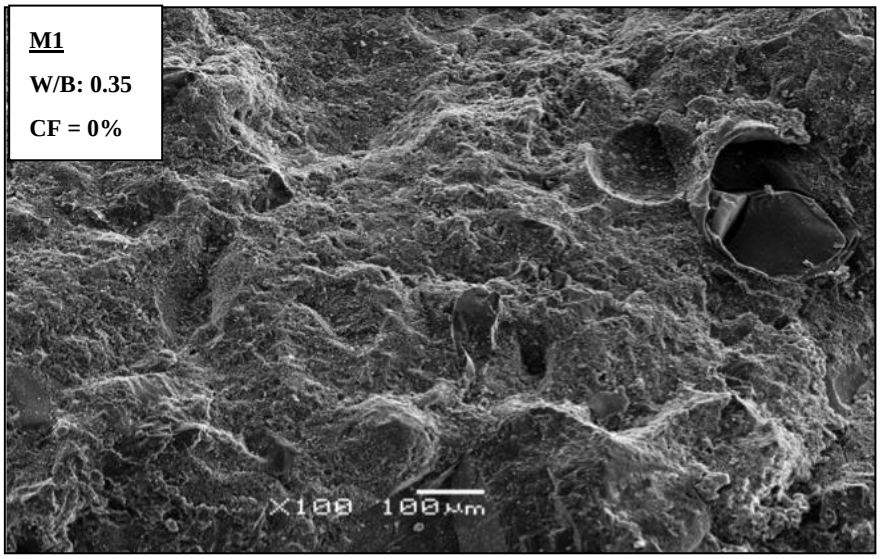


*a) Mix M1: SEM of fracture surface shows no fibers.*

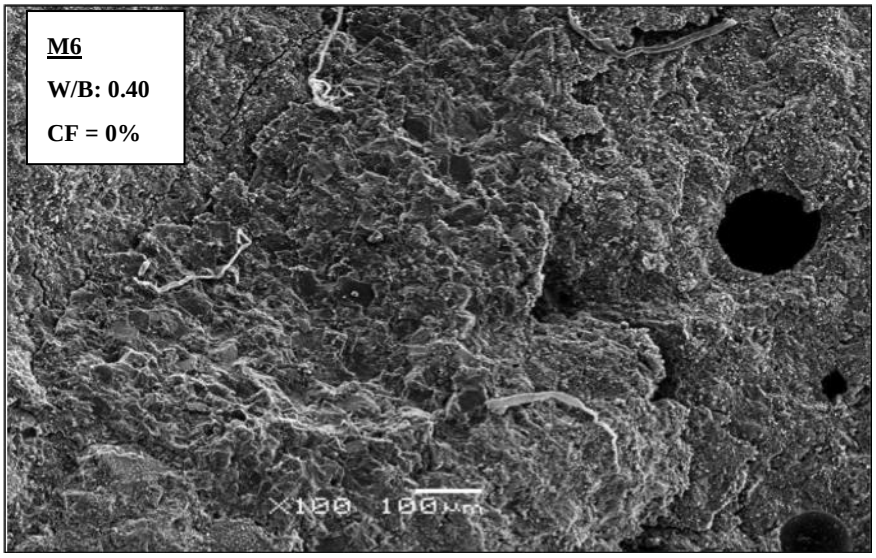


*b) Mix M6: SEM of fracture surface shows no fibers.*

*Figure 4.30 Scanning electron micrographs of M1 and M6 mixtures*

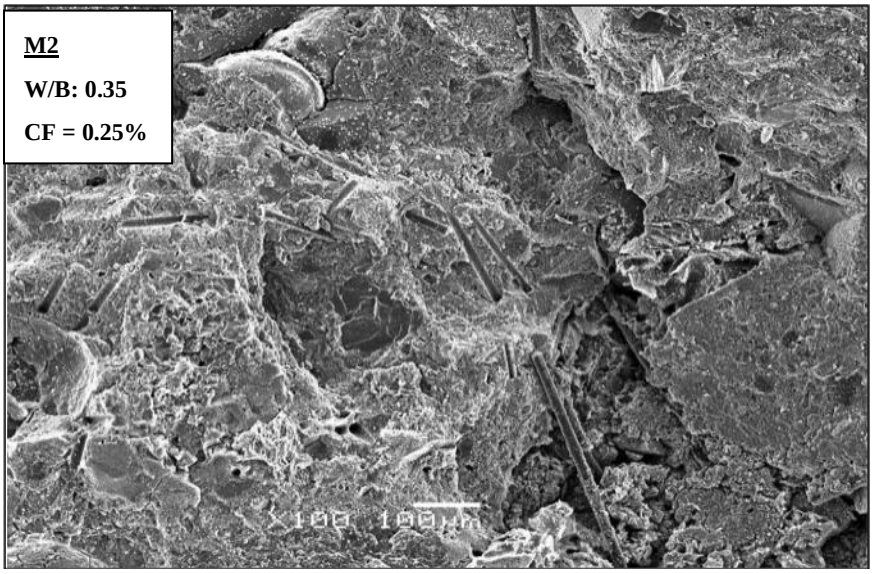


*a) Mix M2: SEM of fracture surface shows good distributed fibers.*

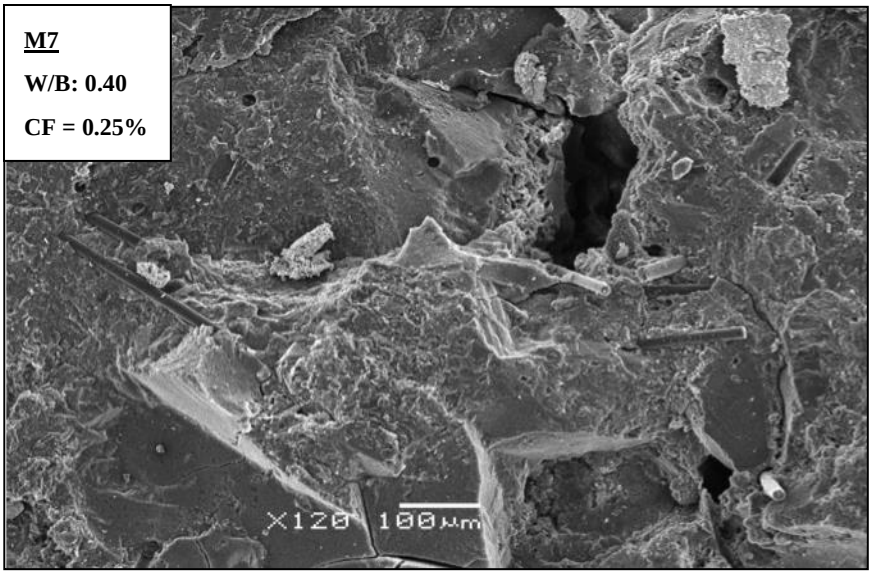


*b) Mix M7: SEM of fracture surface shows good distributed fibers.*

*Figure 4.31 Scanning electron micrographs of M2 and M7 mixtures*

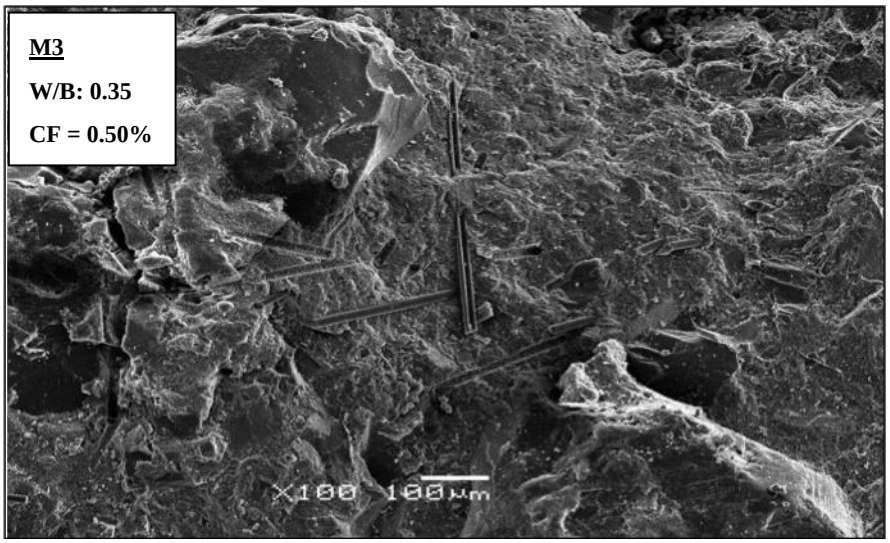


*a) Mix M3: SEM of fracture surface shows good distributed fibers.*

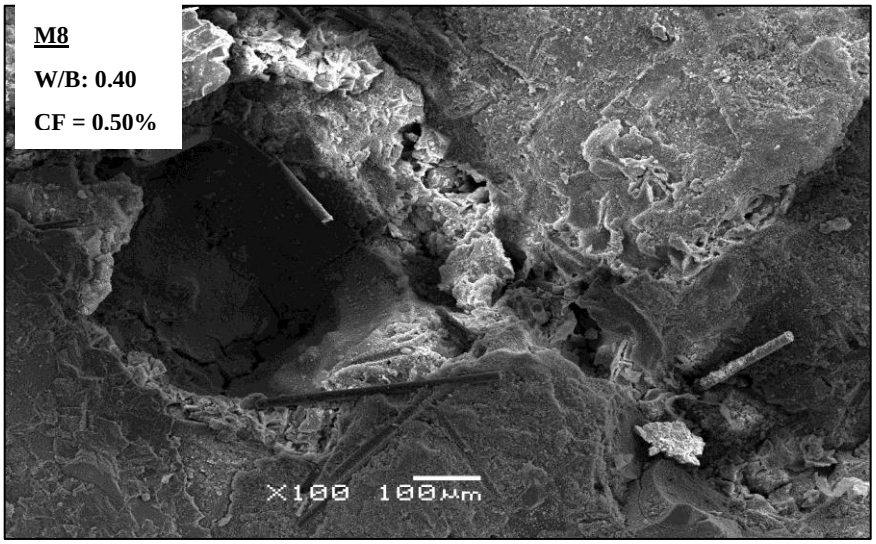


*a) Mix M8: SEM of fracture surface shows good distributed fibers.*

*Figure 4.32 Scanning electron micrographs of M3 and M8 mixtures*

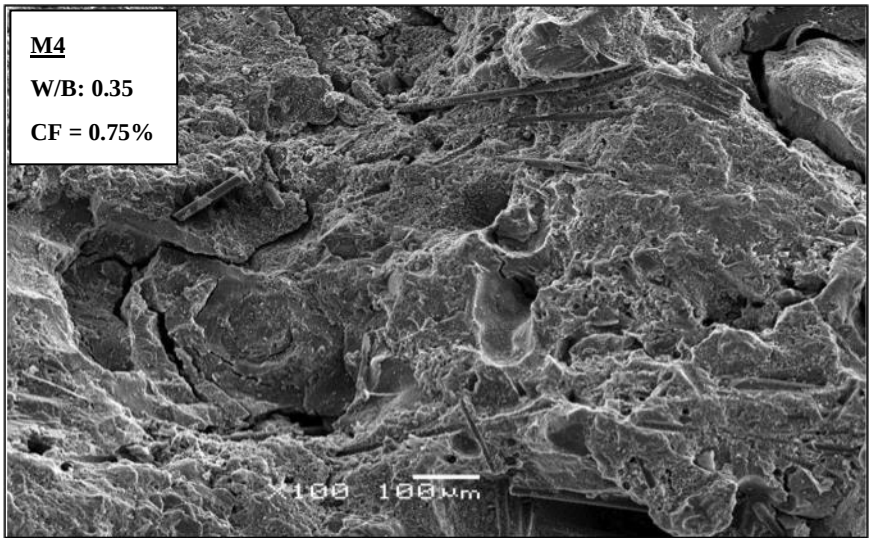


*a) Mix M4: SEM of fracture surface shows good distributed fibers.*

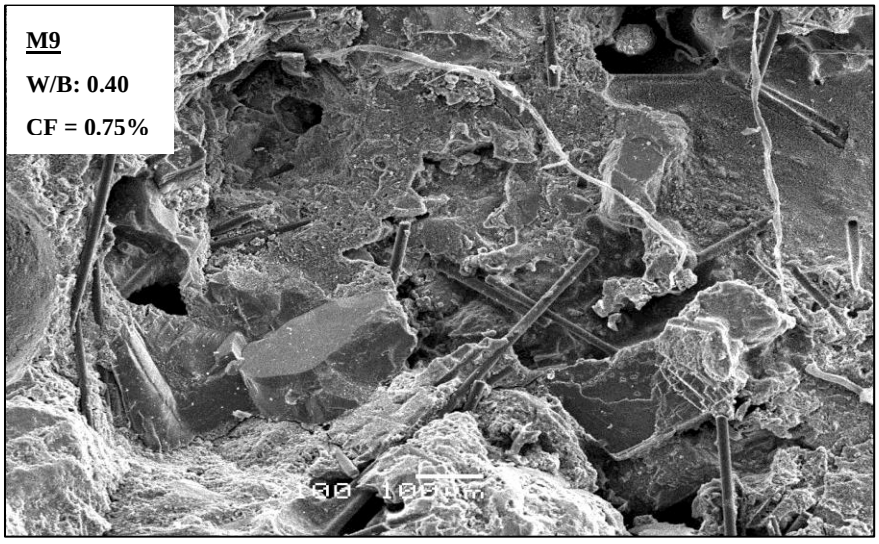


*b) Mix M9: SEM of fracture surface shows good distributed fibers.*

*Figure 4.33 Scanning electron micrographs of M4 and M9 mixtures*

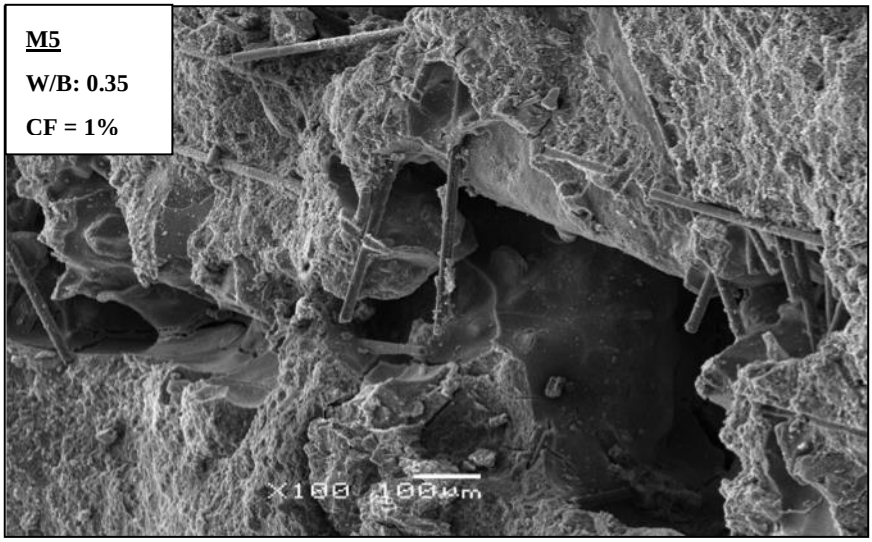


*a) Mix M5: SEM of fracture surface shows good distributed fibers.*

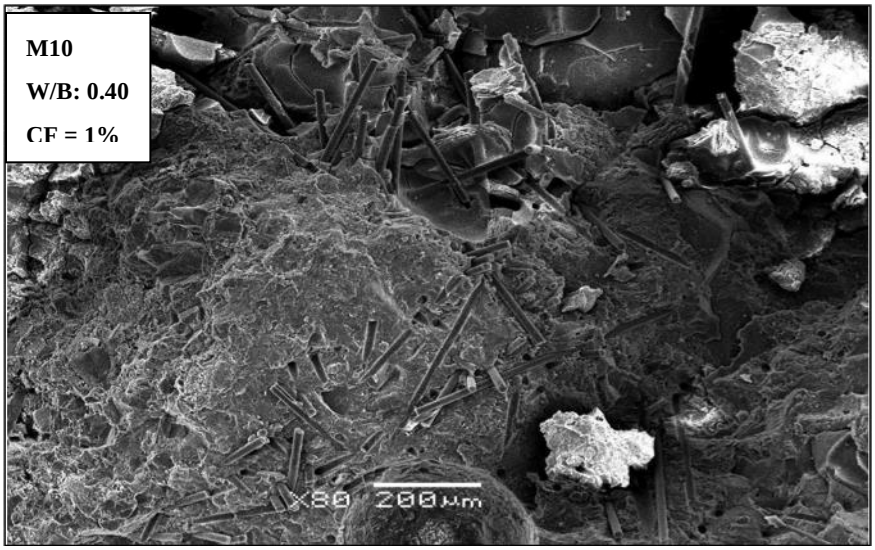


*b) Mix M10: SEM of fracture surface shows good distributed fibers.*

*Figure 4.34 Scanning electron micrographs of M5 and M10 mixtures*

# Chapter 5 Structural Performance of CFRSCC Patch Repaired Beams

## 5.1 General

Eleven RC beams were tested to investigate three different repair configurations: a flexural-top patch, a flexural bottom patch and a shear span patch. Three different repair patch materials were used. The flexural beams were divided into three groups: the first group had one control beam; the second group had three beams that were repaired in the compression zone (top patch); and the third group had three beams that were repaired in the tension zone (bottom patch). The shear beams had one control beam and three repaired beams that were repaired using three different patch materials in one shear span. This chapter will present the observed behaviour, failure mode and load-deflection responses for the different repaired beams.

## 5.2 Effect of repair material on structural performance of flexural beams

Table 5.1 summarizes the critical stages of the flexural beam results. The individual beam load-deflection response in terms of the strain in longitudinal reinforcement and strain in top concrete are shown in Appendix B. The following sections will present and discuss the observed behaviour, load-deflection behaviour, load-strain behaviour, flexural stiffness, yield load, ultimate load and ductility for the patch-repaired flexural beams.

**Table 5.1 Summary of flexural test results**

| Beam designation | | Cracking | | Yielding | | Ultimate | | Mode of failure |
|---|---|---|---|---|---|---|---|---|
| | | $P_{cr}$ | $\Delta_{cr}$ | $P_y$ | $\Delta_y$ | $P_u$ | $\Delta_u$ | |
| | | kN | mm | kN | mm | kN | mm | |
| Flexural control | | 23 | 2 | 102 | 8 | 122 | 28 | Concrete crushing |
| Flexural top patch | Sikacrete-08 SCC | 23 | 2 | 100 | 10 | 130 | 58 | Concrete crushing |
| | Mix M1 | 23 | 2 | 103 | 8 | 122 | 43 | Concrete crushing |
| | Mix M3 | 30 | 2 | 109 | 8 | 130 | 39 | Concrete crushing |
| Flexural bottom patch | Sikacrete-08 SCC | 23 | 2 | 102 | 9 | 121 | 26 | Concrete crushing |
| | Mix M1 | 35 | 2 | 103 | 8 | 120 | 34 | Concrete crushing |
| | Mix M3 | 45 | 2 | 100 | 8 | 115 | 26 | Concrete crushing |

### 5.2.1 Observed flexural behaviour

#### 5.2.1.1 Control beam

The beam was loaded at rate of 1.2mm/min and crack formation was monitored. The first cracks that appeared were flexural cracks and were located randomly within the constant moment region at a load of 23kN. As the load increased, the shear cracks started to appear between the point loading and the support, meanwhile the flexural cracks started to become wider and extended to the compression zone. As the load continued to increase, the flexural and shear cracks increased. When the load reached 122kN, which is the ultimate load, the cracks at the compression zone developed and the concrete crushed. The failure mode of the beam was by concrete crushing in the compression zone as shown in Figure 5.1.

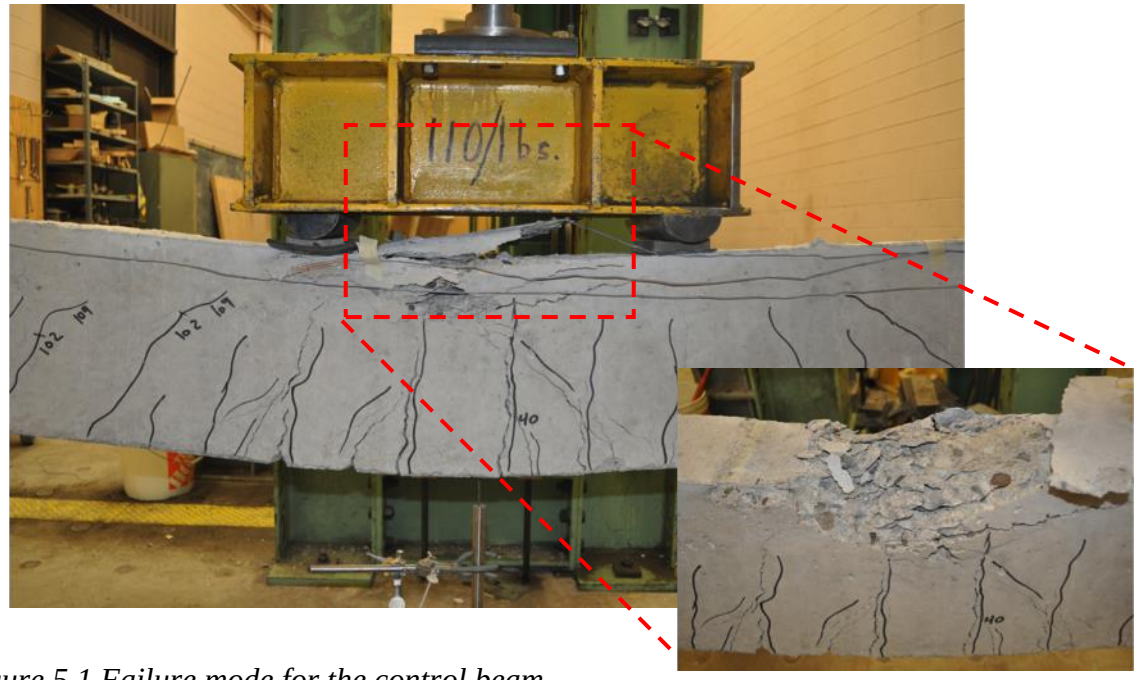


*Figure 5.1 Failure mode for the control beam*

#### 5.2.1.2 Beams repaired in tension zone

Figures 5.2 to 5.4 show the observed flexural cracks, shear cracks, and the failure mode in the bottom-patch repaired beams in tension zone. The first cracks that appeared were the flexural cracks within the constant moment region at loads of 23kN, 23kN and 30kN for bottom-patch repaired beams with Sikacrete-08 SCC, mix M1 (SCC, no fibers), and mix M3 (CFRSCC, 0.50% fibers), respectively. Beyond the cracking load, the shear cracks started to appear between the point loading and the support, meanwhile the flexural cracks became wider and extended to the compression zone. As the load continued to increase, the flexural and shear cracks increased. For the beams that were repaired with Sikacrete-08 SCC and mix M1, the cracks propagated in the repair material itself and between the old concrete and the repair material at the bond line, but for the beam that was repaired with mix M3 (CFRSCC, 0.5% fibers) the cracks did not appear between the old concrete and the repair material. The beams failed when the load reached

121kN, 120kN, and 115kN for the repaired beams with Sikacrete-08 SCC, mix M1, and mix M3, respectively. The concrete in the compression zone was crushed and the beams failed.

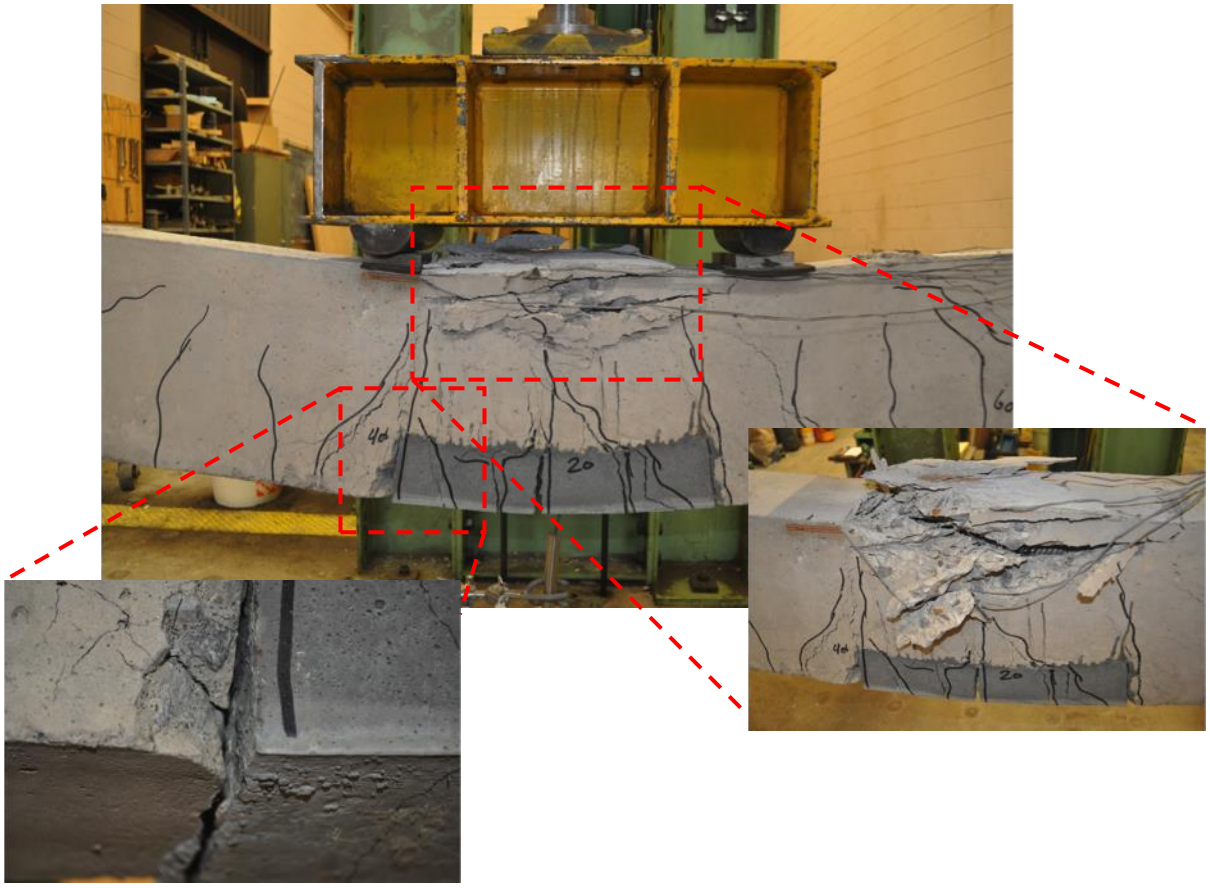

*Figure 5.2 Failure mode for the bottom-patch repaired beam with Sikacrete-08SCC*

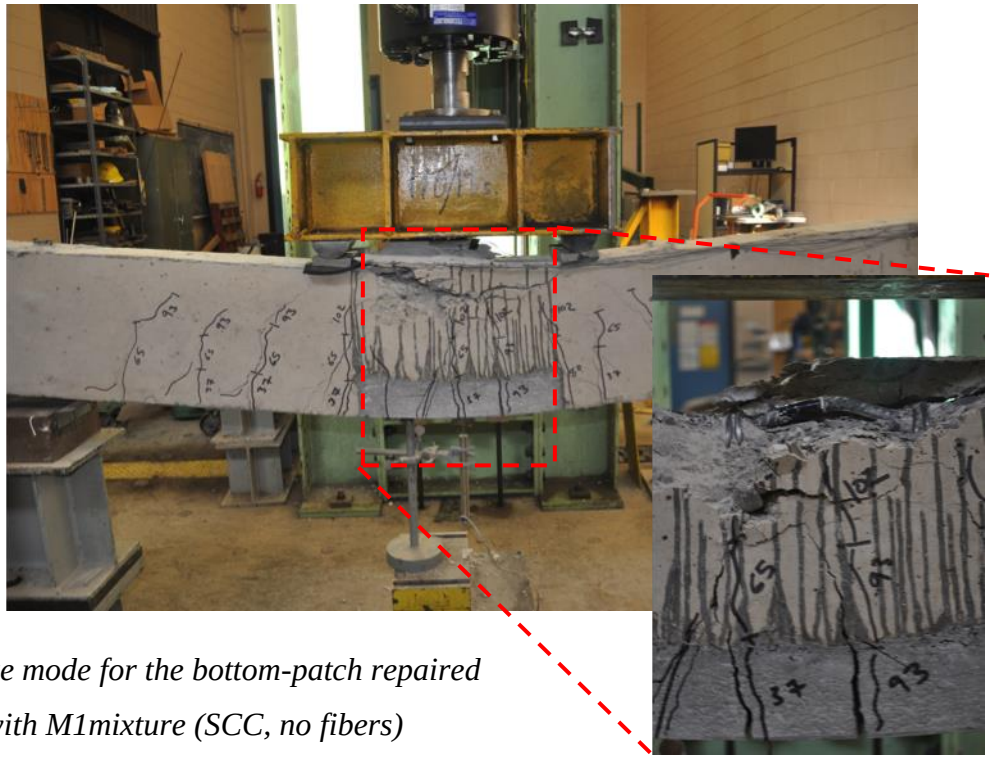

*Figure 5.3 Failure mode for the bottom-patch repaired beam with M1mixture (SCC, no fibers)*

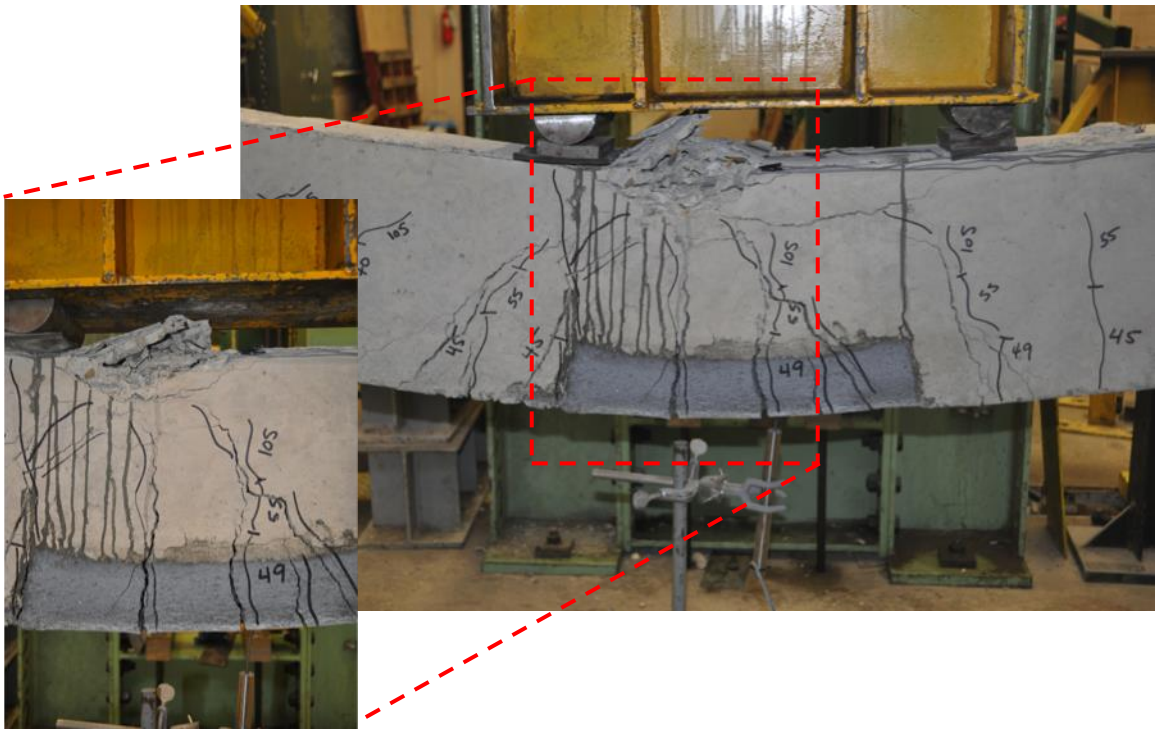

*Figure 5.4 Failure mode for the bottom-patch repaired beam with M3 mixture (CFRSCC, 0.50% fibers)*

#### 5.2.1.3 Beams repaired in compression zone

Figures 5.5 to 5.7 show the observed flexural cracks, shear cracks, and the failure mode in the top-patch repaired beams in the compression zone. Flexural cracks appeared first within the constant moment region at loads of 23kN, 35kN, and 45kN for the top-patch repaired beams with Sikacrete-08 SCC, mix M1 (SCC, 0 fibers), and mix M3 (CFRSCC, 0.50% fibers), respectively. Then as loading increased, the shear cracks started to appear between the point loading and the supports, meanwhile the flexural cracks started to become wider and extended to the compression zone. As the load continued to increase, the flexural and shear cracks increased. For the beams that were repaired with Sikacrete-08 SCC and mix M1, a big diagonal crack appeared and extended from the tension zone towards the compression zone as shown in Figures 5.5 and 5.6. The beams failed when the load reached 130kN, 122kN, and 130kN for the repaired beams with Sikacrete-08 SCC, mix M1, and mix M3, respectively. In all cases, the old concrete crushed under the point loading and Sikacrete-08 SCC and mix M1 did not crush. Sikacrete-08 SCC and mix M1 with stood more load and the stresses at these materials were higher than that of the old concrete. However, the repaired beam with M3 showed no difference from the control (unrepaired) beam as shown in Figure 5.7. The failure mode of the beams was concrete crushing in the compression zone.

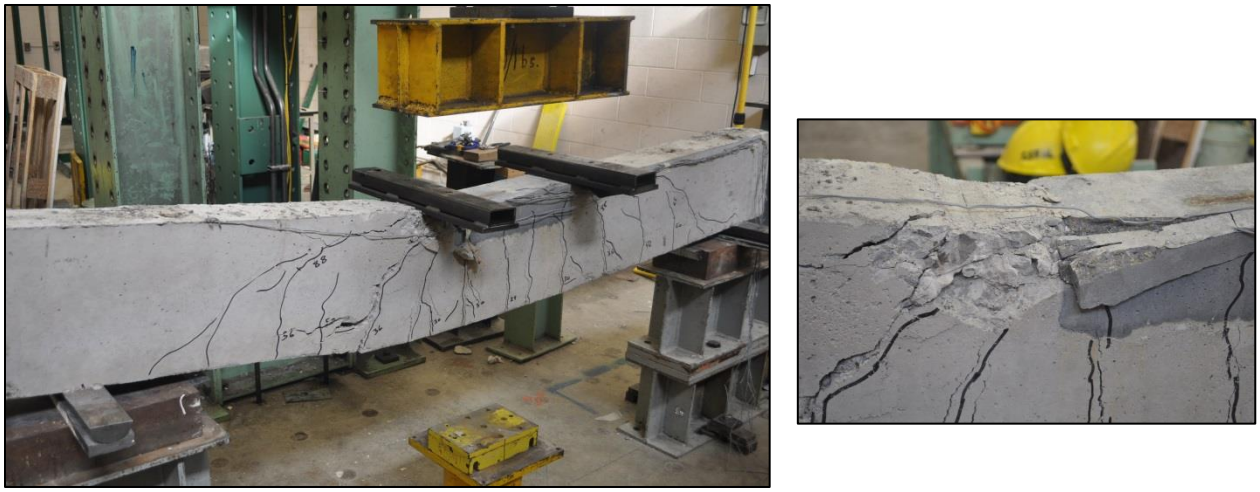

*Figure 5.5 Failure mode for the top-patch repaired beam with Sikacrete-08 SCC*

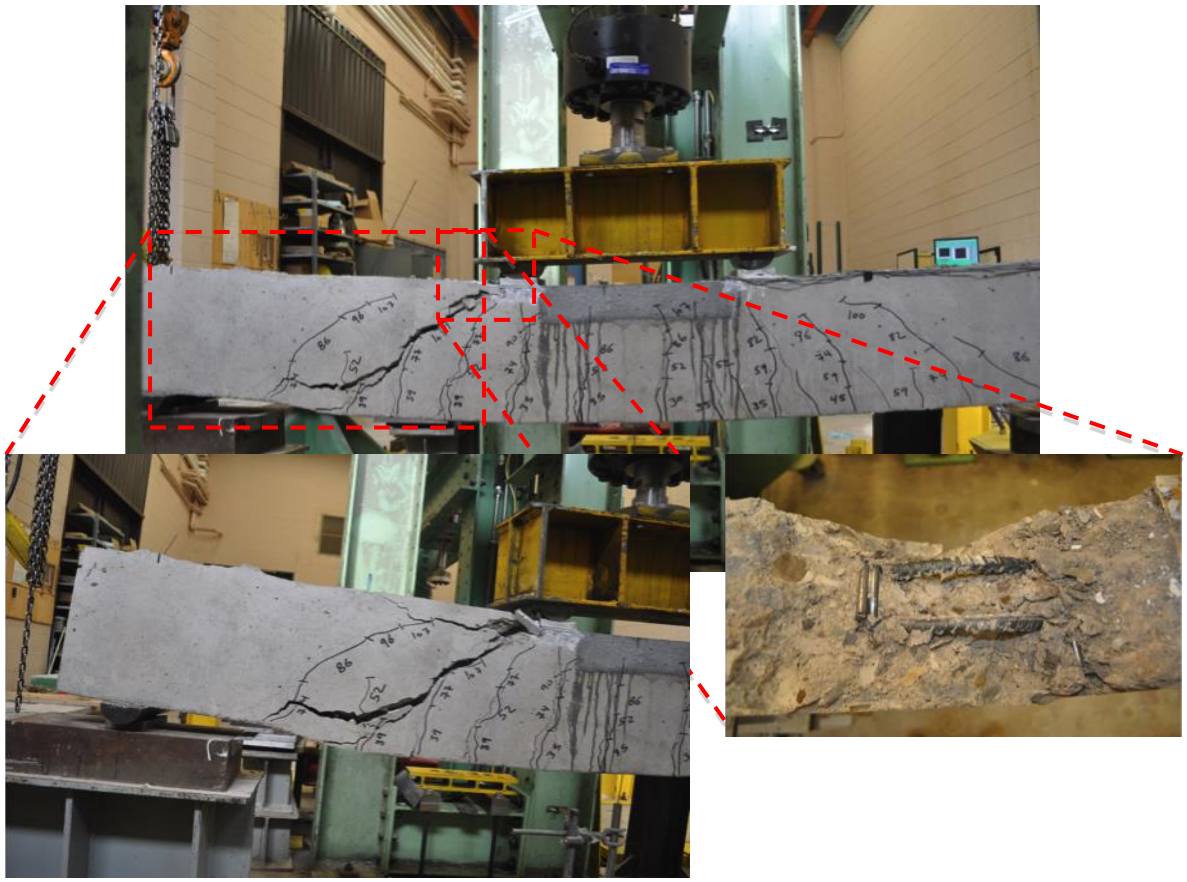

*Figure 5.6 Failure mode for the top-patch repaired beam with mix M1 (SCC, no fibers)*

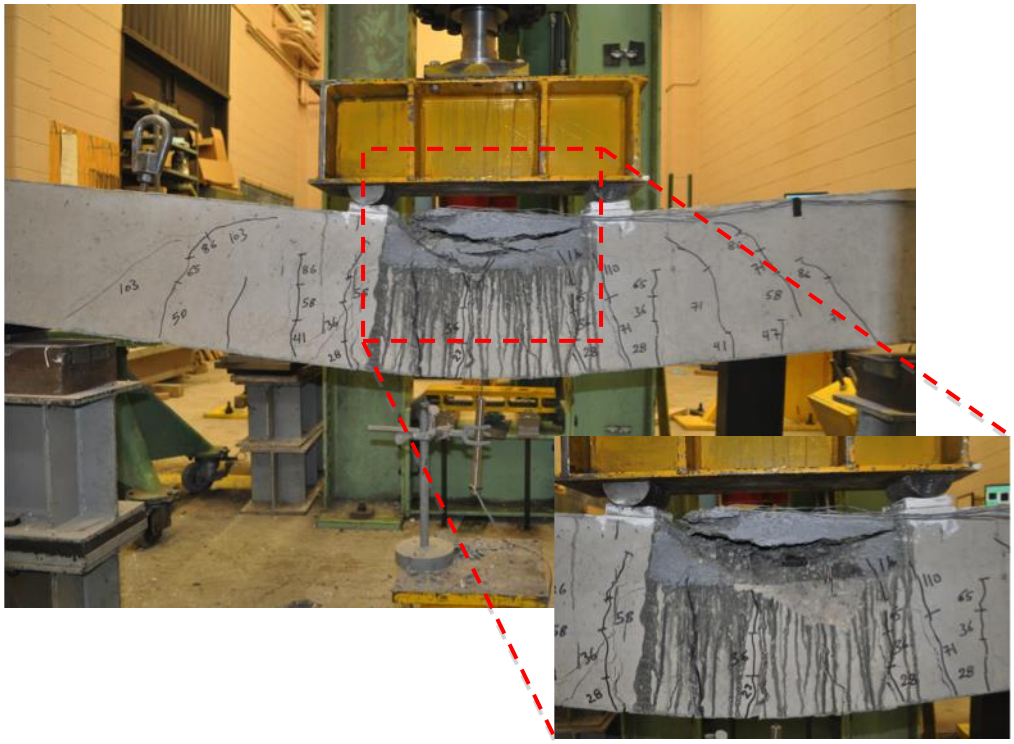

*Figure 5.7 Failure mode for the top-patch repaired beam with mix M3 (CFRSCC, 0.50% fibers)*

### 5.2.2 Load-deflection behaviour

Figure 5.8 and Figure 5.9 show the load-deflection curves for beams repaired in tension and compression zone, respectively. The load-deflection curves exhibited a tri-linear response with cracking yield and ultimate stage. Initially, the beams were uncracked and as the load was increased the tension stress in the bottom concrete exceeded the tensile strength of the concrete and flexural cracks appeared. The load-deflection curve increased linearly with a lesser slope until the longitudinal reinforcement yielded. After post yielding, the beam continued to resist the load at a significantly reduced rate with deflection increasing until the ultimate load. After this load point, the beam failed by concrete crushing; however, the deflection continued to increase and the load gradually decreased in the post-peak response. Few differences to note about the

response of the repaired vs. control beams (Table 5.1). In case of repair in tension zone (bottom patch), the cracking loads increased with two repair materials (Mix M1 and Mix M3) versus that of the control beam. The cracking load was not affected in case of repair in compression zone (top patch) except with mix M3 versus that of the control beam. The deflection at cracking was the same for all beams. Patch repair slightly affected the yield load when applied as a top patch (compression zone), but had no effect on yield load when applied as a bottom patch (tension zone). The deflection at yield was not affected by patch repair. Patch repair had no effect or a slightly negative effect on the ultimate load when the repair materials were applied as a bottom patch (tension zone), but had a positive effect with two repairs (Mix M1 and Mix M3) when applied as a top patch. Deflection at ultimate was significantly improved with top patch versus the control beam and no effect or slight improvement was evident with bottom patch versus the control beam.

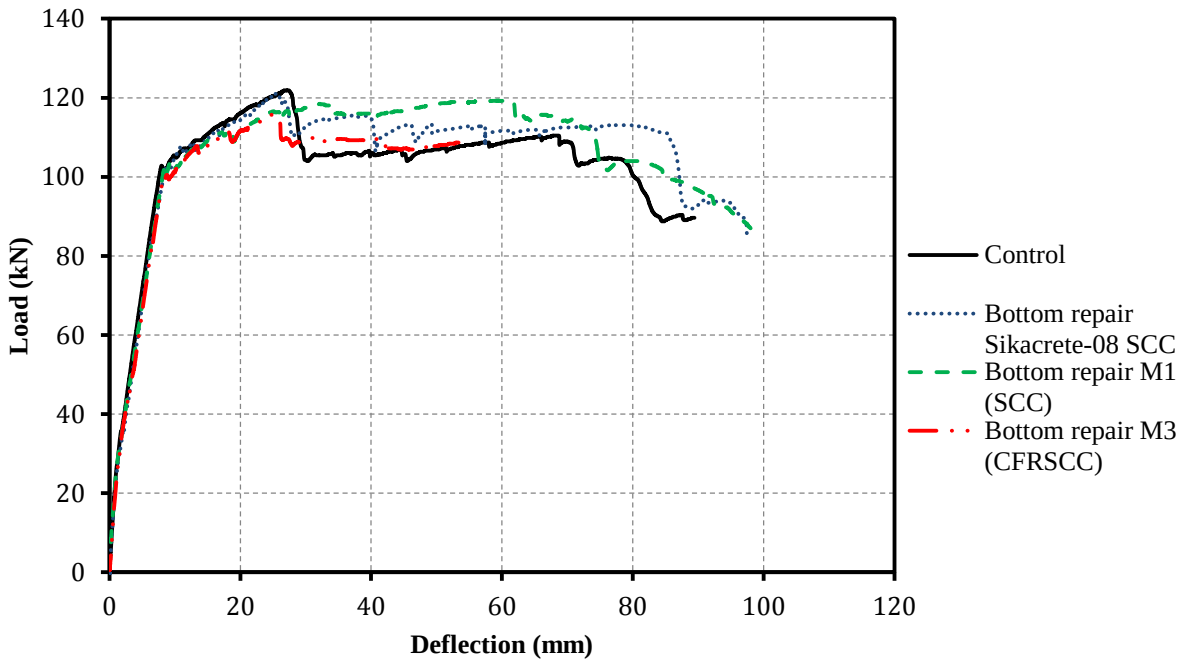


*Figure 5.8 Load vs. deflection curves of the control and bottom flexural repaired beams*

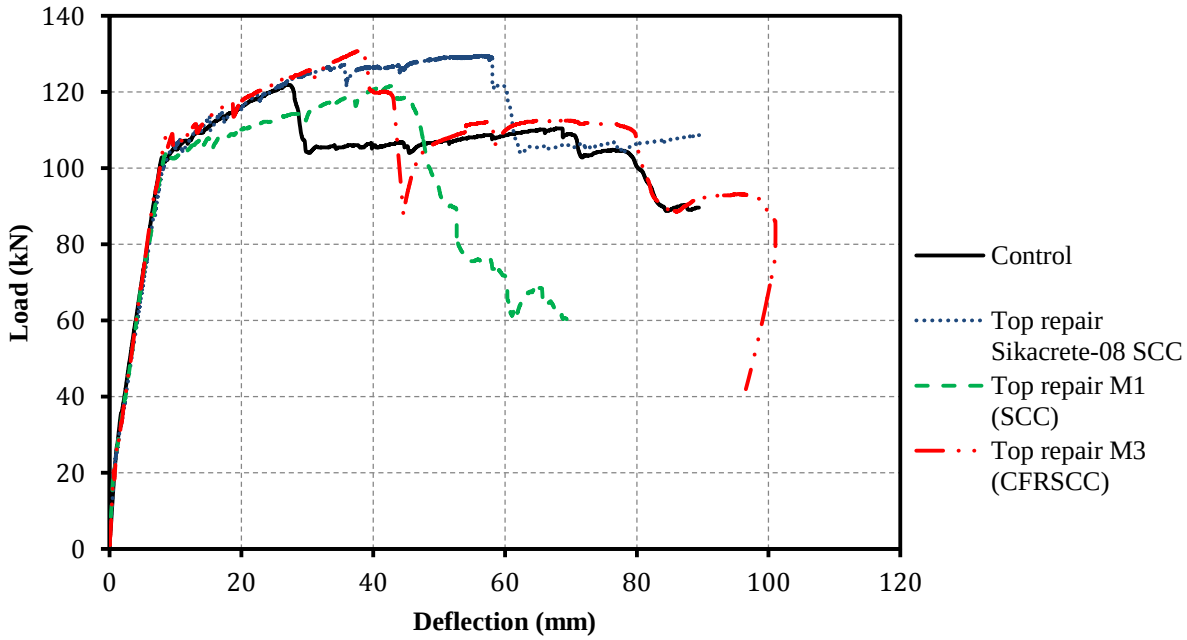


*Figure 5.9 Load vs. deflection curves of the control and top flexural repaired beams*

### 5.2.3 Load-strain behaviour

Figures 5.10 to 5.13 show the load-strain curves of the bottom patch repaired beams. The tensile strain for the bottom longitudinal reinforcement and the compressive strain for the top concrete are shown respectively in Figure 5.10 and Figure 5.11 for the bottom patch repaired beams. The strain values were measured at one section at the middle span of the beams. The strain for the longitudinal steel and concrete increased, as the load increased. The yield strain value for the longitudinal steel is 2435 microstrain, the yield strain for the stirrup is 1900 microstrain and the strain value of the concrete crushing is 3500 microstrain. It is evident from Figure 5.10 and Figure 5.11 that the strain in the longitudinal steel rebar exceeded the yield strain and that the strain value in the top concrete reached the crushing strain. However, the strain values in the stirrups did not reach the yield strain. This means that the longitudinal steel rebar resisted the applied load.

The load-strain behaviour of the longitudinal steel rebar and top concrete of the bottom patch repaired beams were slightly different from that of the control beam. Figures 5.12 and 5.13 show the load-strain curves of the steel rebar and concrete of the top patch repaired beams, respectively. The strain in the longitudinal steel rebar exceeded the yield strain in all the bottom patch repaired beams and similar to the control beam. It is evident from Figure 5.13 that the strain values in the top concrete were different than that of the control beam. The strain values of the top patch repaired beams were higher than that of the control beam. This increase in strain values means that the patch materials had higher strength than that of the conventional concrete.

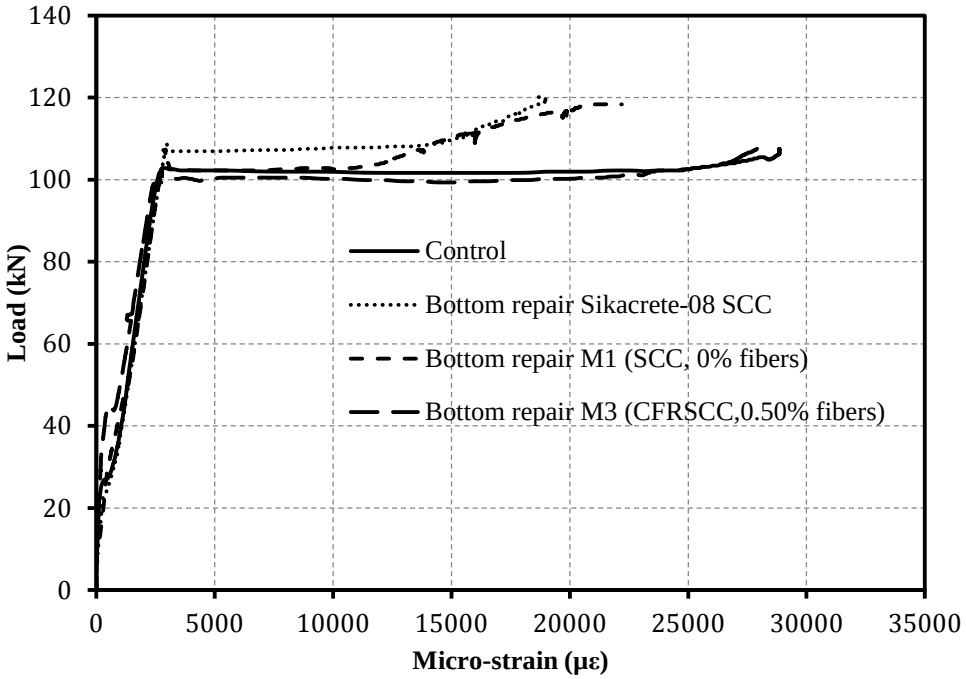


*Figure 5.10 Load-strain behaviour of the longitudinal steel rebar for the bottom patch repaired beams vs. control beam*

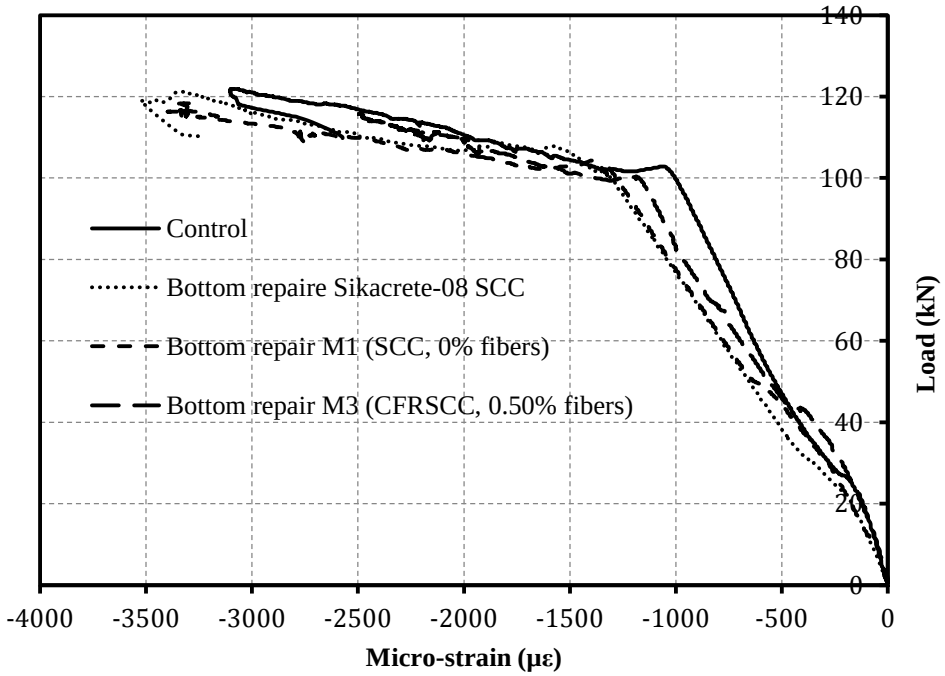


*Figure 5.11 Load-strain behaviour of the top concrete for the bottom patch repaired beams vs. control beam*

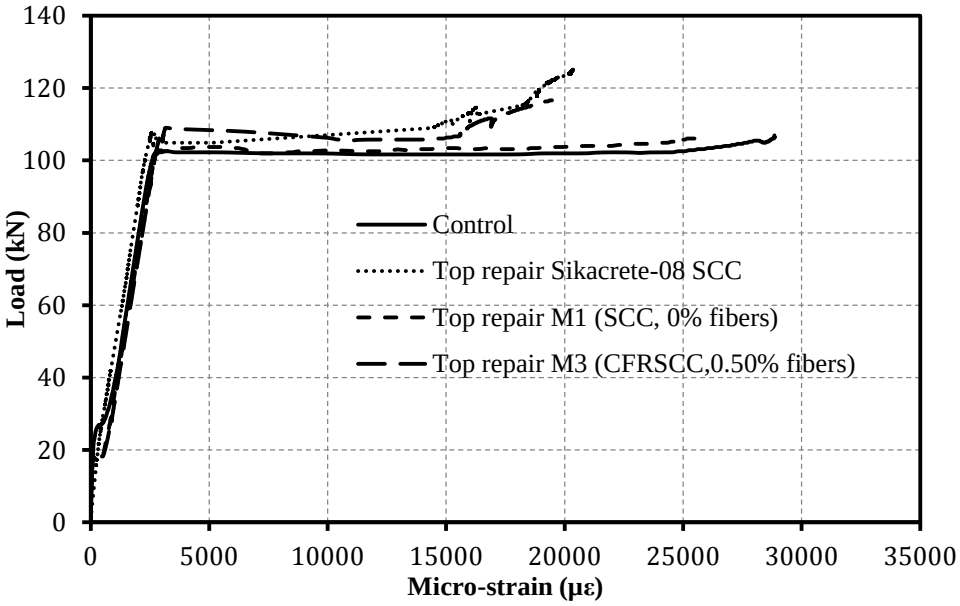


*Figure 5.12 Load-strain behaviour of the longitudinal steel rebar for the top patch repaired beams vs. control beam*

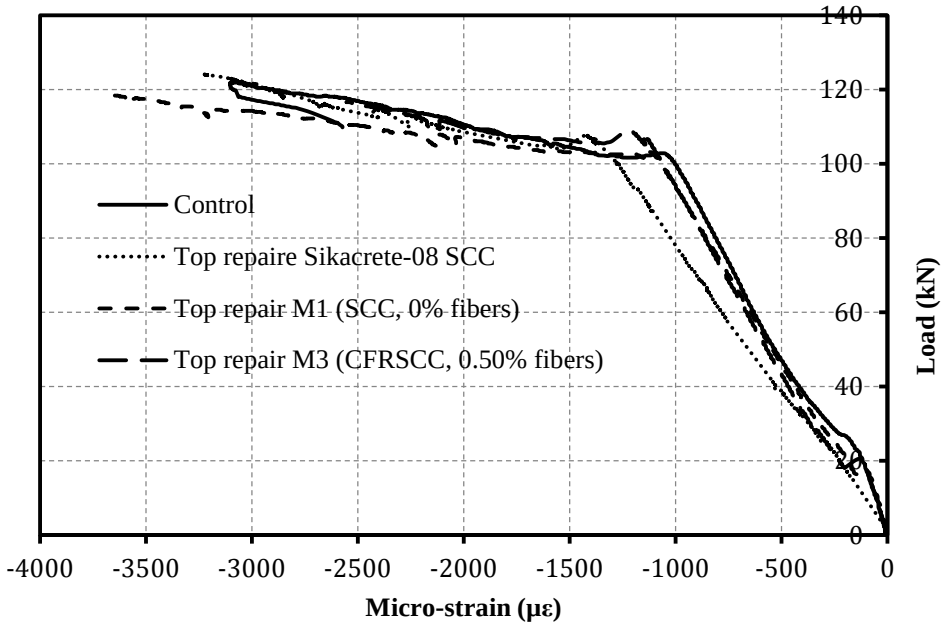


*Figure 5.13 Load-strain behaviour of the top concrete for the top patch repaired beams vs. control beam*

### 5.2.4 Flexural stiffness

Table 5.2 lists the flexural stiffness of all flexural beams at different stages. In the uncracked stage, the top patch repaired beams showed no improvement in flexural stiffness with Sikacrete-08 SCC and mix M1 versus the control beam but the flexural stiffness for the top patch repaired beam with M3 was 30% higher than that of the control beam. The flexural stiffness for the bottom patch repaired beam with Sikacrete-08 SCC was identical to that for the control beam; however, the flexural stiffness for the bottom patch repaired beams with mix M1 and mix M3 was 52% and 95% higher than that of the control beam, respectively. The increase of flexural stiffness in the uncracked stage is probably because of the higher tensile strength of the repair material and the contribution of the fibers to bridge the growing cracks in the tension zone (bottom patch).

**Table 5.2 summary of the flexure stiffness of the flexural beams**

| Beam designation | | Flexural stiffness (N/mm) | | |
|---|---|---|---|---|
| | | Uncracked | Post-cracking | Post-yield |
| | | $K_u$ | $K_c$ | $K_y$ |
| Control | | 11500 | 12750 | 4357 |
| Top patch | Sikacrete-08 SCC | 11500 | 10000 | 2241 |
| | Mix M1 | 11500 | 12875 | 2837 |
| | Mix M3 | 15000 | 13625 | 3333 |
| Bottom patch | Sikacrete-08 SCC | 11500 | 11333 | 4654 |
| | Mix M1 | 17500 | 12875 | 3529 |
| | Mix M3 | 22500 | 12500 | 4423 |

The post-cracking stiffness and the post-yield stiffness of the repaired beams did not show improvement versus the control beam and in some cases the patch repair had a negative effect on the post-cracking and post-yield stiffness.

### 5.2.5 Yield load

Figure 5.14 shows a bar chart comparison of the yield load for all flexural beams. The yield loads for the top patch repaired beams were slightly higher than the control beam. The yield load for the control beam was 102kN. The yield load for the top patch repaired beams with Sikacrete-08 SCC, mix M1, and mix M3 were 100kN, 103kN, and 109kN, respectively. The maximum increase in yield load versus the control was 7% probably due to the high compression strength of the repair patch. However, the yield loads for the bottom patch repaired beams were same as the control beam. The yield load for the bottom patch repaired beams with Sikacrete-08 SCC, mix M1, and mix M3 were 102kN, 103kN, and 100kN, respectively. The repair materials had no effect on the yield loads for the bottom patch repaired beams.

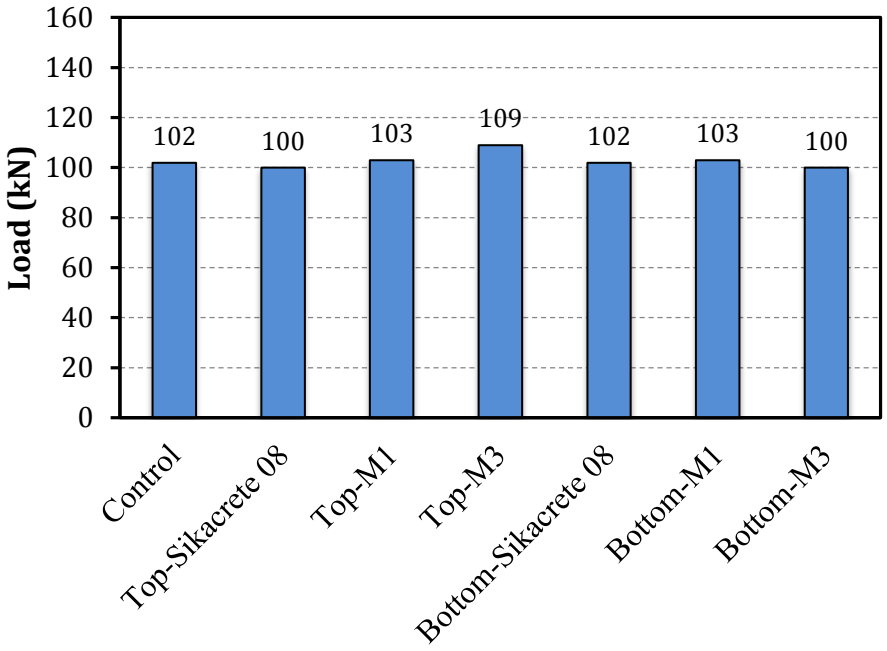


*Figure 5.14 The yield load of the repaired beams vs. the control beam*

### 5.2.6 Ultimate load

Figure 5.15 shows a bar chart comparison of the ultimate load for all flexural beams. The ultimate loads for the top patch repaired beams were slightly higher than the control beam. The ultimate load for the control beam was 122kN. The ultimate load for the top patch repaired beams with Sikacrete-08 SCC, mix M1, and mix M3 were 130kN, 122kN, and 130kN, respectively. Two of the top patch repaired beams had a 6% increase in ultimate load versus the control probably due to the high compression strength of the repair patch. However, the ultimate loads for the bottom patch repaired beams were reduced as result of the repair. The ultimate load for the bottom patch repaired beams with Sikacrete-08 SCC, mix M1, and mix M3 were 121kN, 120kN, and 115kN, respectively. The slight reduction in the ultimate loads was considered within experimental error.

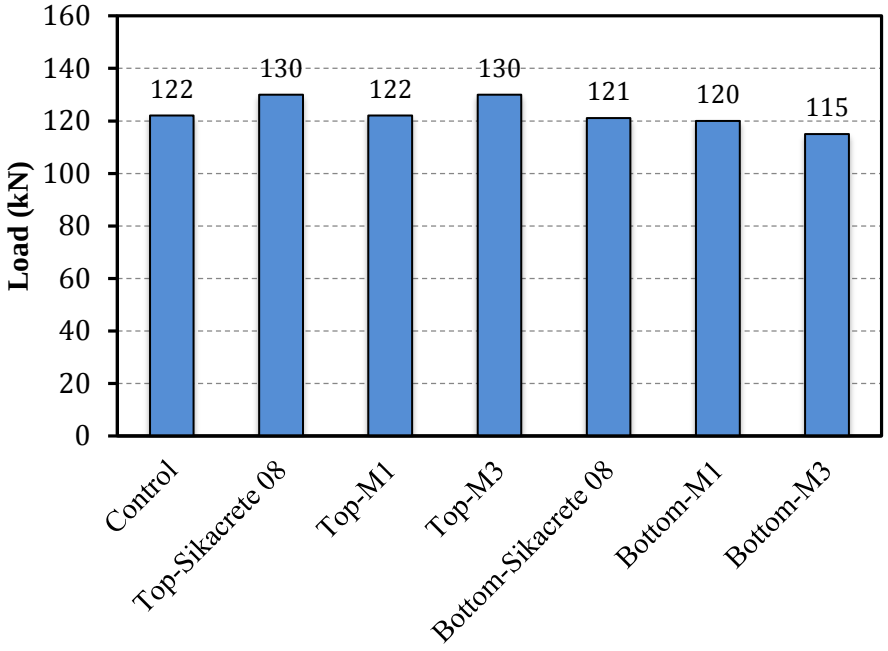


*Figure 5.15 The ultimate load of the repaired beams vs. the control beam*

### 5.2.7 Ductility

Ductility can be defined as the ultimate deflection divided by the yield deflection. Figure 5.16 shows a bar chart comparison of the ductility for the flexural beams. The ductility for the control beam was 3.5. The ductility for the top patch repaired beams was 50% higher than that of the control beam. One of the factors that affect the ductility of RC beams is the compression strain in the concrete. As it can be seen from the load-strain curves in Appendix B, the compression strains in the repaired patches were higher than that of the control beam at midspan. Also, the compressive strength of the repaired material was higher than that of the normal concrete. The ductility of the bottom patch repaired beams with Sikacrete-08 SCC and mix M3 was not significantly improved versus the control beam, but the ductility of the bottom patch repaired beam with M1 was 21% higher than the control beam.

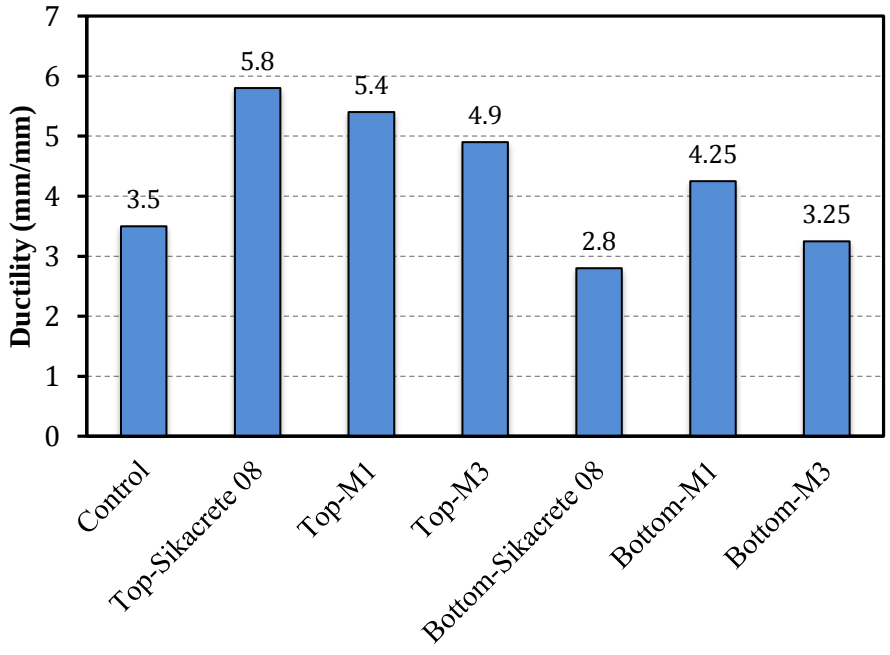


*Figure 5.16 The ductility of the repaired beams vs. control beam*

## 5.3 Effect of repair material on structural performance of shear beams

Table 5.3 summarizes the critical stages of the shear beams. The detailed results of the individual beams (load-deflection and strain responses) are given in Appendix B.

**Table 5.1 Summary of shear test results**

| Beam designation | | Cracking | | Yielding | | Ultimate | | Mode of failure |
|---|---|---|---|---|---|---|---|---|
| | | $P_{cr}$ | $\Delta_{cr}$ | $P_y$ | $\Delta_y$ | $P_u$ | $\Delta_u$ | |
| | | kN | mm | kN | mm | kN | mm | |
| Shear zone patch | Control | 40 | 2 | 190 | 6.8 | 270 | 10 | Diagonal tension shear |
| | Sikacrete-08 SCC | 45 | 2 | 215 | 7.5 | 345 | 14.5 | Diagonal tension shear |
| | Mix M1 | 42 | 2 | 220 | 7.5 | 320 | 11.5 | Diagonal tension shear |
| | Mix M3 | 50 | 2 | 265 | 9 | 355 | 14.9 | Concrete crushing |

### 5.3.1 Observed shear behaviour

#### 5.3.1.1 Control beam

Flexural cracks appeared first and were located in the constant moment region at a load of 40kN. As the load increased, an inclined crack appeared between the loading point and the support in one span at a load of 143kN. As the load increased, the shear or inclined crack extended towards the loading point. As the inclined crack widened in the right side of the beam, the stirrups started to share the load resistance and the beam continued to carry more load until the concrete crushed. The failure mode of the control beam was diagonal tension shear by loss of aggregates interlock. The shear failure is shown in Figure 5.17.

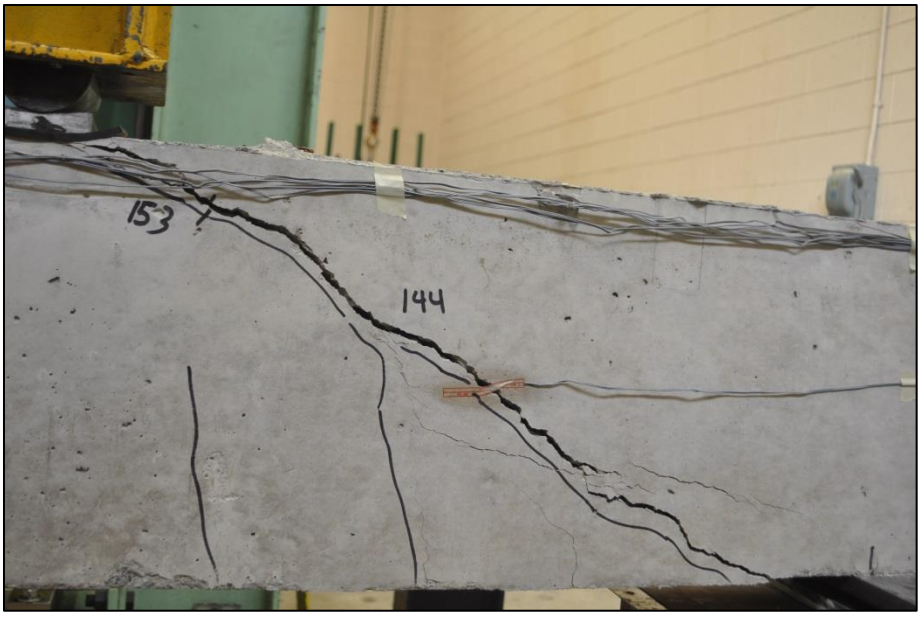


*Figure 5.17 Failure mode of control beam*

#### 5.3.1.2 Repaired beams

The repair was applied on the right side of the beam and the left side of the beam was cast with additional stirrups to ensure that failure would occur in the right span. The flexural cracks appeared first and they were located in the constant moment region at loads of 45kN, 42kN, and 50kN for the shear-span repaired beams with Sikacrete-08 SCC, mix M1, and mix M3, respectively. As the load increased, the shear crack appeared between the loading point and supports at loads of 143kN, 120kN, and 135kN for the repaired beams with Sikacrete-08 SCC, mix M1, and mix M3 respectively. As the load was further increased, the shear (inclined) crack grew and extended towards the loading point. After the appearance of the inclined crack in the right side of the repaired beam with Sikacrete-08 SCC the stirrups started to share the load resistance and the beam continued to carry load until the concrete crushed as shown in Figure 5.18. However, the shear-span repaired beam with M1 (SCC, no fibers) showed that the failure inclined crack appeared in the left side of the beam (control) instead of the patched zone in the

right side of the beam. The failure mode of the repaired beam was diagonal tension shear by loss of aggregates interlock as shown in Figure 5.19.

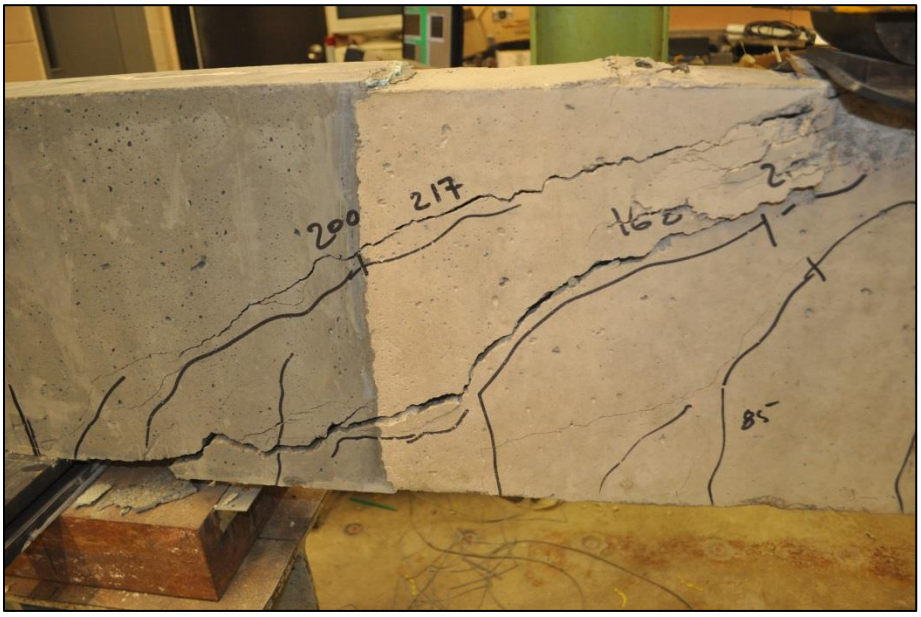


*Figure 5.18 Failure mode of the shear-span repaired beam with Sikacrete-08 SCC*

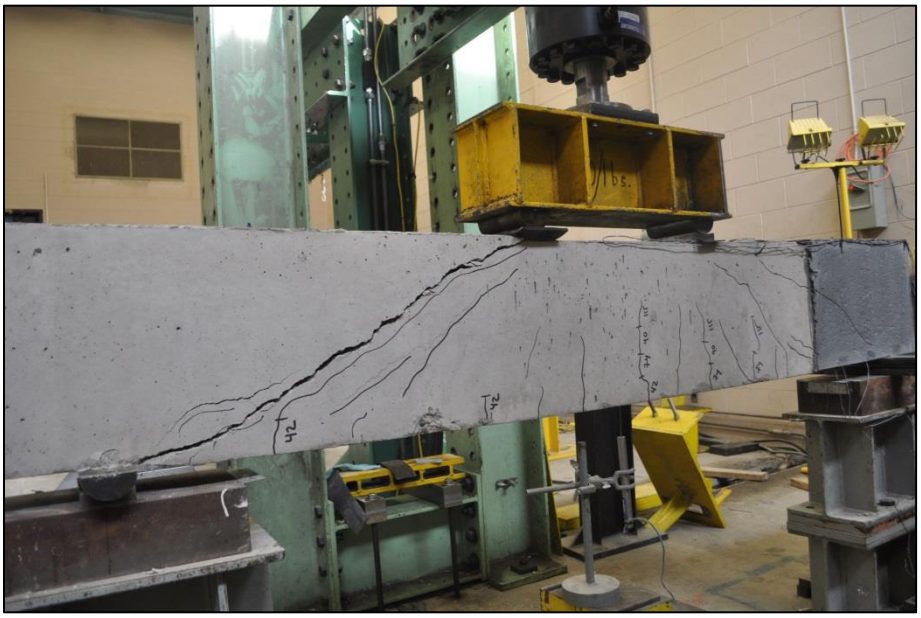

*Figure 5.19 Failure mode of shear-span repaired beam with mix M1 (SCC, no fibers)*

On the other hand, the shear-span failure mode of the repaired beam with mix M3 (CFRSCC, 0.50% fibers) changed from a shear failure (brittle failure) to a flexural failure (ductile failure) due to the contribution of carbon fibers in resisting the cracks growth in the shear-span as shown in Figure 5.20. At failure, the flexural load capacity of the beam was 355kN. This result means that the shear capacity was significantly increased beyond the flexural capacity.

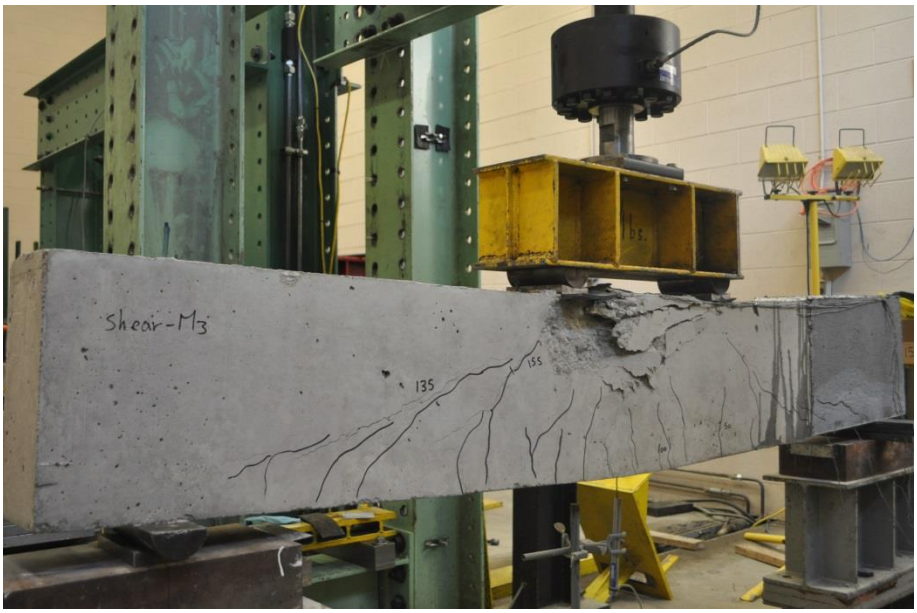


*Figure 5.20 Failure mode of the shear-span repaired beam with mix M3 (CFRSCC, 0.50% fibers)*

### 5.3.2 Load-deflection behaviour

Figure 5.21 shows a comparison the load-deflection curves for the shear-span repaired vs. control beam. The load deflection behaviour can be divided into three distinct stages: first stage where the concrete was uncracked up to the appearance of the flexural cracks, the load-deflection curve was a straight line. Stage two; the concrete was fully cracked and the stiffness of the beam

decreased. This stage continued until the diagonal crack appeared. Stage three; the diagonal crack appeared and more flexural cracks appeared. Upon completion of this last stage, the load reached its peak value, then noticeably decreasing rapidly afterwards. This drop in the load occurred because the shear reinforcement was no longer taking more load. It is evident that the shear-span patch repair increased the ultimate load as well as the deflection at failure. The shape of the load-deflection curve during the post-peak response was similar with a rapid drop in load for patch repair with Sikacrete-08 SCC and mix M1 (SCC, no fibers). However, the repaired beam with mix M3 (CFRSCC, 0.50% fibers) patch exhibited a more ductile flexural failure mode with a gradual decrease in load. This behaviour is attributed to the presence of the carbon fibers that helped in bridging in the cracks as evident in the failure mode as shown in Figure 5.21. The stiffness of the repaired beams was almost identical to that of the control beam during all stages of loading. The only exception is for repaired beam with mix M3 (CFRSCC, 0.50% fibers) where the post-peak stiffness was much higher than the rest of the beams (which exhibited no peak stiffness) because of the change in mode of failure of that beam.

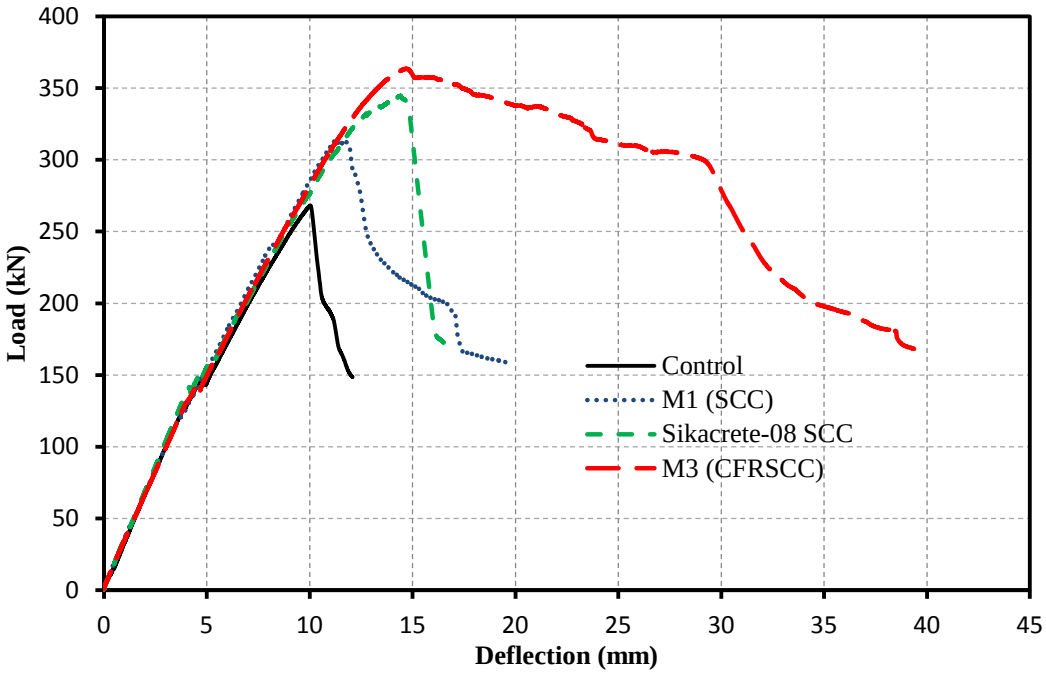


*Figure 5.21 Load vs. deflection curves of the control and the shear-span repaired beams*

### 5.3.3 Load-strain behaviour

Figures 5.22 and 5.23 show the load-strain curves of the shear-span repaired beams. The strain in the bottom longitudinal steel rebar, the strain in the stirrups, and the strain in the top concrete are shown in Figure 5.22 and Figure 5.23. The strain values were measured at the middle span of the beams. The yield strain for the longitudinal steel rebar is 2060 microstrain, the yield strain for the stirrup is 1900 microstrain, and the concrete crushing strain is 3500 microstrain. It is evident from Figure 5.23 that the strain value in the longitudinal steel rebar did not reach the yield and the strain value in the top concrete did not reach the crushing strain. However, the strain values in the stirrups exceeded the yield strain for the shear-span repaired beams with Sikacrete-08 SCC and M1 (SCC, 0% fibers) and the control beam. After the concrete cracked in shear, the

aggregate interlock was lost and the stirrups started to share in the load resistance. It is evident from Figure 5.23 that the strain values in the longitudinal steel and the top concrete were identical to that of the control beam. The shear-span repaired beam with M3 (CFRSCC, 0.50% fibers) showed that the mode of failure changed from a brittle failure to ductile failure. It is evident that from this beam the strain in longitudinal steel rebar exceeded the yield strain and the strain value in concrete reached the crushing strain. The stirrups did not reach the yield. Figures 5.24 to 5.27 show the strain profile in the stirrups for the shear-span repaired beams and control beam. It is evident that strains in the stirrups were very small (less than 500 με) up to cracking. Once the inclined shear crack occurred, the strains (for stirrups S2 and S3) jumped to values above 1500 με and continued to increase as loading was increased. In most cases, the peak strain was measured by S2 which was located at 150 mm from the support. The beam repaired with M3 exhibited lower stirrups strains than the other beams because this beam failed in flexure.

The stirrup strain profiles also showed that the strain value increased, as the distance from the support increased. This means that the stirrup which was placed close to the support did not contribute as other stirrups to share in resistance of the diagonal crack whereas the stirrups which were placed far from the support contributed in resisting diagonal crack.

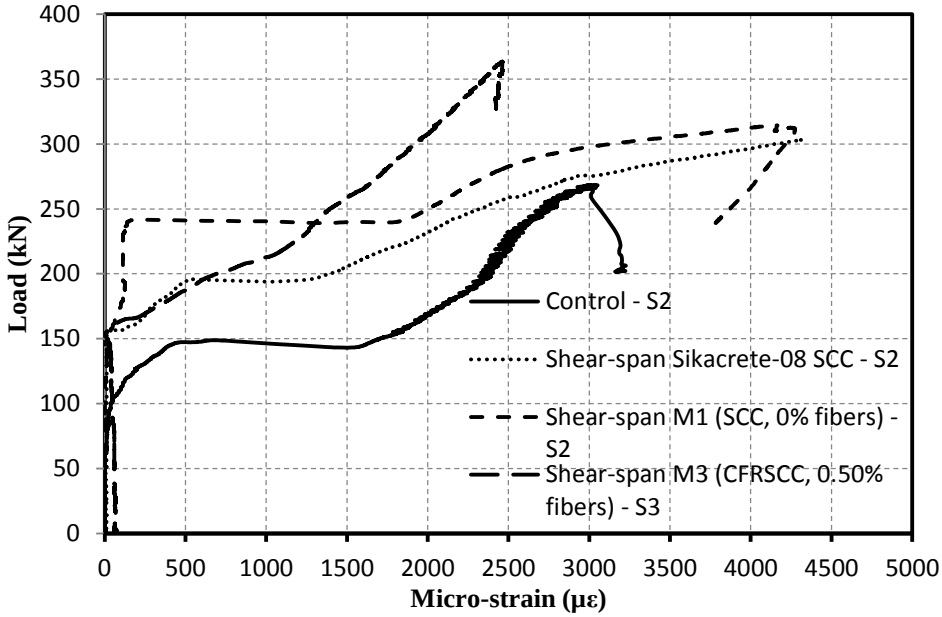


*Figure 5.22 Load-strain behaviour of the stirrup for the shear-span repaired beams vs. control beam*

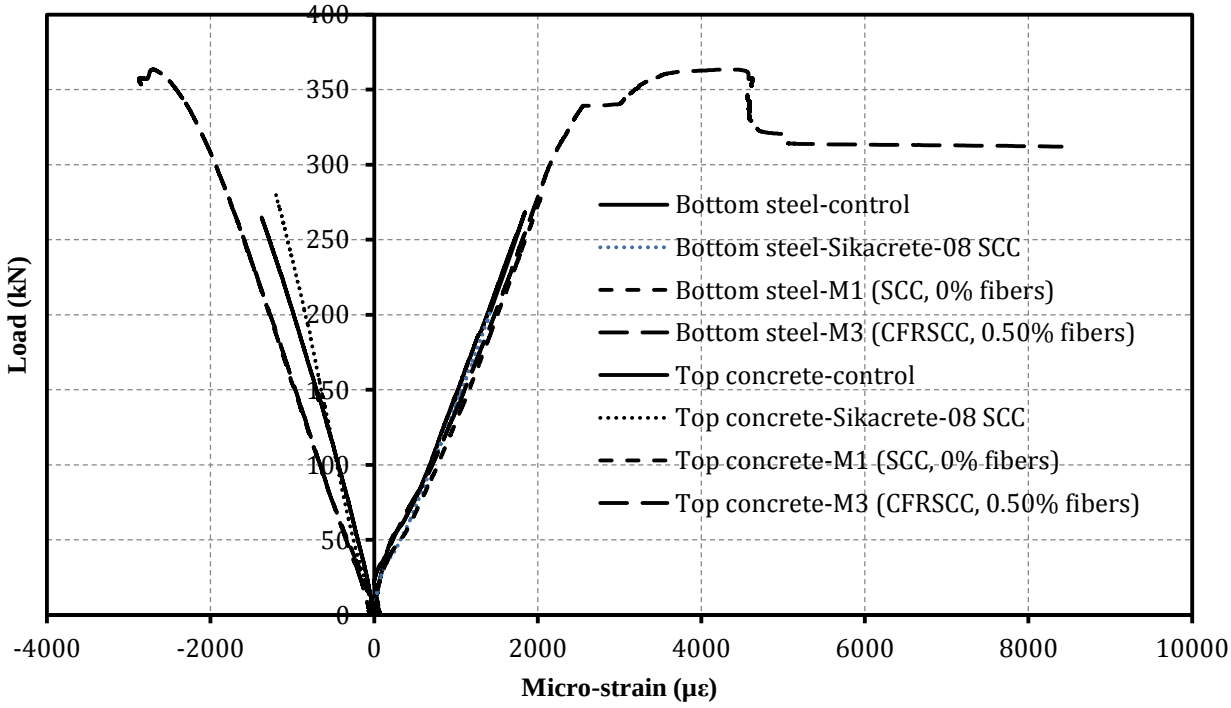


*Figure 5.23 Load-strain behaviour of the stirrups for the shear-span repaired beams vs. control beam*

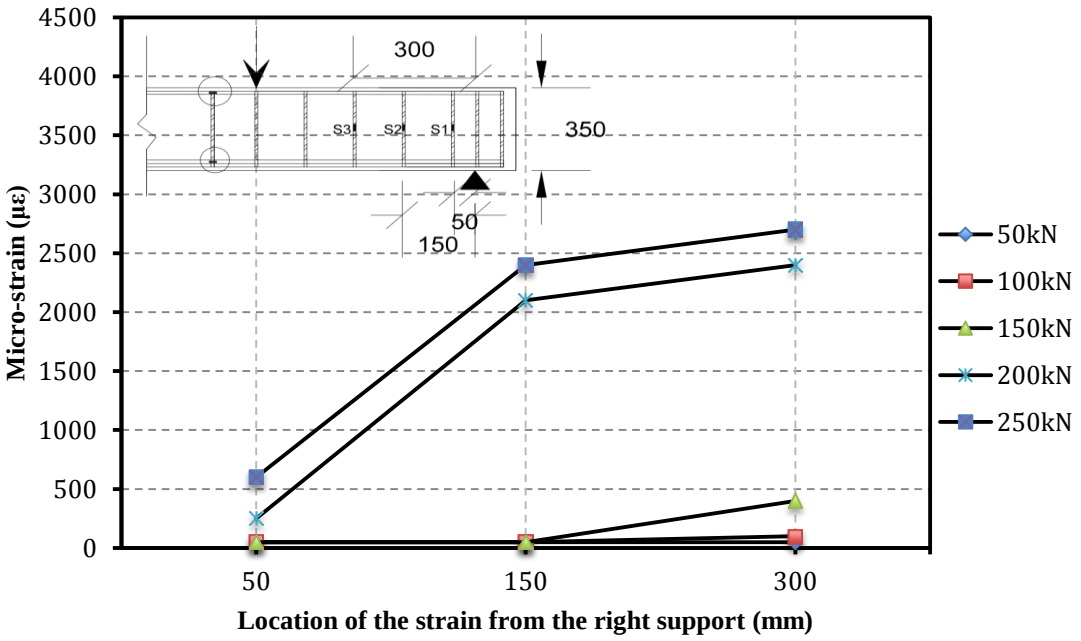


*Figure 5.24 Stirrups strain profile of control beam*

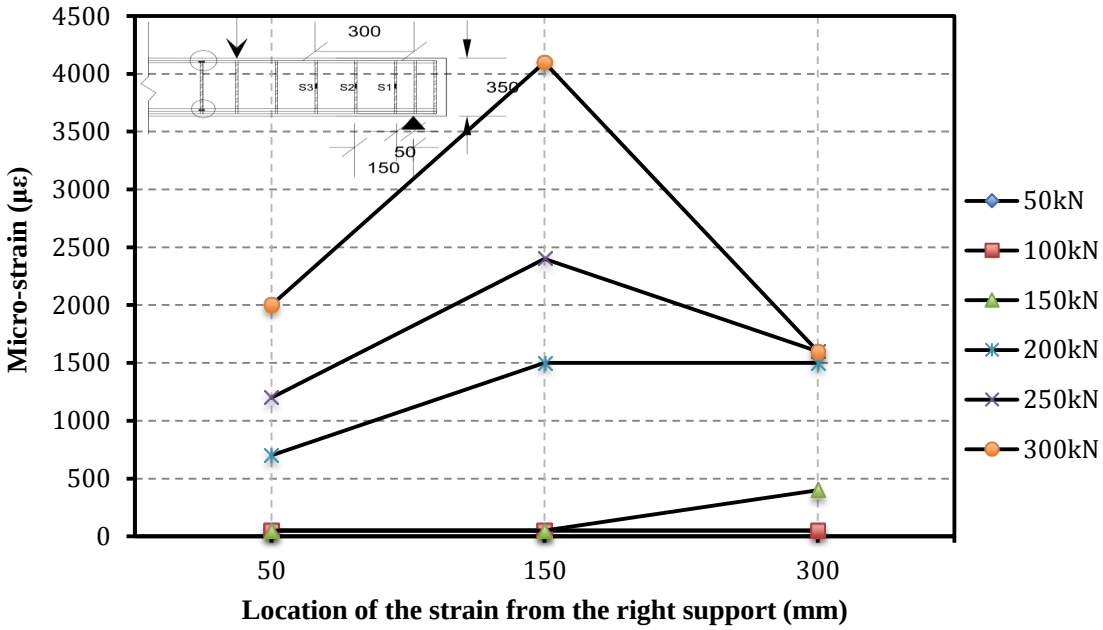


*Figure 5.25 Stirrups strain profile of shear-span repaired beam with Sikacrete-08 SCC*

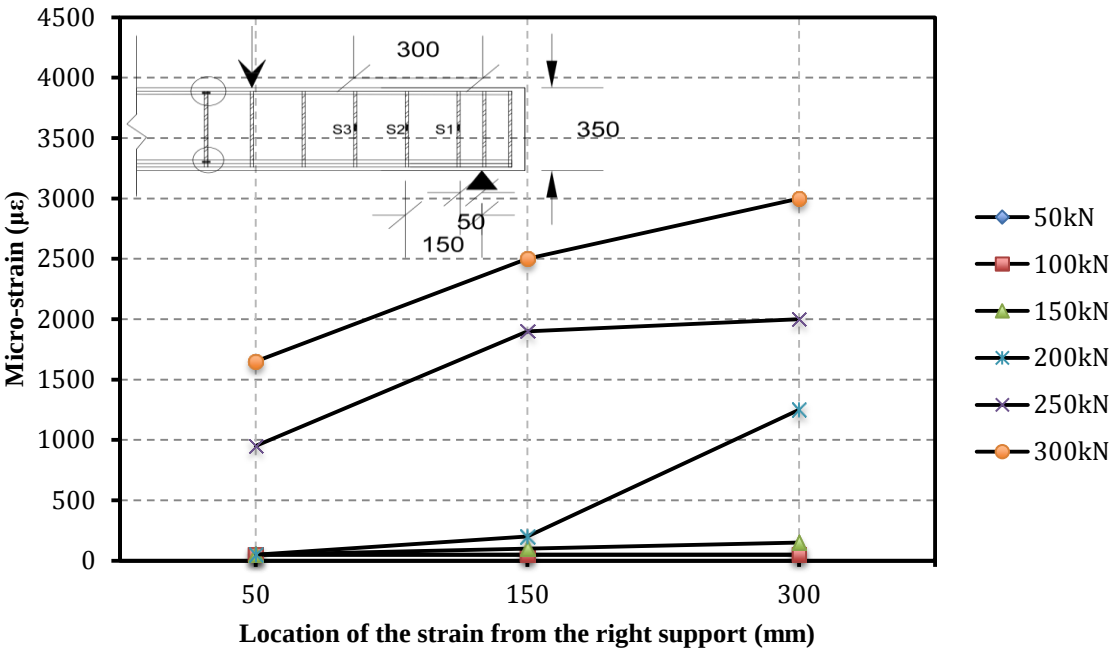


*Figure 5.26 Stirrups strain profile of shear-span repaired beam with mix M1 (SCC, 0% fibers)*

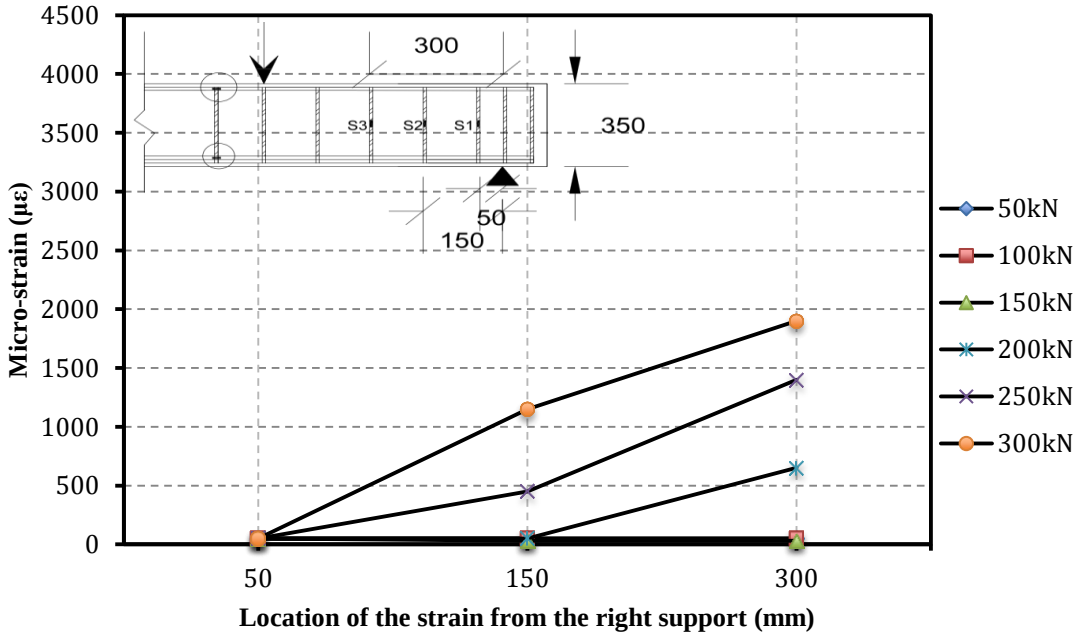


*Figure 5.27 Stirrups strain profile of shear-span repaired beam with mix M3 (SCC, 0.5% fibers)*

### 5.3.4 Yield load

A comparison of the yield loads for the shear-span repaired beams with Sikacrete-08 SCC, mix M1 (SCC, 0% fibers), and mix M3 (CFRSCC, 0.50% fibers) versus the control beam is shown in Figure 5.28. It is evident that the yield load increased by about 13%, 16%, and 39.5% for the repaired beams with Sikacrete-08 SCC, mix M1, and mix M3, respectively. This increase is due to the contribution of the repair materials, which were stronger than the normal concrete. The compressive and tensile strengths of the repair materials were higher than that of normal concrete. Also, carbon fibers played a very important role in controlling the growth of cracks in the beam repaired with mix M3 (CFRSCC, 0.5% fibers).

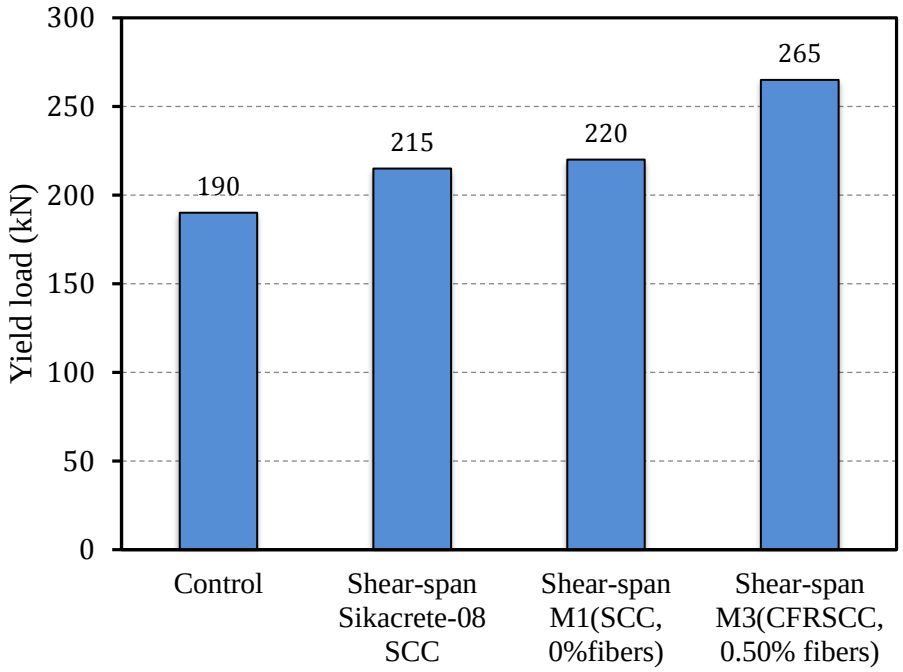


*Figure 5.28 The yield loads for the shear-span repaired beams vs. the control beam*

### 5.3.5 Ultimate load

The ultimate loads for the shear-span repaired beams with Sikacrete-08 SCC, mix M1 (SCC, no fibers), and mix M3 (CFRSCC, 0.50% fibers) are compared with the control beam as shown in Figure 5.29. The ultimate load increased by about 27.8%, 18.5%, and 31.1% for repaired beams with Sikacrete-08 SCC, mix M1, and mix M3, respectively. This increase is likely due to the contribution of repair materials, which had higher compressive and tensile strengths than that of normal concrete. Also, carbon fibers played very important role in reducing the growth of cracks and changing failure mode from a brittle to ductile failure for failure for beam repaired with M3 (CFRSCC, 0.5% fibers).

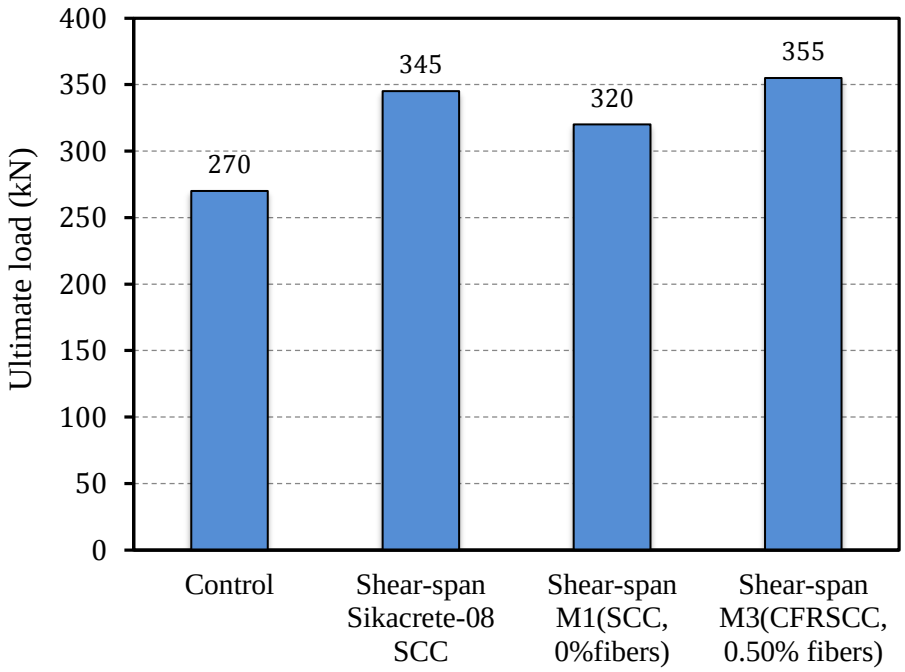


*Figure 5.29 The ultimate loads for the shear-span repaired beams vs. the control beam*

### 5.3.6 Ultimate deflection

A comparison of the ultimate deflection for the shear-span repaired beams with Sikacrete-08 SCC, mix M1 (SCC, no fibers), and mix M3 (CFRSCC, 0.50% fibers) versus the control beam is shown in Figure 5.30. It is evident that the ultimate deflection increased by about 40%, 20%, and 200% for the repaired beams with Sikacrete-08 SCC, mix M1, and mix M3, respectively. This increase is due to the contribution of the repair materials, which were stronger than the normal concrete. The compressive strengths and tensile strength of the repair materials were higher than that of normal concrete. Also, carbon fibers played a very important role in reducing controlling the growth of cracks in the CFRSCC repaired beams.

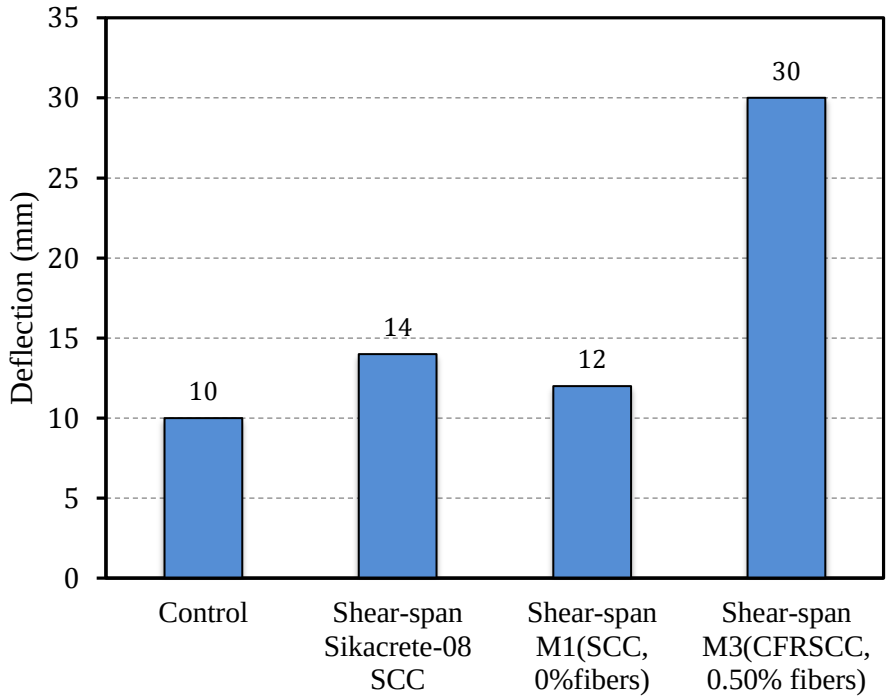


*Figure 5.30 Deflection for the shear-span repaired beams vs. control beam*

# Chapter 6 Conclusions and recommendations

## 6.1 Summary

The main objective of this research was to investigate the effect of carbon fibers on the fresh and hardened properties of self-consolidating concrete mixtures. The efficiency of CFRSCC as a patch material was also evaluated in shear and flexural repairs. The experimental research consisted of concrete materials work and structural performance of repaired RC beams.

Twenty trial mixtures were done to achieve the optimum fresh properties of CFRSCC mixtures. The HRWR dosages varied until the CFRSCC fresh properties fulfilled the limits of SCC set by ASTM standards. Ten concrete mixtures were finally batched. Two W/B ratios were used 0.35 and 0.40. The carbon fiber content (CF) ranged from 0 to 1%. The HRWR ranged from 1.5 to 8% for mixes 1 to 5 and from 1 to 7% for mixes 5 to 10.

A total of eleven reinforced concrete beams were tested. Group (1) consisted of four beams designed to study the behaviour of shear-span patch repair of reinforced concrete beams; group (2) consisted of seven beams designed to study the behaviour of top patch and bottom patch repaired reinforced concrete beams. The test variables were: the repair materials (SCC (M1), CFRSCC (M3), and Sikacrete-08 SCC), location of repair (shear, tension, and compression), and loading configuration (flexure, shear).

## 6.2 Conclusions

### 6.2.1 Fresh and hardened properties tests

Based on the test results for the fresh and hardened properties of CFRSCC, the following conclusions can be made:

- SCC with CF can be made to meet the fresh properties.
- Carbon fibers affected the filling ability, passing ability, and segregation resistance of SCC mixtures. HRWR facilitated achieving the target filling ability and passing ability properties of the SCC mixtures with carbon fibers.
- The CFRSCC mixtures with 1% by volume of carbon fibers (mixtures M5 and M10) required a very high amount of HRWR to improve their fresh properties. The CFRSCC mixtures with carbon fiber content up to 0.75% and HRWR up to 3% satisfactorily passed the requirements of SCC.
- All CFRSCC mixtures achieved the segregation resistance requirement as their segregation index was below the maximum limit (18%).
- The $T_{50}$ slump flow time was increased with the increase in carbon fibers content because the inclusion of fibers slowed the flow of CFRSCC mixtures by making it more viscous.
- The blocking index for all SCC mixtures was below the maximum limit of 50 mm because of their relatively high flowing ability and high segregation resistance.
- The visual stability index (VSI) of the freshly mixed CFRSCC mixtures revealed that the concrete mixtures were highly stable (VSI =0) to stable (VSI =1), thus indicating excellent and good segregation resistance, as observed from the sieve stability test.

- The compressive strength of the CFRSCC mixtures decreased as the carbon fibers increased and the splitting tensile strength of the CFRSCC increased as the carbon fibers increased.
- For mixes with 0.35 W/b ratio achieved higher compressive strength than mixes with 0.4 W/B ratio.
- The modulus of rupture for mixes with W/B ratio of 0.35 increased with the increase of carbon fibers. However, the modulus of rupture for mixes with W/B ratio of 0.40 did not increase with the increase of carbon fibers. These results were different from those of mixes with 0.35 W/B ratio.
- The toughness or the fracture energy of mixes with 0.35 W/B ratio increased when the carbon fibers were added.
- SEM images of the fracture surface showed that the carbon fibers were well distributed with the concrete matrix, and no fiber balling occurred.
- SEM images revealed that fibers failure was by both fiber pullout and by fiber breakout.

### 6.2.2 Structural load tests

Conclusions for the structural performance of patch repaired RC beams are as follows:

- The patch repair had a more significant effect in shear-span patches versus bottom-patch and top-patch flexural repairs.
- The uncracked flexural stiffness of the top patch repaired beams with Sikacrete-08 SCC and mix M1 were identical to that for the control beam but the flexural stiffness for the

top patch repaired beam with mix M3 was 30% higher than the flexural stiffness of the control beam.

- The flexural stiffness for the bottom patch repaired beam with Sikacrete-08 SCC was identical to that for the control beam; however, the flexural stiffness for the bottom patch repaired beams with mix M1 and mix M3 was 52% and 95% higher than that of the control beam, respectively.
- The ultimate loads of the top patch repaired beams were identical or higher than that of the control beam. The ultimate loads for the bottom patch repaired beams were similar or slightly lower than that of the control beam.
- The ductility for the top patch repaired beams was 50% higher than that of the control beam. The ductility of the bottom patch repaired beams with Sikacrete-08 SCC and mix M3 was not improved, but the ductility of the bottom patch repaired beam with M1 was 21% higher than the control beam.
- The ultimate load for the shear-span repaired beams with Sikacrete-08 SCC, mix M1, and mix M3 increased by about 27.8%, 18.5%, and 31.1%, respectively.
- All beams had the same type of failure, which is diagonal tension shear by loss of aggregates interlock, except the shear-span repaired beam with mix M3.
- In this study, the repair material M3 (CFRSCC, 0.50% carbon fibers) changed the failure mode from a shear failure to flexural failure. This is due to the contribution of fibers in resisting the cracks growth.
- Mix M3 is recommended to be sued in the repair application.

## 6.3 Recommendations of future work

- Research on other size and type of carbon fibers to produce SCC is required to find obtained more information.
- More hardened properties tests are needed such as impact resistance, freeze and thaw, and conductivity resistance to find the effect of carbon fibers on the these tests.
- Research is needed to investigate the concrete shear resistance ($V_c$) which means using CFRSCC on RC beams without stirrups.
- Investigate the bond behaviour between the concrete and repair materials M1 and M3 (SCC and CFRSCC).
- Investigate the repair materials M1 and M3 on improving repaired corroded RC beams.

# Bibliography

ACI Committee 211.4R-08. (2008). "Guide for Selecting Proportions for High-Strength Concrete Using Portland Cement and Other Cementitious Materials". American concrete institute, Farmington Hills, USA, pp. 1-29.

ACI Committee 237R-07. (2007). "Self –consolidating concrete", American concrete institute, Farmington Hills, USA, pp. 1-30.

Ali A., Majumdar J., and Rayment L. (1972). "Carbon fiber reinforcement of cement," Cement and Concrete Research, Vol. 2, No. 2, pp. 201-212.

Aydin, A. (2007). "Self-compatibility of high volume hybrid fiber reinforced concrete," Construction and Building Materials, Vol. 21, No. 6, 1149-1154.

ASTM C29/C29M – 09. (2009). "Standard test method for bulk density ("unit weight") and voids in aggregate", *Annual book of ASTM standard*, American Society for Testing and Materials, Philadelphia, USA.

ASTM C33/C33M. (2008). "Standard specification for concrete aggregate", *Annual book of ASTM standard*, American Society for Testing and Materials, Philadelphia, USA.

ASTM C127 – 07. (2007). "Standard test method for density, relative density (specific gravity), and absorption of coarse aggregate", *Annual book of ASTM standard*, American Society for Testing and Materials, Philadelphia, USA.

ASTM C128 – 07a. (2007). “Standard test method for density, relative density (specific gravity), and absorption of fine aggregate”, *Annual book of ASTM standard*, American Society for Testing and Materials, Philadelphia, USA.

ASTM C136 – 06. (2006). “Standard test method for sieve analysis of fine and coarse aggregates”, *Annual book of ASTM standard*, American Society for Testing and Materials, Philadelphia, USA.

ASTM C150/C150M – 09. (2009). “Standard specification for portland cement”, *Annual book of ASTM standard*, American Society for Testing and Materials, Philadelphia, USA.

ASTM C231/C231M – 09b. (2009) “Standard test method for air content of freshly mixed concrete by the pressure method”, *Annual book of ASTM standard*, American Society for Testing and Materials, Philadelphia, USA.

ASTM C494/C494M – 10. (2010). “Standard specification for chemical admixtures for concrete”, *Annual book of ASTM standard*, American Society for Testing and Materials, Philadelphia, USA.

ASTM C566 – 97. (1997). “Standard test method for total evaporable moisture content of aggregate by drying”, *Annual book of ASTM standard*, American Society for Testing and Materials, Philadelphia, USA.

ASTM C 1116/C 1116M – 09. (2009). “Standard specification for fiber-reinforced concrete”, *Annual book of ASTM standard*, American Society for Testing and Materials, Philadelphia, USA.

ASTM C1240 – 05. (2005). “Standard specification for silica fume used in cmentitious mixtures”, *Annual book of ASTM standard*, American Society for Testing and Materials, Philadelphia, USA.

ASTM C1611/C 1611M – 09b. (2009). “Standard test method for slump flow of self-consolidating concrete”, *Annual book of ASTM standard*, American Society for Testing and Materials, Philadelphia, USA.

ASTM C1621/C 1621M – 09b. (2009). “Standard test method for passing ability of self-consolidating concrete by J-ring”, *Annual book of ASTM standard*, American Society for Testing and Materials, Philadelphia, USA.

Azam, R. (2010). “Behaviour of shear critical RC beams with corroded longitudinal steel reinforcement,” Masters of Applied Science Thesis, University of Waterloo, Waterloo, ON, Canada.

Badawi, M. (2003). “Flexural response of uniform and shear-span corroded RC beams repaired with CFRP laminates,” Masters of Applied Science Thesis, University of Waterloo, Waterloo, ON, Canada.

Banthia, N., and Soleimani, S. (2005). “Flexural response of hybrid fiber-reinforced cementitious composites”. *ACI Materials Journal*, V. 102, No. 6, pp. 382-389.

Barluenga G., and Hemández-Olivares F. (2007). “Cracking control of concrete modified with short AR-glass fibers at early age; Experimental results on standard concrete and SCC”. *Cement and Concrete Research*, Vol. 37, No. 12, pp. 1624 – 1638.

Bharatkumar, B., Narayanan, R., Raghuprasad, B., and Ramachandramurthy, D. (2001). "Mix proportioning of high performance concrete". *Cement & Concrete Composites,* Vol. 23, No. 1, pp. 71-80.

Brown, M., Ozyildirin, C., and Duke, W. (2010). "Investigation of fiber-reinforced self-consolidating concrete". Virginia transportation research council. Charlottesville, Virginia, USA.

Brown, M., Ozyildirim, C., and Duke W. (2010). "Investigation of steel and polymer fiber-reinforced self-consolidating concrete". *ACI SP-274-5, American Concrete Institute*, Farmington Hills, Michigan, USA, pp. 69-78.

CAN/CSA-A23.3-04, (2004). "Design of concrete structures". *Canadian Standard Association*, Rexdale, Ontario, Canada, 240p.

Carlswärd, J., and Emborg, M. (2010). "Prediction of stress development and cracking in steel fiber-reinforced self-compacting concrete overlays due to restrained shrinkage". *ACI SP-274-3, American concrete institute*, Farmington Hills, Michigan, USA, pp. 31-50.

Chang C., Ho M., Song G., Mo L., and Li H. (2010) "Improvement of electrical conductivity in carbon fiber-concrete composites using self-consolidating technology". *Earth and Space 2010: Engineering, Science, Construction, and Operation in Challenging Environments*, Honolulu, pp. 3553-3558.

Chung D. (2000) "Cement reinforced with short carbon fibers: a multifunctional material". *Composites*. Part B., Vol. 31 No. 6-7, pp. 511-526.

Chung D. (1992). "Carbon fiber reinforced concrete". *Strategic highway research program: National Research Council*, University of New York, Buffalo, USA.

Chung D., and Chen P. (1993). “Concrete reinforced with up to 0.2 vol% of short carbon fibers”. *Composites*, Vol. 24, No. 1, pp. 33-52.

Cunha, V., Barros, J., and Sena-Cruz, J. (2010). “Tensile behavior of steel fiber-reinforced self-compacting concrete”. *ACI SP-274-4, American Concrete Institute*, Farmington Hills, Michigan, USA, pp. 51-68.

Daczko, J. (2012). “Self-consolidating concrete: ch. 4 hardened properties of SCC”. New York, USA.

De schutter, G. (2005). “Guidelines for testing fresh self-compacting concrete”. *European research project: Measurement of properties of fresh self-compacting concrete*. pp. 1-7.

Ding, Y., You, Z., and Jalali, S. (2011). “The composite effect of steel fibers and stirrups on the shear behaviour of beams using self-consolidating concrete”. *Engineering Structures*, Vol. 33, No. 1, pp. 107-117.

Douglas, R. P. (2004). “Properties of self-consolidating concrete containing type F fly ash: with a verification of the minimum paste volume method,” Masters of Applied Science Thesis, Northwestern University, USA.

EFNARC. (2002). “Specification and guidelines for self-compacting concrete”. *European Federation of Supplies of Specialist Construction Chemicals*, Farnham, Surrey, UK.

Ferraris C. F., Brower L., Ozyildirim C., and Daczko J. (2000). “Workability of self-compacting concrete”. *Preeeding of the PCI/FHWA/FIB international symposium on high performane concrete*. Precast/prestressed Concrete Institute, Chicago, pp. 398-407.

Ferrara, L. Prisco, M., and Ozyurt, N. (2010). "Self-consolidating high-performance SFRC: an example of structural application in Italy". *ACI SP-274-8, American Concrete Institute,* Farmington Hills, Michigan, USA, pp. 109-128.

Forgeron, D., and Omer, A. (2010). "Flow characteristics of macro-synthetic fiber-reinforced self-consolidating concrete". *ACI SP-274-1, American Concrete Institute,* Farmington Hills, Michigan, USA, pp. 1-14.

Gao D., Mo L., and Peng L. (2010). "Mechanical and electrical properties of carbon-nanofiber self-consolidating concrete". *Earth and Space 2010: Engineering, Science, Construction, and Operation in Challenging Environments,* Honolulu, pp. 2577-2585.

Gao D., Mo L., and Peng L. (2011). "Electrical resistance of self-consolidating concrete containing carbon nanofibers". *Journal of Sichuan University (Engineering Science Edition),* Vol. 43, No. 5, pp. 52-58.

Goodier. C. (2003). "Development of self-compacting concrete". *Structures and buildings 156, Proceeding of the Institution of Civil Engineers,* London, SB4, pp. 405-414.

Greenough, T., and Nehdi, M. (2008). "Shear behavior of fiber-reinforced self-consolidating concrete slender beams". *ACI Materials Journal,* V. 105, N0.5, pp. 468-477.

Grünewald, S., and Walraven, J. (2010*).* "Maximum fiber content and passing ability of self-consolidating fiber-reinforced concrete". *ACI SP-274-2, American concrete institute,* Farmington Hills, Michigan, USA, pp. 15-30.

Grünewald, S., Walraven, J., Emborg, M., Carlswärd, J., and Hedin C. (2004). "Summary report of workpackage 3.1 Test methods for filling ability of SCC". Delft University of Technology. Betongindustri, pp. 1-6.

Hadiwidodo, Y., and Mohd, S., (2005). "Review of testing methods for self compacting concrete". *International Conference on Construction and Building Technology 2008 – A – (05),* pp. 69-82.

Hitchen, S., Ogin, L., and Smith P. (1995). "Effect of fiber length on fatigue of short carbon fiber/ epoxy composite". *Composites*. Vol. 29, No. 4, pp. 303-308.

Ivorra, S., Garcés, P., Catalá, G., Andión, L., and Zornoza, E. (2009). "Effect of silica fume particle size on mechanical properties of short carbon fiber reinforced concrete". *Materials and design*, Vol. 31, No. 3, pp. 1553-1558.

Khayat, K. H. (2000). "Optimization and performance of air-entrained, self-consolidating concrete". *ACI Materials Journal*, Vol. 97, No. 5, pp. 526-535.

Khrapko, M. "Self-compacting concrete – a solution for technology hungry concrete construction". CBE consultancy Ltd., Finland.

Kosmatka, S., Kerkhoff, B., and Panarese, W. (2002). "Design and control of concrete mixtures". *14th edition, Portland Cement Association*, Skokie, Illinois, USA.

Liao, W., Chao, S., Park, S., and Naaman, A. (2006) "Self-consolidating high performance fiber reinforced concrete". University of Michigan, USA, 0-10.

Liao, W., Chao, S., and Naaman, A. (2010). "Experience with self-consolidating high-performance fiber-reinforced mortar and concrete". *ACI SP-274-6, American Concrete Institute*, Farmington Hills, Michigan, USA, pp. 79-94.

Mobasher, B., and Destrée, X. (2010). "Design and construction aspects of steel fiber-reinforced concrete elevated slabs". *ACI SP-274-7, American Concrete Institute*, Farmington Hills, Michigan, USA, pp. 95-108.

Nagataki, S., and Fujiwara, H. (1995). "Self-compacting property of high flowable concrete". *Proceedings of the second CANMET/ACI international symposium on advances in concrete technology, SP-154*, V.M. Malhotra, ed., American Concrete Institute, Farmington Hills, Michigan, USA, pp. 301-314.

Nehdi M. and Ladanchuk J. (2004). "Fiber synergy in fiber-reinforced self-consolidating concrete". *ACI Material Journal*, USA, Vol. 101, No. 6, pp. 508-517.

Nehdi, M., Pardhan, M., and Koshowski, S. (2004). "Durability of self-consolidating concrete incorporating high-volume replacement composite cements". *Cement and Concrete Research*, Vol. 34, No. 11, pp. 2103-2112.

Okamura, H., (1997). "Self-compacting high-performance concrete". *Concrete International*, Farmington Hills, Vol. 19, No. 7, pp. 50-54.

Okamura, H. and Ouchi, M. (1999). "Self-compacting concrete. Development". *Present use and future. 1st International RILEM symposium on self –compacting concrete*, Stockholm, Sweden.

Okamura, H., and Ouchi, M. (2003). “Self-compacting concrete”. *Journal of Advanced Concrete Technology,* Vol. 1, No. 1, pp. 5-15.

Ouchi, M., Nakamura, S., Osterberg, T., Halberg, S., and Lwin, M. (2003). “Application of self-compaction in Japan”. *Europe and the United State. Federal Highway Administration*, Washington, D.C., U.S.A.

Perez N., Romero H., Hermida G., and Cuellar G. (2002). “Self-compacting concrete on the search and finding of an optimized design”. *Proceeding of the first North Amerian Conference on the design and use of self-consolidating concrete*. Hanley-Wood, LLC, Illinois, USA, pp. 101-107.

Ramachandran V. S. (1995). “Concrete admixtures handbook, Properties, Science, and Technology: Superplasticizers”. Second edition. Park Ridge, New Jersey, USA, pp. 410-517.

Safiuddin, Md. (2008). “Development of self-consolidating high performance concrete incorporating rice husk ask”. Ph.D Thesis. University of Waterloo, Waterloo, ON, Canada.

Safiuddin, Md. (2010). “High performance mortar with carbon fibers: Properties and mix optimization”. Saarbrücken, Germany.

Safiuddin, Md., West, J.S., and Soudki, K. A. (2010). “Flowing ability of self-consolidating concrete and its binder paste and mortare component incorporating rice husk ash”. *NRC research press,* Can. J. Civ. Eng., Vol. 37, No. 3, pp. 401-412.

Schutter, G. (2005). “Measurement of properties of fresh self-compacting concrete”. *Guidelines for testing fresh self-compacting concrete*. University of Paisley, UK.

Srinivasa Rao P., Vishwanadh G., Sravana P., and Sekhar, T. (2009). "Flexural behaviour of reinforced concrete beams using self-compacting concrete". *34th conference on our world in concrete & structures*, Singapore.

Takefumi S., and Yasunori M. (2003). "Development of combination-type self-consolidating concrete and evaluation test method". *Journal of Advanced Concrete Technology*. Vol. 1, No. 1, pp. 26-36.

Yin, J., and Wu, Z., S. (2003). "Structural performance of short steel-fiber reinforced concrete beams with externally bonded FRP sheets". *Construction and Building Materials*, pp. 463-470.

Zhang, H., Zhong, Z., and Friedrich, K. (2007). "Effect of fiber length on the wear resistance of short carbon fiber reinforced epoxy composites". *Composites Science and Technology*, Vol. 67, No. 2, pp. 222-230.

# Appendix A

## Flexural design:

| **Beam length:** | | |
|---|---|---|
| L | 2400 | mm |
| a | 800 | mm |
| b | 500 | mm |

| | | |
|---|---|---|
| Cover | 30 | mm |
| Φ stirrups | 6 | mm |
| Φ' | 10M | |

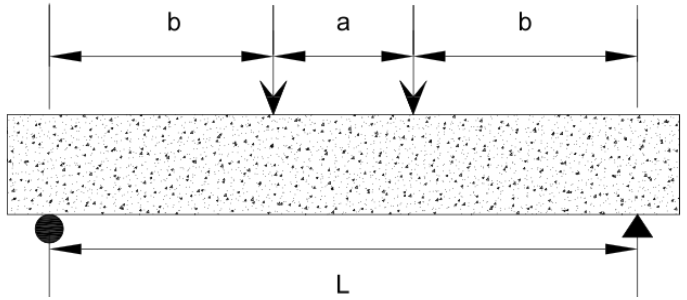


| **Section properties:** | | |
|---|---|---|
| b | 150 | mm |
| h | 300 | mm |
| d | 256.5 | mm |
| $d_v$ | 230.85 | mm |

| | |
|---|---|
| a/d | 3.1 |

| | | |
|---|---|---|
| No. | 2 | |
| Φ | 15 | 15M |
| $A_s$ | 353.25 | $mm^2$ |
| d' | 41 | mm |
| $A_s'$ | 200 | $mm^2$ |
| As stirrup | 56.52 | $mm^2$ |

| **Concrete and steel properties:** | | |
|---|---|---|
| $f'_c$ | 40 | MPa |
| $f_y$ | 400 | MPa |
| $E_s$ | 200000 | MPa |
| $\theta_c$ | 1 | |
| $\theta_s$ | 1 | |

**Calculation of bending moment:**

| P | |
|---|---|
| 82 | kN |

| α | β | ρ | ρ' | $K_r$ | $K_r'$ | $M_r$ | $M_f=P\times a/2$ | $P=Mr\times 2/a$ | P/2 |
|---|---|---|---|---|---|---|---|---|---|
| 0.790 | 0.870 | 0.00398 | 0.00520 | 1.553 | 1.747 | 32.57 | 32.8 | 81.42 | 41 |

| $\rho_b$ | 0.0437 |
|---|---|

**Calculation of shear:**

**Simplified method:**

| β | θ | $V_f$ | $V_c$ | S | $V_r$ max | $0.125\times\lambda\times\Phi\times C\times f'_c\times b_w\times d_v$ | s required | $S_{used}$ | $V_s$ | $V_r$ |
|---|---|---|---|---|---|---|---|---|---|---|
| 0.21 | 42 | 41 | 45.99 | -2321 | 346.2 | 173.14 | 161.60 | 133.5 | 86.8 | 132.8 |

## Shear design:

**Beam length:**

| | | | | | |
|---|---|---|---|---|---|
| L | 2400 | mm | Cover | 30 | mm |
| a | 800 | mm | a/d | 2.7 | |
| b | 500 | mm | | | |

**Beam Section:**

| | | | |
|---|---|---|---|
| b | 150 | mm | |
| h | 350 | mm | |
| d | 294 | mm | |
| dv | 264.6 | mm | |
| Φ | 20 | 20M | |
| No. | 4 | *bandeld* | |
| As | 1256 | $mm^2$ | |
| d' | 40.5 | mm | |
| $A_s'$ | 353.25 | $mm^2$ | 2-15M bar |
| As stirrup | 56.52 | $mm^2$ | 6M bar |

**Concrete and steel properties:**

| | | |
|---|---|---|
| $f'_c$ | 40 | MPa |
| $f_y$ | 400 | MPa |
| $E_s$ | 200000 | MPa |
| $\theta_c$ | 1 | |
| $\theta_s$ | 1 | |

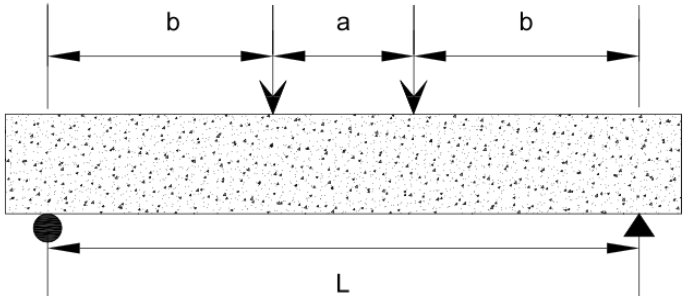

**Calculation of bending moment:**

| P | 270 | kN | | | | | | |
|---|---|---|---|---|---|---|---|---|
| α | β | ρ | ρ' | $K_r$ | $K_r'$ | $M_r$ | $M_f=P\times a/2$ | $P_r$ |
| 0.790 | 0.870 | 0.02047 | 0.00801 | 7.127 | 2.763 | 128.23 | 108 | 320.6 |
| $\rho_b$ | 0.0437 | | | | | | | |

**Calculation of shear:**

**Simplified method:**

| β | θ | $V_f$ | $V_c$ | S | $V_r$ max | | S maximum | $V_s$ | $V_r$ | $V_f$ | $S_{used}$ |
|---|---|---|---|---|---|---|---|---|---|---|---|
| 0.21 | 42 | 135 | 52.7 | 161.39 | 396.9 | 198.45 | 185.22 | 59.8 | 112.6 | 135 | 180 |

**General method:**

| $M_f$ | $V_f$ | $\varepsilon_x$ | β | θ | $V_c$ | S | $V_{r\,max}$ | | $s_{max}$ | $s_{used}$ | $V_s$ | $V_r$ |
|---|---|---|---|---|---|---|---|---|---|---|---|---|
| 72.3 | 135 | 0.00081 | 0.18 | 34.7 | 45.3 | 192.63 | 396.9 | 198.45 | 185.22 | 180 | 48.0 | 93.3 |

**Check:**

Pr(flexure)/Pr(shear)

2.85 %

Mr/Vr

1.14 %

## Design of CFRSCC mixtures:

**Sample #1 for W/B of 0.35**

| **Mix Design proportion:** | | | | | | |
|---|---|---|---|---|---|---|
| W/B ratio | 0.35 | | | | | |
| Water Weight | 189.85 | First estimate of water from Table 2.3 | | | | |
| Oven Dry Unit Weight | 115 | | | | | |
| Relative Density (dry) | 2.65 | | | | | |
| Void Content % | 30.45 | | | | | |
| The Mixing Water Adjustment | -21.56 | $Kg/m^3$ | | | | |
| The Total Mixing Water Required | 168.29 | $Kg/m^3$ | | | | |
| Binder | 480.82 | kg | | | | |
| Silica Fume 10% | 48.08 | kg | | | | |
| Air Entrapped % | 2 | | | | | |
| Cement | 432.74 | | | | | |
| Carbon Fibers % | **0** | | | | | |
| | 0.0 | | | | | |
| HRWR 1% of Binder | **1.5** | | | | | |
| | 7.212 | kg | | | | |
| Solids Contents of HRWR (%) | 0.330 | | | | | |
| Sand/Aggregate ratio | 0.55 | | | | | |
| Concrete Component: | Coarse | Fine | Silica Fume | Cement | Carbon | HRWR |
| Relative Density(SSD) | 2.74 | 2.68 | 2.2 | 3.15 | 1.9 | 1.064 |
| Absorption(OD) % | 1.13 | 1.15 | - | - | - | - |
| Moisture Content % | 0.393 | 0.144 | - | - | - | - |
| Bulk Density $kg/m^3$ | - | 1843.14 | - | - | | - |
| Absorption(AD) % | 1.264 | 1.15 | - | - | - | - |

| **Calculation of concrete mixture:** | | | | |
|---|---|---|---|---|
| W/B | 0.35 | | | |
| Water Weight | 168.29 | kg | 0.16875 | $m^3$ |
| Cement | **432.74** | kg | 0.13775 | $m^3$ |
| Silica Fume | **48.08** | kg | 0.02192 | $m^3$ |
| HRWR | **7.21** | kg | 0.00680 | $m^3$ |
| Carbon | **0.00** | kg | 0.00000 | $m^3$ |
| Total | | | 0.3352 | |
| FA | | | 0.55*TA/2.68*997.28 | |
| CA | | | 0.45*TA/2.74*997.28 | |
| The absolute volume of total agg. | | | 1742.6739 | |
| FA | 958.47 | kg | | |
| CA | 784.20 | kg | | |
| Adjusted FA | **948.92** | kg | | |
| Adjusted CA | **777.43** | kg | | |
| Adjusted Water | **179.77** | kg | | |

## Sample #1 for W/B of 0.40

| **Mix Design proportion:** | | |
|---|---|---|
| W/B ratio | 0.40 | |
| Water Weight | 189.85 | First estimate of water from Table 2.3 |
| Oven Dry Unit Weight | 115 | |
| Relative Density (dry) | 2.65 | |
| Void Content % | 30.45 | |
| The Mixing Water Adjustment | -21.56 | $Kg/m^3$ |
| The Total Mixing Water Required | 168.29 | $Kg/m^3$ |
| Binder | 480.82 | kg |
| Silica Fume 10% | 48.08 | kg |
| Air Entrapped % | 2 | |
| Cement | 378.65 | |
| Carbon Fibers % | **0** | |
| | 0.0 | |
| HRWR 1% of Binder | **1.00** | |
| | 4.207 | kg |
| Solids Contents of HRWR (%) | 0.330 | |
| Sand/Aggregate ratio | 0.55 | |

| Concrete Component: | Coarse | Fine | Silica Fume | Cement | Carbon | HRWR |
|---|---|---|---|---|---|---|
| Relative Density (SSD) | 2.74 | 2.68 | 2.2 | 3.15 | 1.9 | 1.064 |
| Absorption (OD) % | 1.13 | 1.15 | - | - | - | - |
| Moisture Content % | 0.393 | 0.144 | - | - | - | - |
| Bulk Density $kg/m^3$ | - | 1843.14 | - | - | | - |
| Absorption (AD) % | 1.264 | 1.15 | - | - | - | - |

| **Calculation of concrete mixture:** | | | | |
|---|---|---|---|---|
| W/B | 0.40 | | | |
| Water Weight | 168.29 | kg | 0.16875 | $m^3$ |
| Cement | **378.65** | kg | 0.12053 | $m^3$ |
| Silica Fume | **42.07** | kg | 0.01918 | $m^3$ |
| HRWR | **4.21** | kg | 0.00396 | $m^3$ |
| Carbon | **0.00** | kg | 0.00000 | $m^3$ |
| Total | | | 0.3124 | |
| FA | | | 0.55*TA/2.68*997.28 | |
| CA | | | 0.45*TA/2.74*997.28 | |
| The absolute volume of total agg. | | | 1804.27 | |
| FA | 992.35 | kg | | |
| CA | 811.92 | kg | | |
| Adjusted FA | **982.46** | kg | | |
| Adjusted CA | **804.91** | kg | | |
| Adjusted Water | **182.36** | kg | | |

## Calculation of aggregates properties:

### Relative Density and Absorption of Fine Aggregates:

| Sample ID | Pan. Wt.(g) | Water Temp. C | Pycnomete Wt (g) | Pycnometer sand Wt. g | SSD Wt sand | Sand, Water Pycnometer | Mass of water Pycnometer | Oven Dry Wt.Pan (g) | Oven Dry Wt. (g) |
|---|---|---|---|---|---|---|---|---|---|
| | | | | | [D] | [C] | [B] | | [A] |
| A | 149.48 | 23 | 165.9 | 664 | 498.1 | 976.39 | 664.38 | 691.66 | 492.18 |
| B | 122.72 | 22.1 | 166.73 | 667.43 | 333.97 | 874.32 | 664.38 | 452.86 | 330.14 |
| C | 183.57 | 21.7 | 165.46 | 669.24 | 503.78 | 979.92 | 663.68 | 681.82 | 498.25 |

**Calculation**

| Sample | BRD | SSD | Apparent S.G. | Absorption % |
|---|---|---|---|---|
| A | 2.64 | 2.68 | 2.73 | 1.20 |
| B | 2.66 | 2.69 | 2.75 | 1.16 |
| C | 2.66 | 2.69 | 2.74 | 1.11 |
| | | | | |
| Average | 2.65 | 2.69 | 2.74 | 1.16 |

*SSD: Surface saturated dry, BRD: Bulk relative density, Apparent S.G: Apparent specific gravity.*

**Relative Density and Absorption of Coarse Aggregates:**

| Sample | Pan Wt. (g) | Saturated Surface-Dry (g) | Weight in Water (g) | Oven Dry Wt. with Pan (g) | Oven Dry Wt. without Pan g |
|---|---|---|---|---|---|
| | | [B] | [C] | | [A] |
| A | 150.06 | 1623.18 | 1030.95 | 1755.38 | 1605.32 |
| B | 152.65 | 1656.43 | 1052.12 | 1790.18 | 1637.53 |
| C | 149.65 | 1653.94 | 1051.25 | 1785.09 | 1635.44 |
| **Calculation** | | | | | |
| Sample | BRD | SSD | Apparent S.G | Absorption % | |
| A | 2.71 | 2.74 | 2.79 | 1.11 | |
| B | 2.71 | 2.74 | 2.80 | 1.15 | |
| C | 2.71 | 2.74 | 2.80 | 1.13 | |
| | | | | | |
| Average | 2.71 | 2.74 | 2.80 | 1.13 | |

*SSD: Surface saturated dry, BRD: Bulk relative density, Apparent S.G: Apparent specific gravity.*

# Appendix B

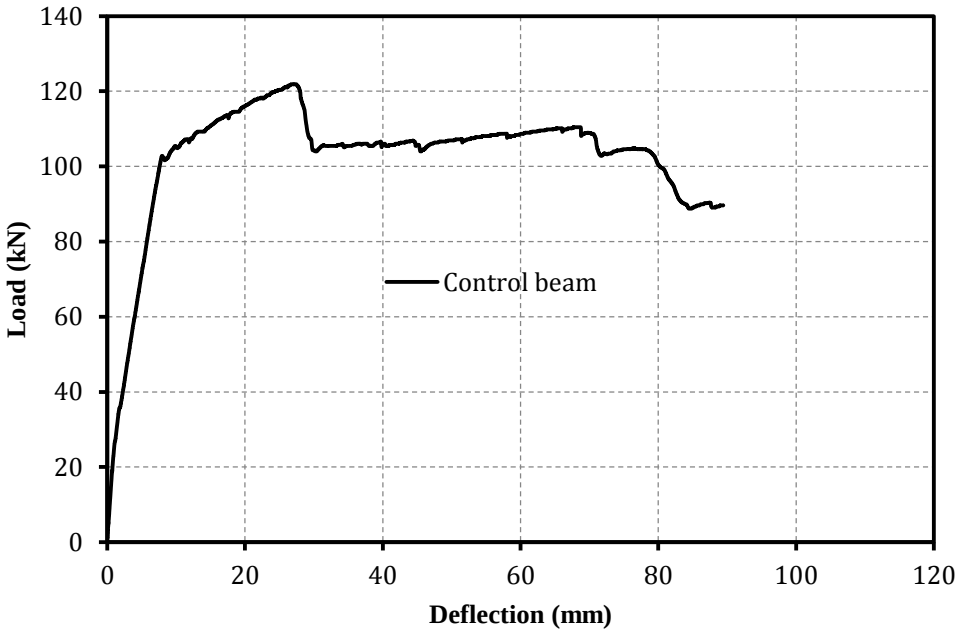


*Figure B.1 Flexural load vs. deflection curve of the control beam*

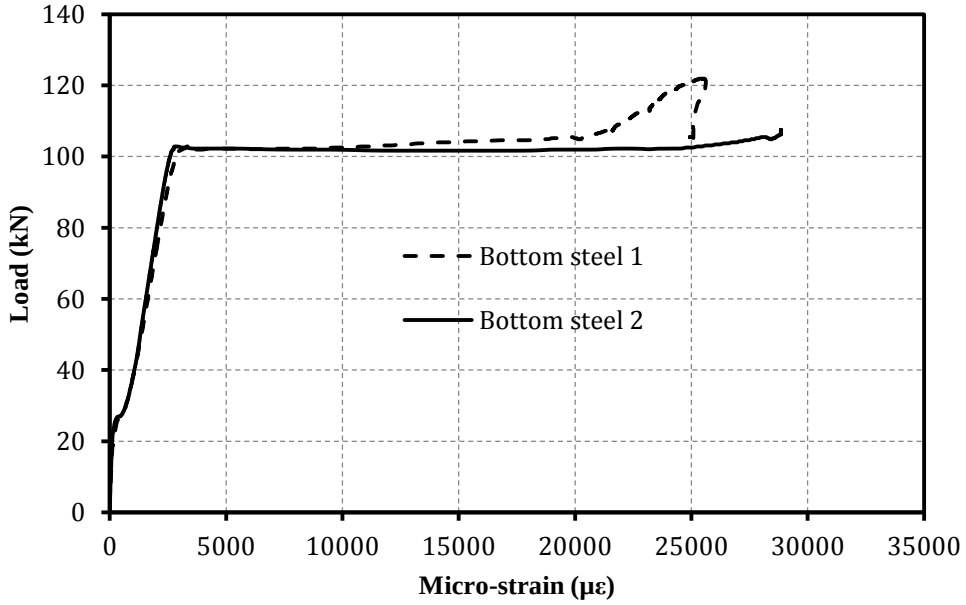


*Figure B.2 Bottom steel strain curves of the control beam*

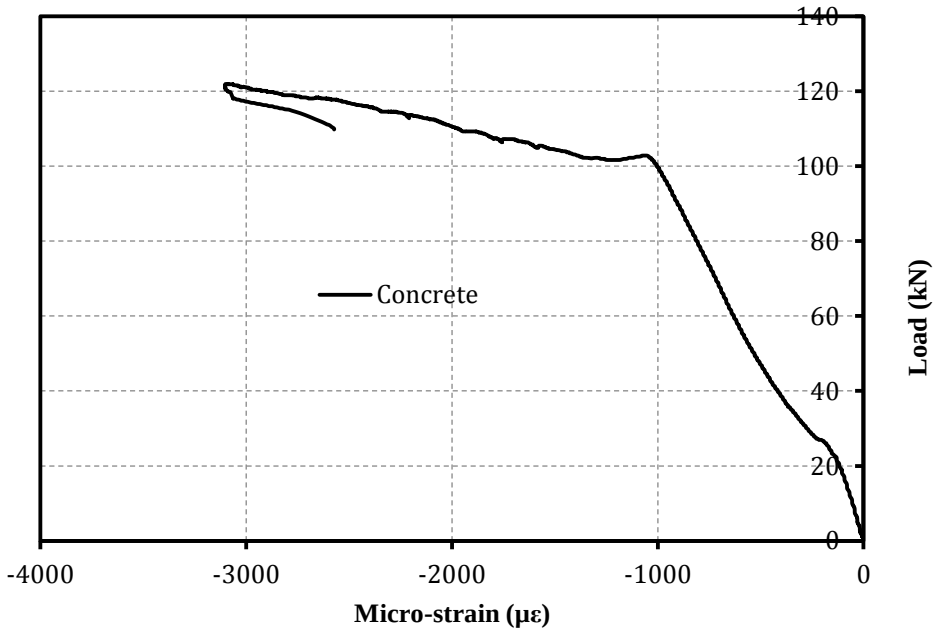


*Figure B.3 Concrete compression strain curve of the control beam*

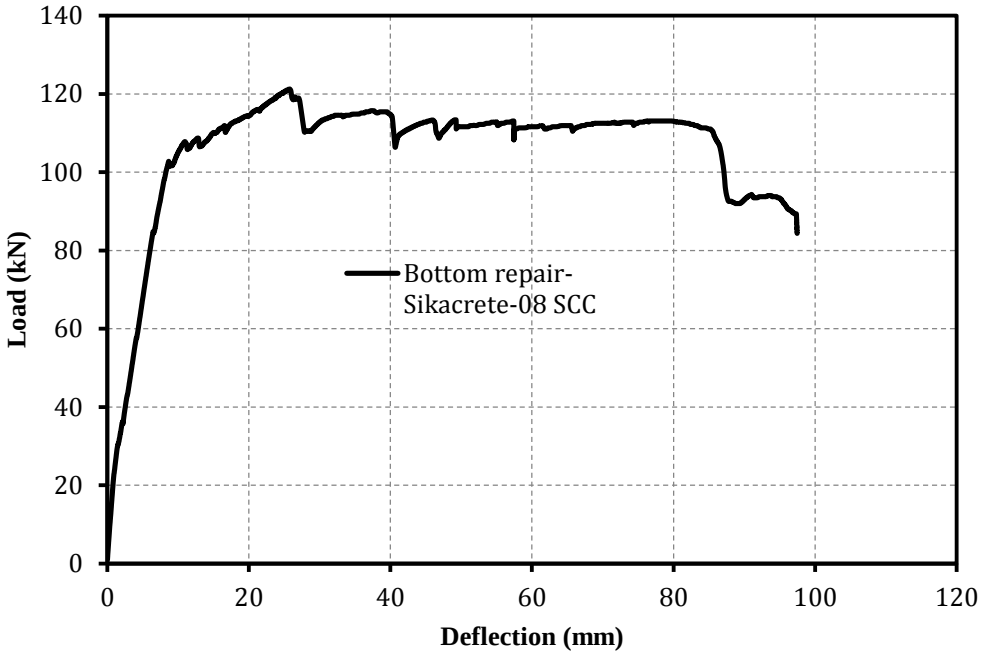


*Figure B.4 Flexural load vs. deflection curve of the bottom patch repaired beam with Sikacrete-08 SCC*

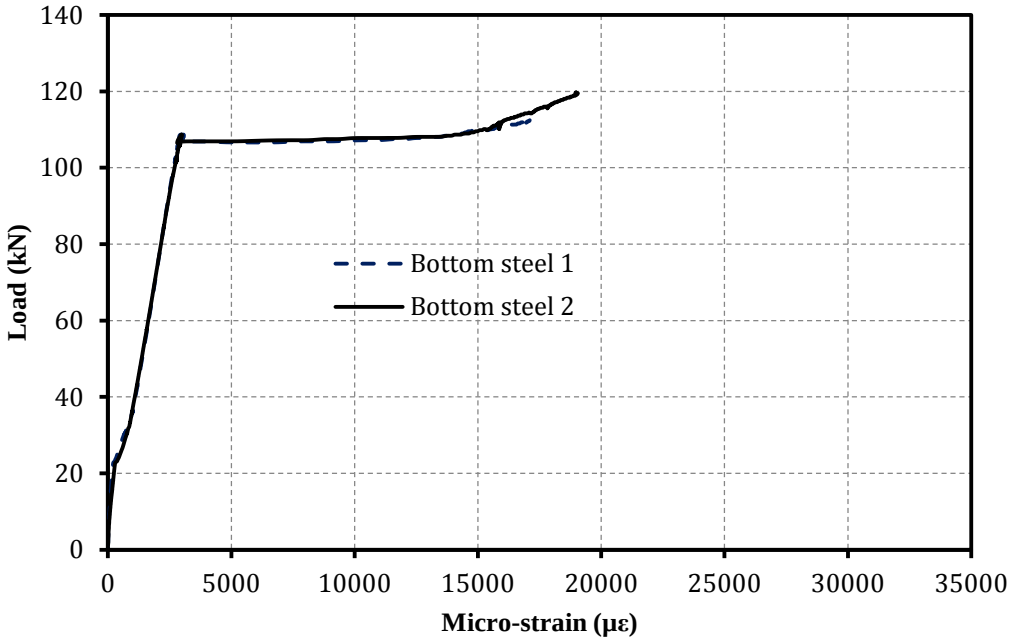


*Figure B.5 Bottom steel strain curves of the bottom patch repaired beam with Sikacrete-08 SCC*

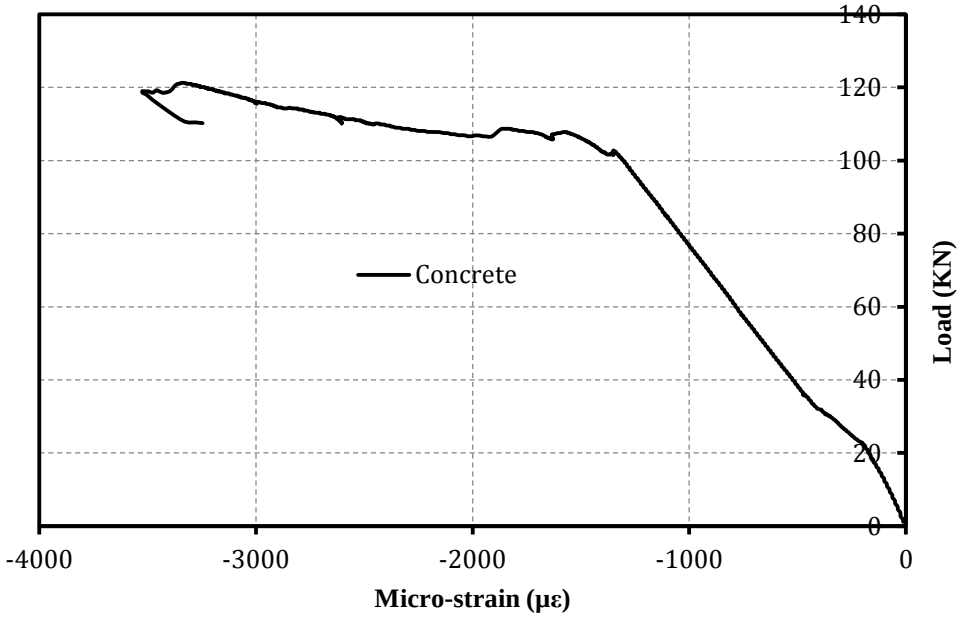


*Figure B.6 Concrete compression strain curve of the bottom patch repaired beam with Sikacrete-08 SCC*

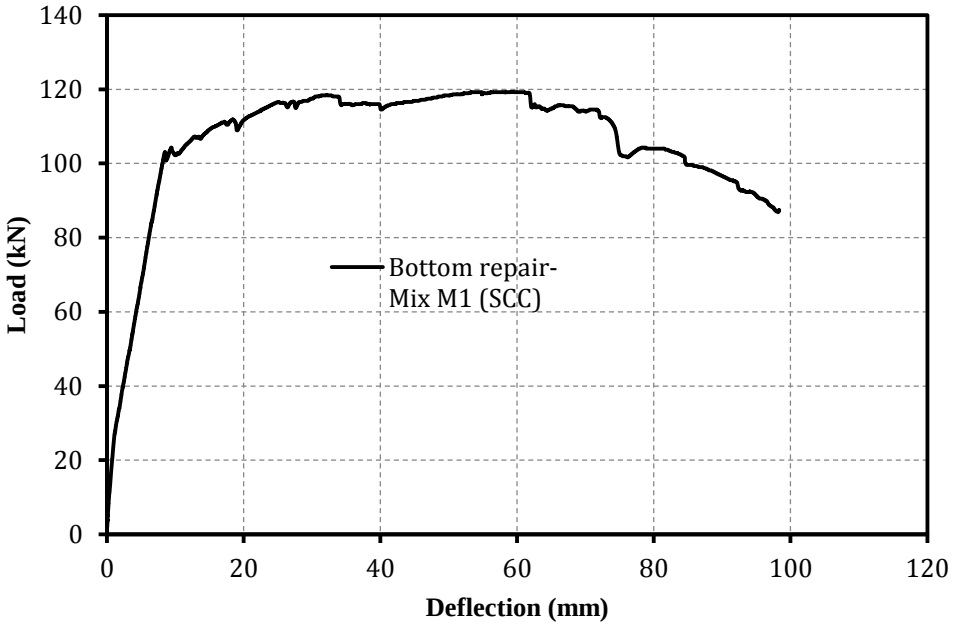


*Figure B.7 Flexural load vs. deflection curve of the bottom patch repaired beam with Mix M1 (SCC, 0%fibers)*

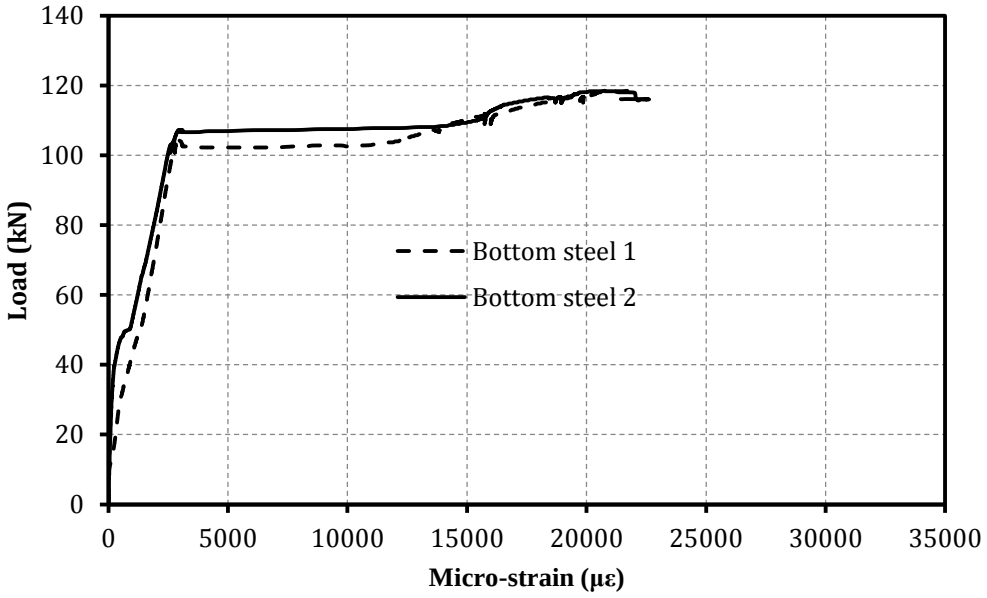


*Figure B.8 Bottom steel strain curves of the bottom patch repaired beam with Mix M1 (SCC, 0% fibers)*

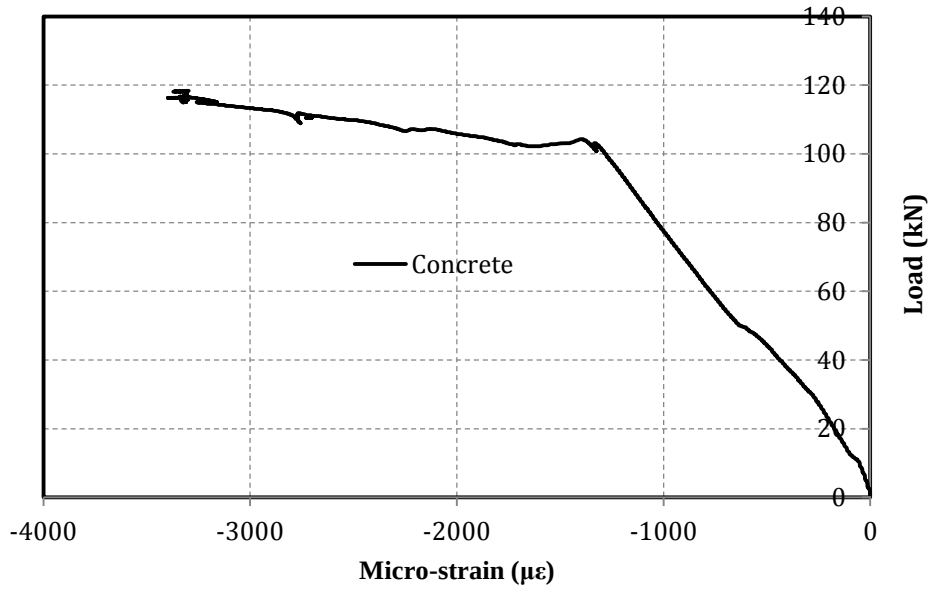


*Figure B.9 Concrete compression strain curve of the bottom patch repaired beam with Mix M1 (SCC, 0%fibers)*

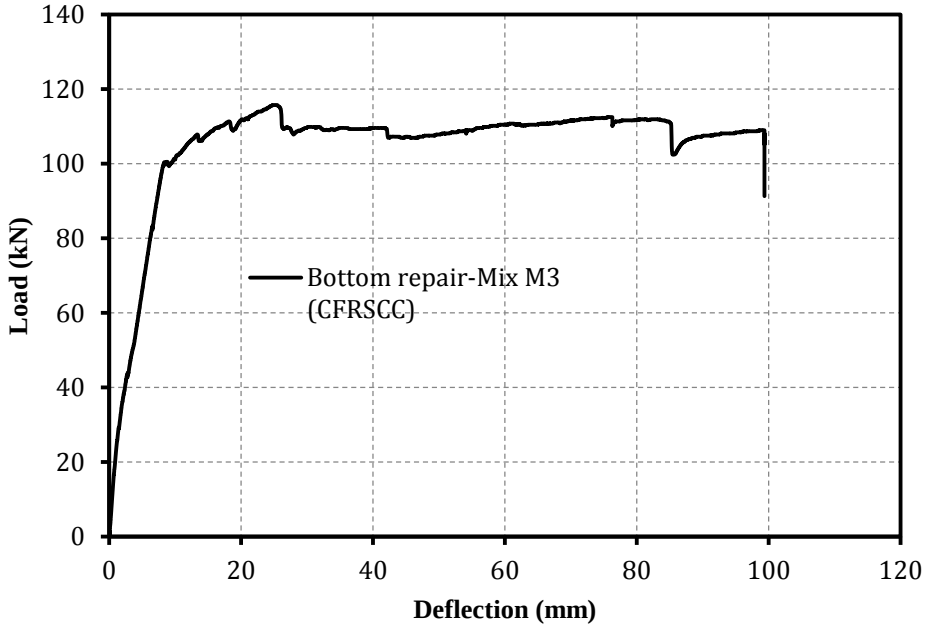


*Figure B.10 Flexural load vs. deflection curve of the bottom patch repaired beam with Mix M3 (CFRSCC, 0.5%fibers)*

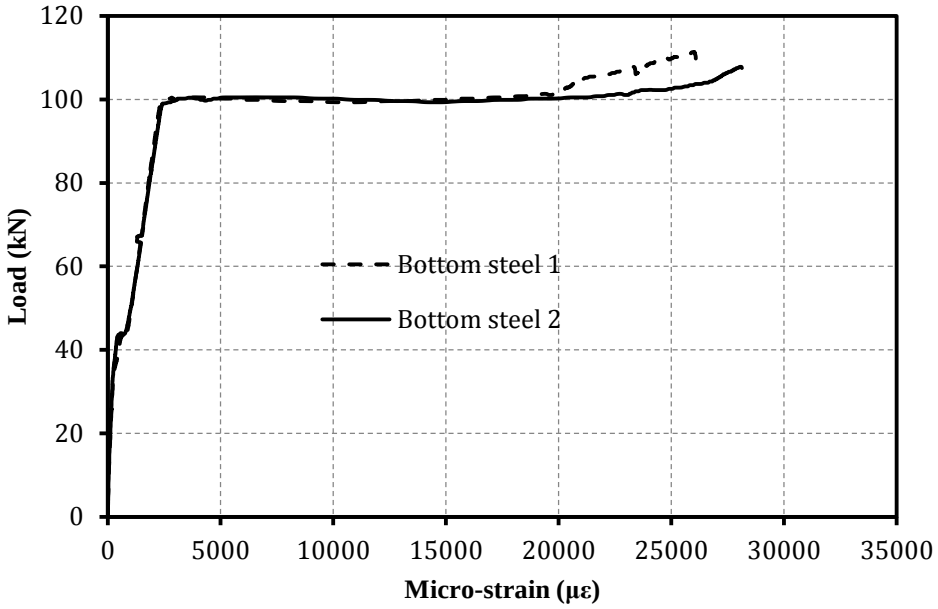


*Figure B.11 Bottom steel strain curves of the bottom patch repaired beam with Mix M3 (CFRSCC, 0.5% fibers)*

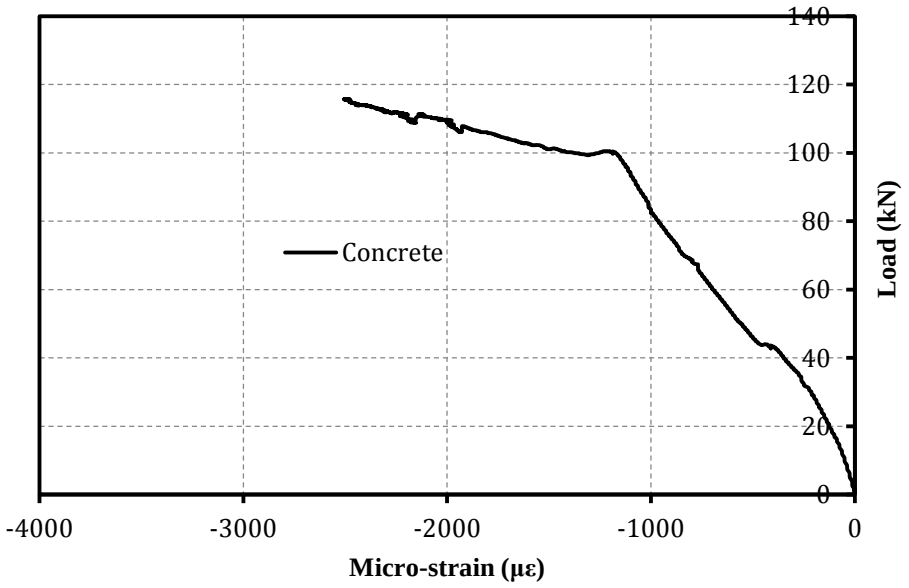


*Figure B.12 Concrete compression strain curve of the bottom patch repaired beam with Mix M3 (CFRSCC, 0.5% fibers)*

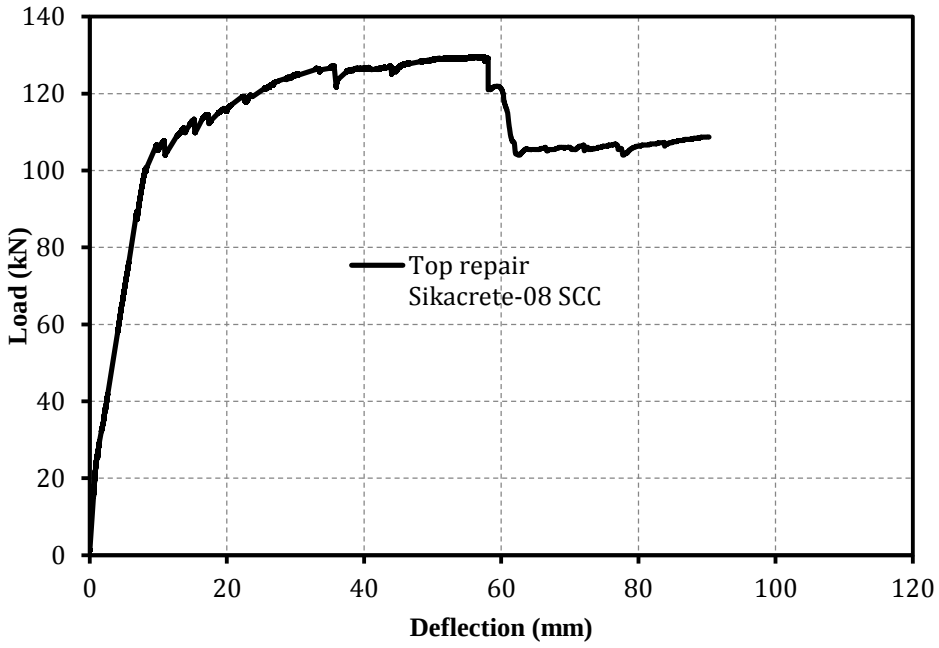


*Figure B.13 Flexural load vs. deflection curve of the top patch repaired beam with Sikacrete-08 SCC*

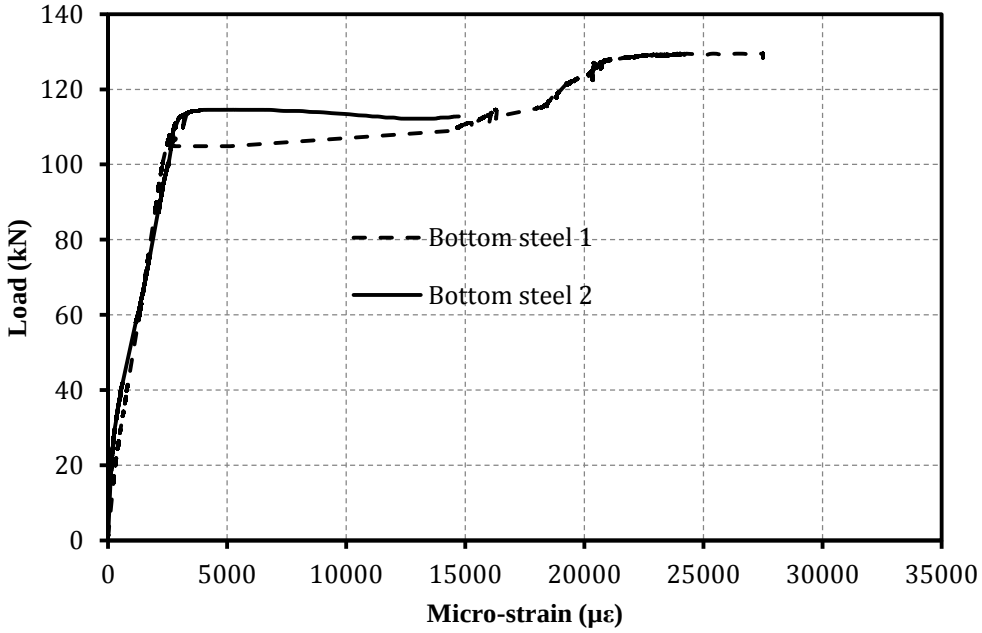


*Figure B.14 Bottom steel strain curves of the top patch repaired beam with Sikacrete-08 SCC*

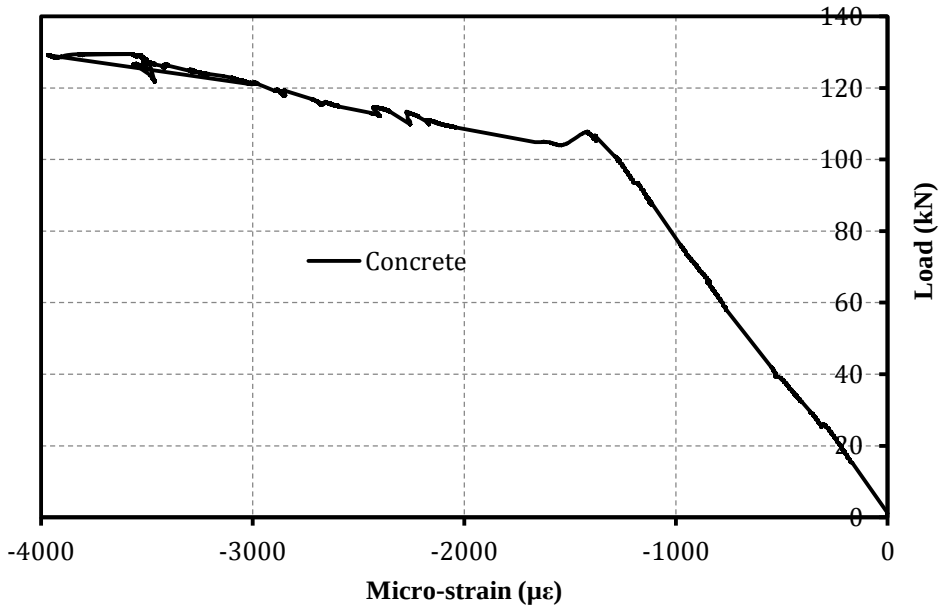


*Figure B.15 Concrete compression strain curve of the top patch repaired beam with Sikacrete-08 SCC*

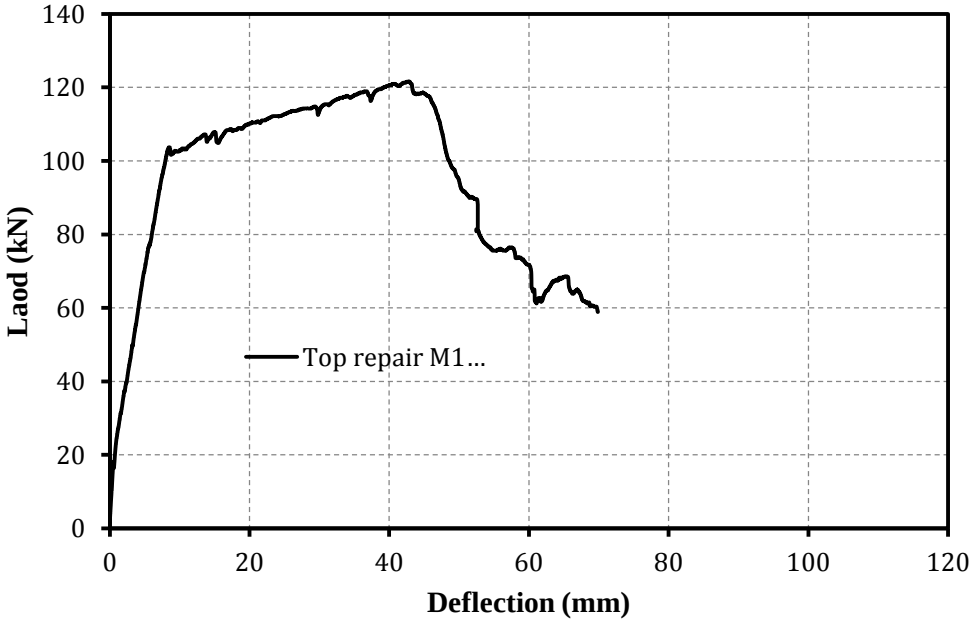


*Figure B.16 Flexural load vs. deflection curve of the top repaired beam with Mix M1 (SCC) 0% carbon fibers*

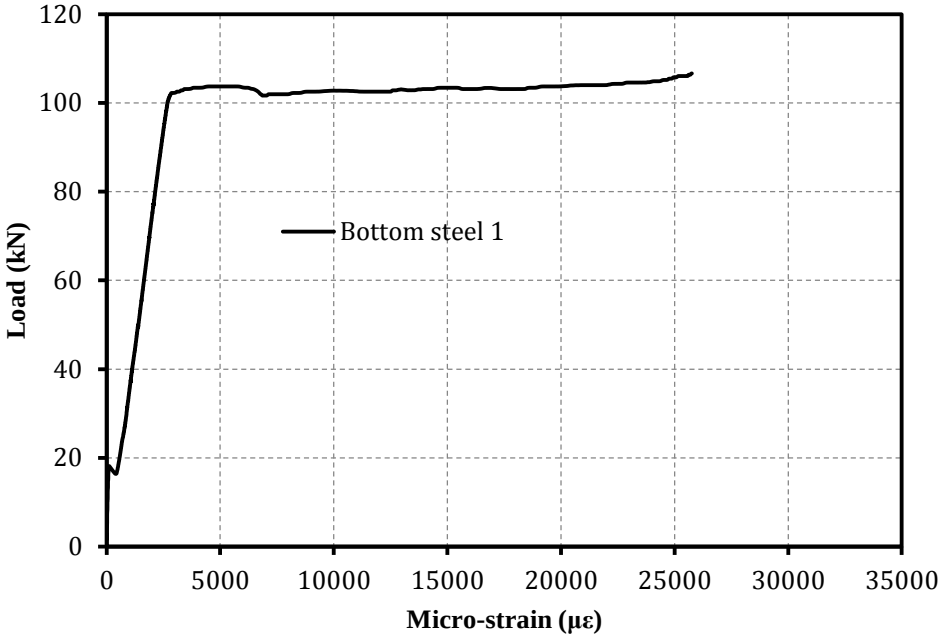


*Figure B.17 Bottom steel strain curves of the top patch repaired beam with Mix M1 (SCC, 0%fibers)*

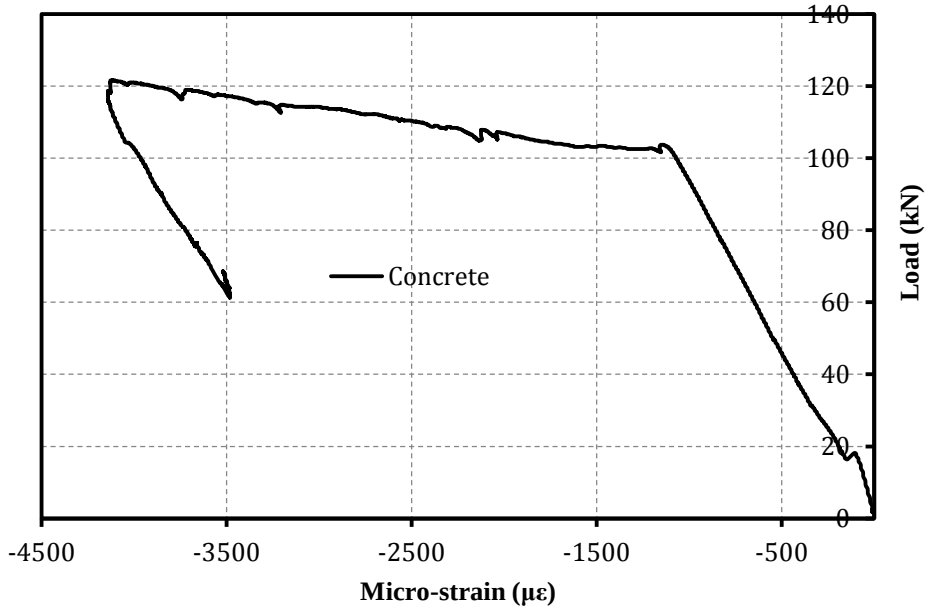


*Figure B.18 Concrete compression strain curve of the top patch repaired beam with Mix M1 (SCC, 0% fibers)*

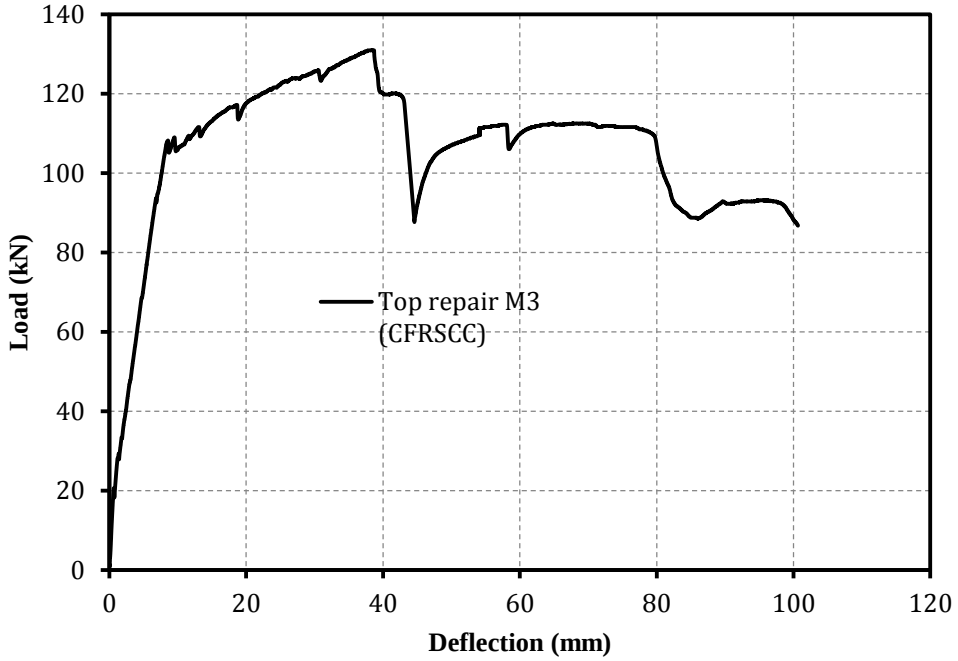


*Figure B.19 Flexural load vs. deflection curve of the bottom patch repaired beam with Mix M3 (CFRSCC, 0.5%fibers)*

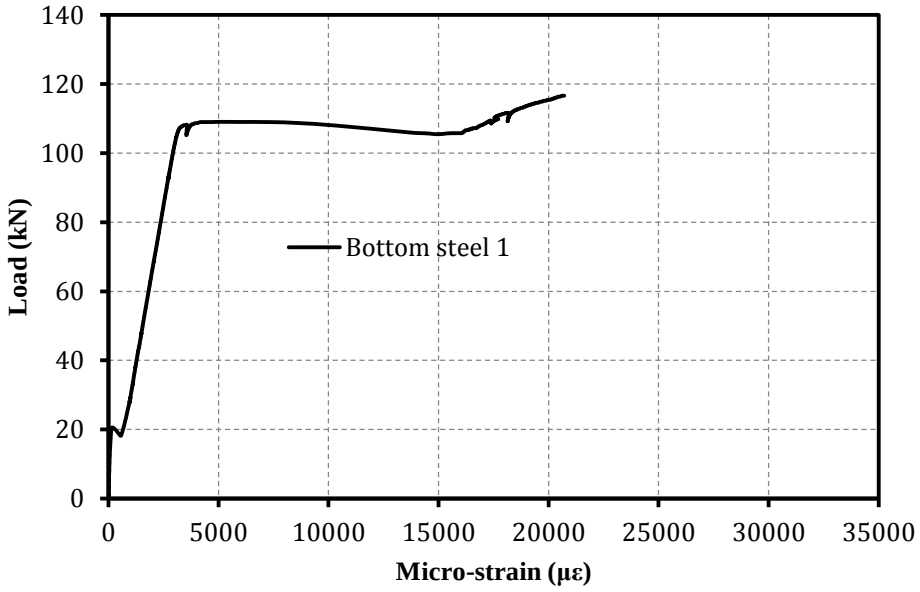


*Figure B.20 Bottom steel strain curve of the top patch repaired beam with Mix M3 (CFRSCC, 0.5%fibers)*

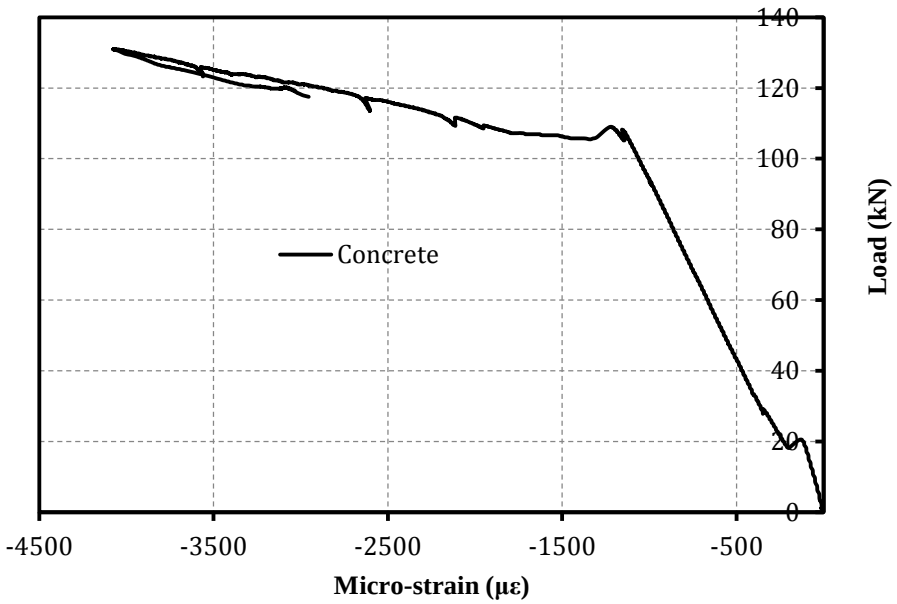


*Figure B.21 Concrete compression strain curve of the top patch repaired beam with Mix M3 (CFRSCC, 0.5% fibers)*

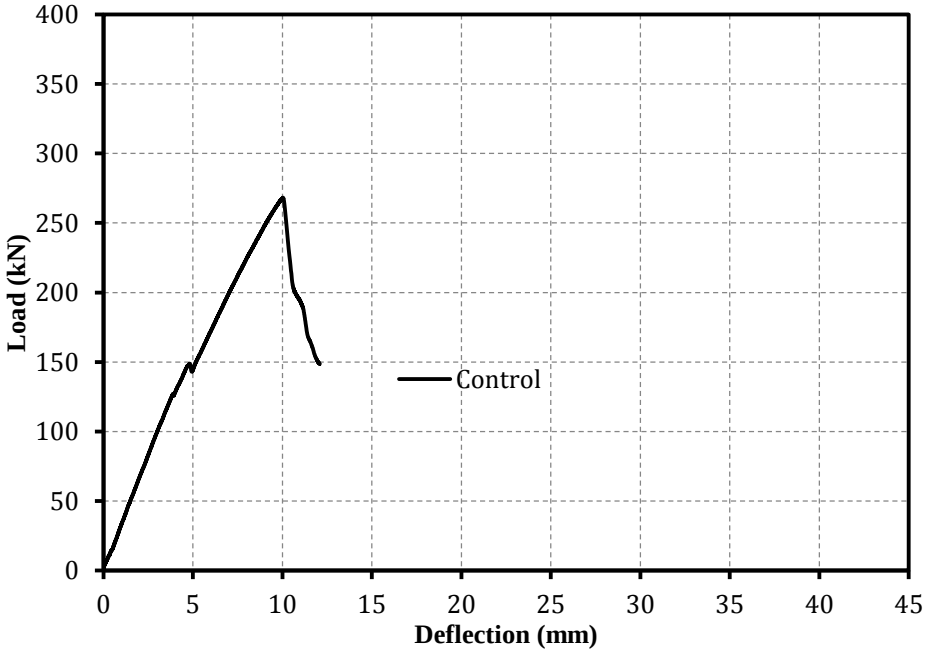


*Figure B.22 Shear load vs. deflection curve of the control*

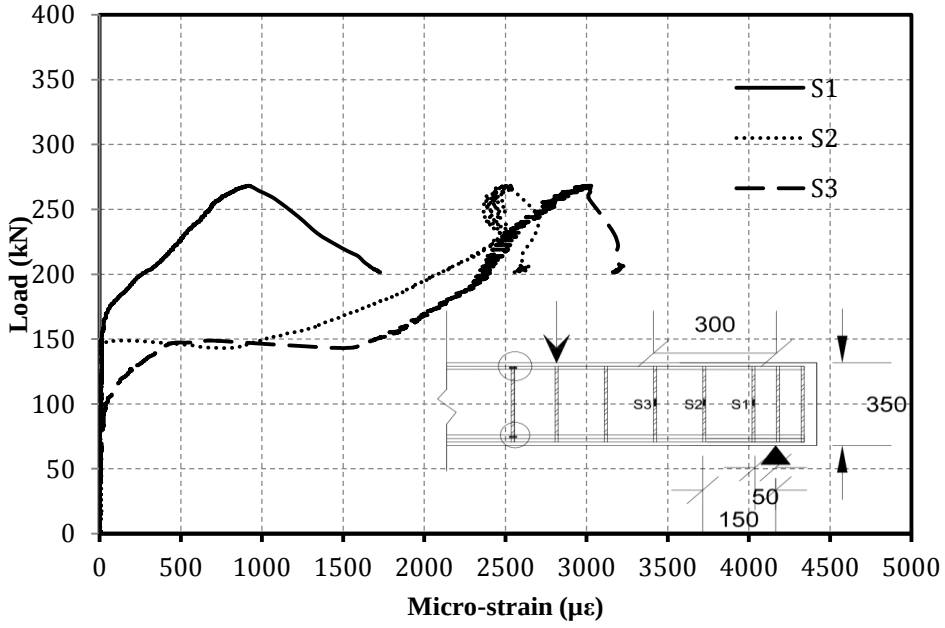


*Figure B.23 Strain curves on the stirrups of the control beam*

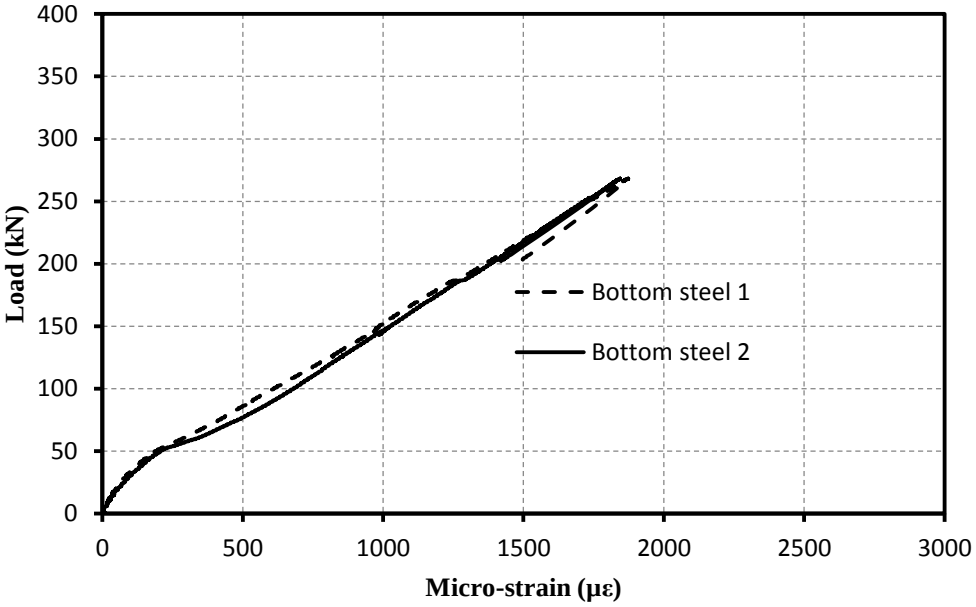


*Figure B.24 Bottom steel strain curves of the control beam*

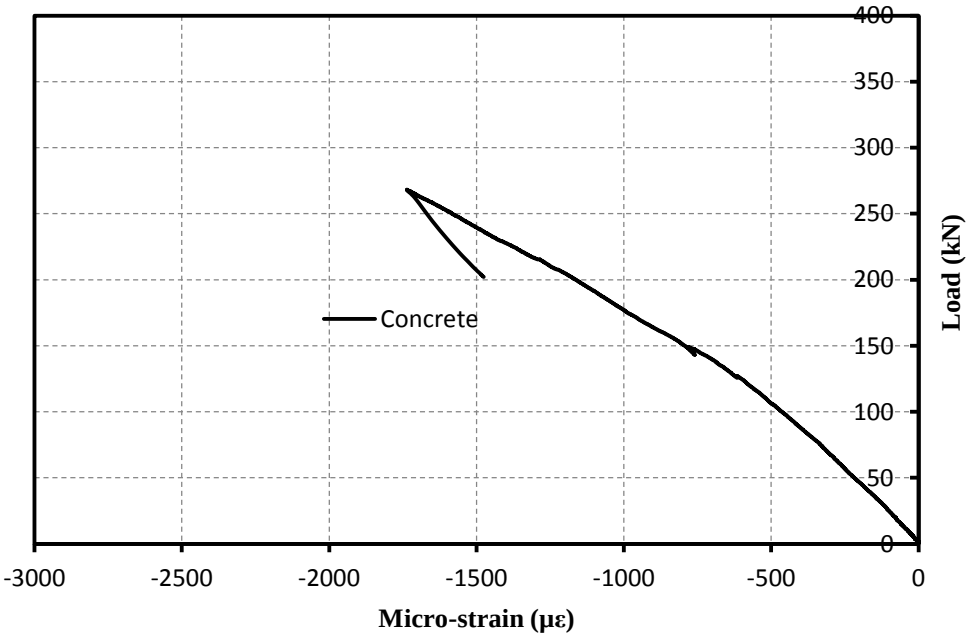


*Figure B.25 Concrete compression strain curve of the control beam*

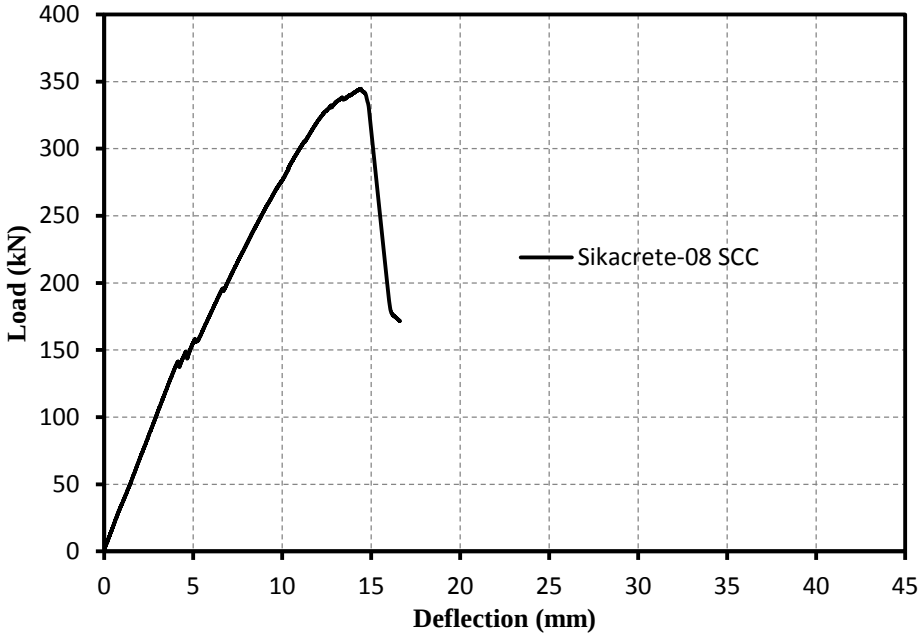


*Figure B.26 Shear load vs. deflection curve of the shear-span repaired beam with Sikacrete-08 SCC*

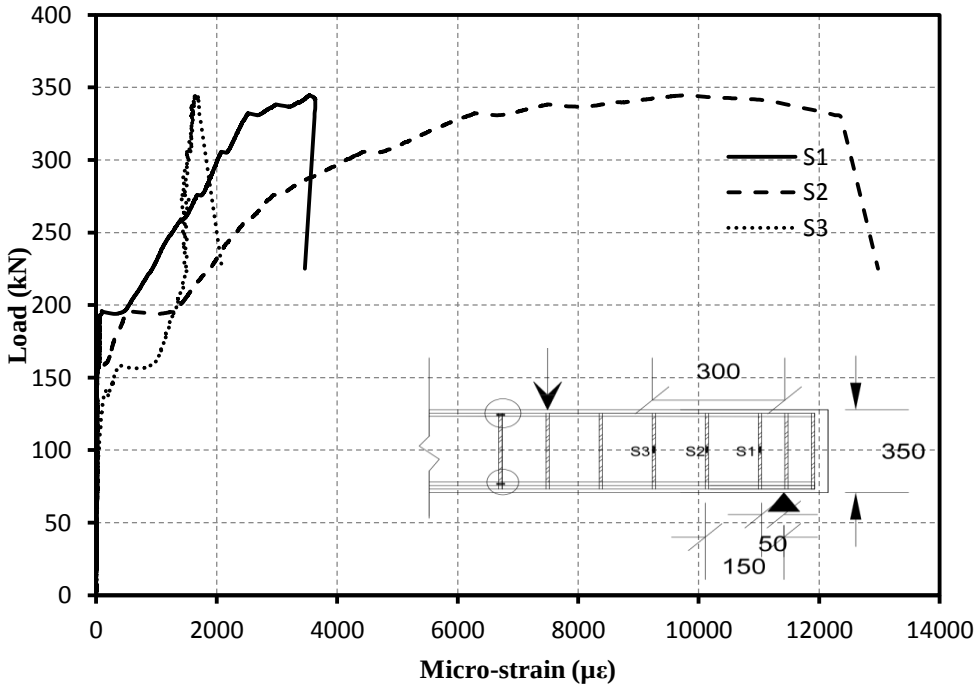


*Figure B.27 Strain curves on the stirrups of the shear-span repaired beam with Sikacrete-08 SCC*

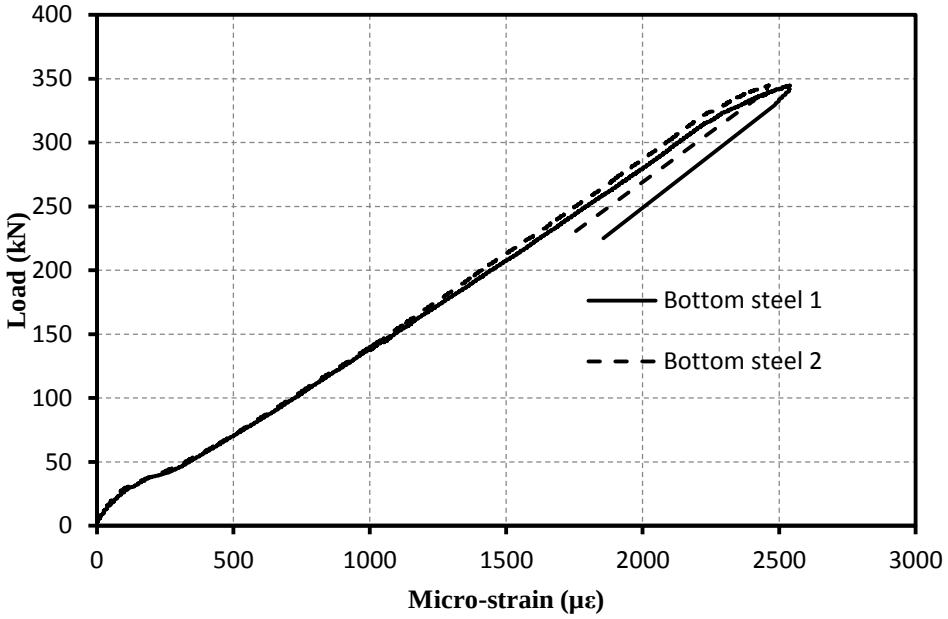


*Figure B.28 Bottom steel strain curves of the shear-span repaired beam with Sikacrete-08 SCC*

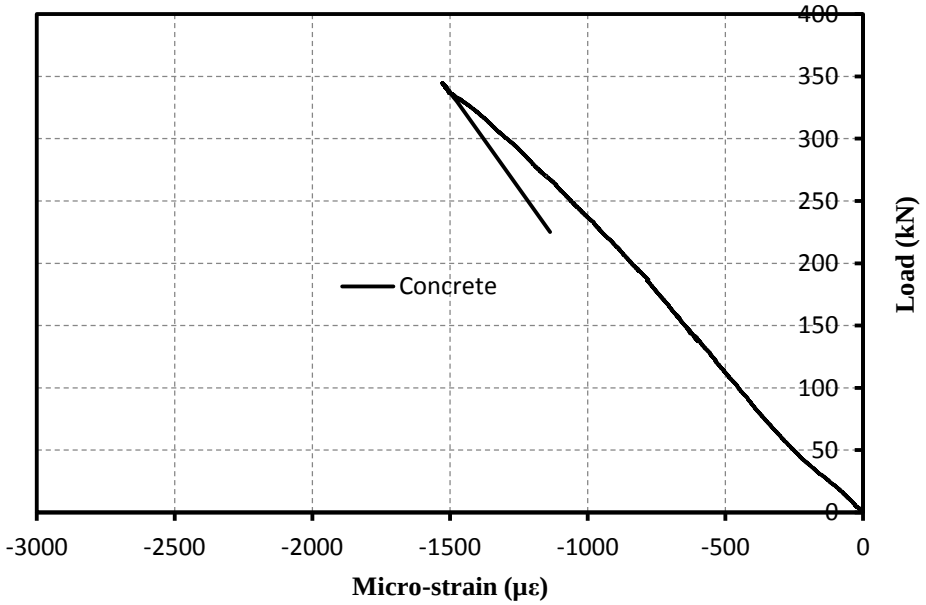


*Figure B.29 Concrete compression strain curve of the shear-span repaired beam with Sikacrete-08 SCC*

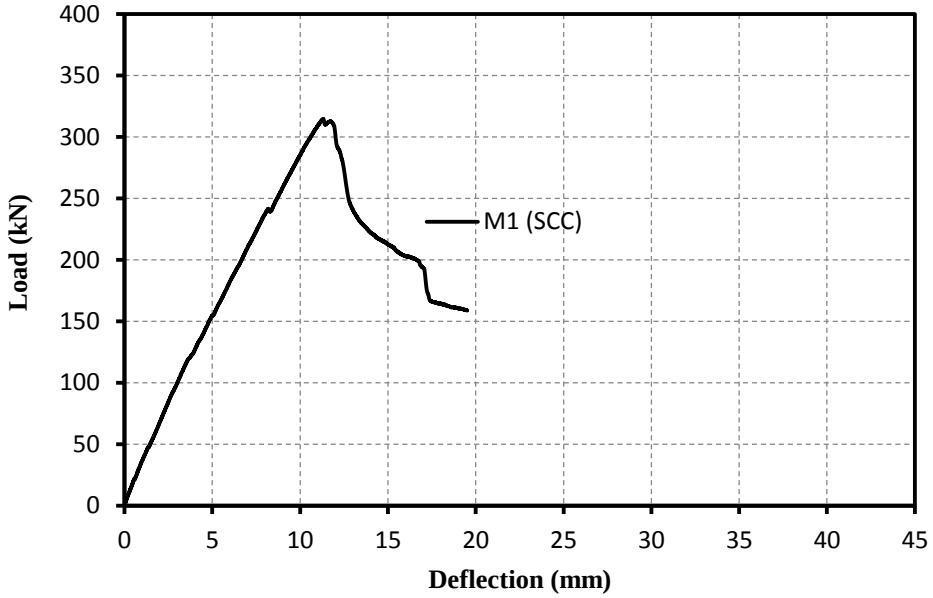


*Figure B.30 Shear load vs. deflection curve of the shear-span repaired beam with Mix M1 (SCC, 0%fibers)*

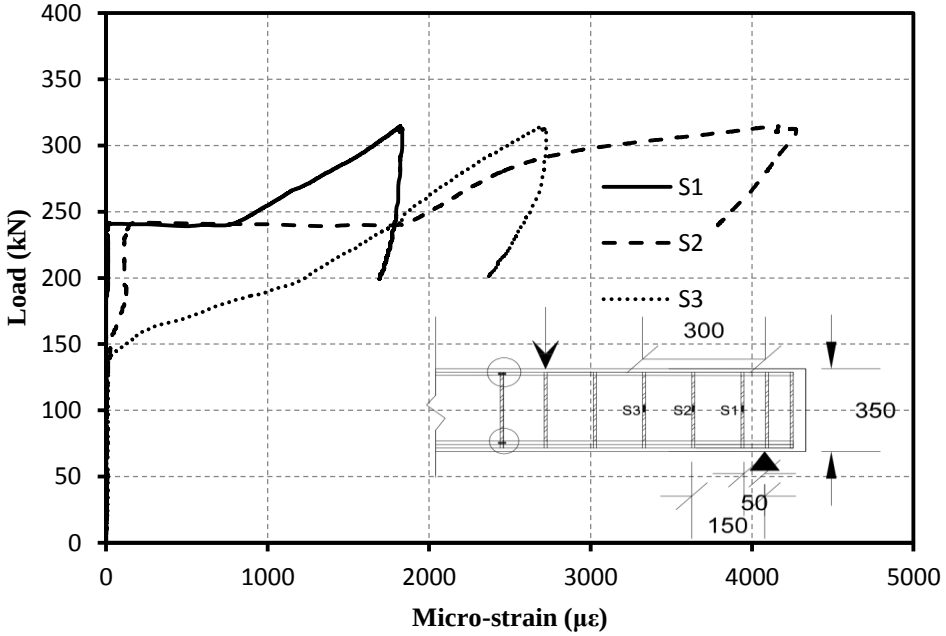


*Figure B.31 Strain curves on the stirrups of the shear-span repaired beam with Mix M1 (SCC, 0% fibers)*

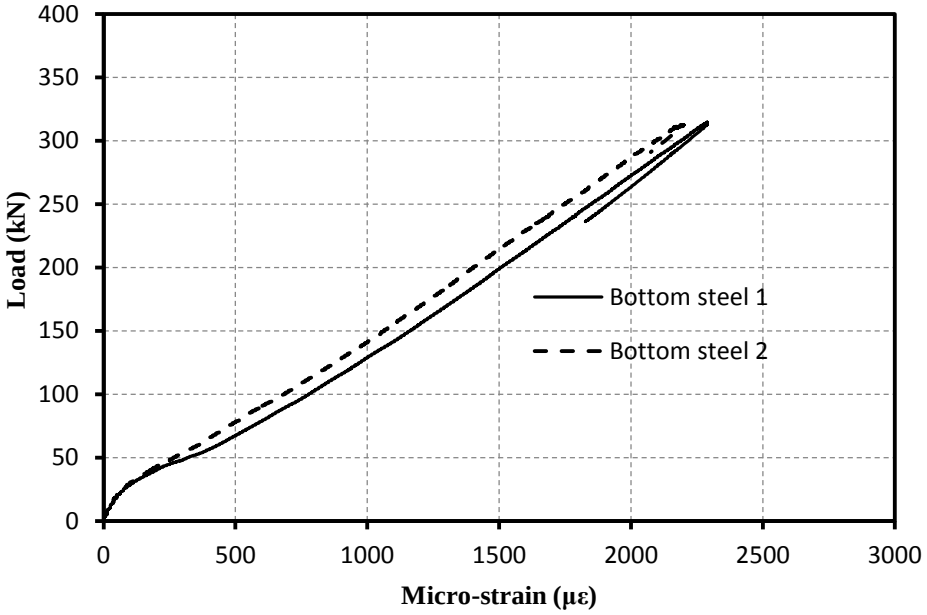


*Figure B.32 Bottom steel strain curves of the shear-span repaired beam with Mix M1 (SCC, 0%fibers)*

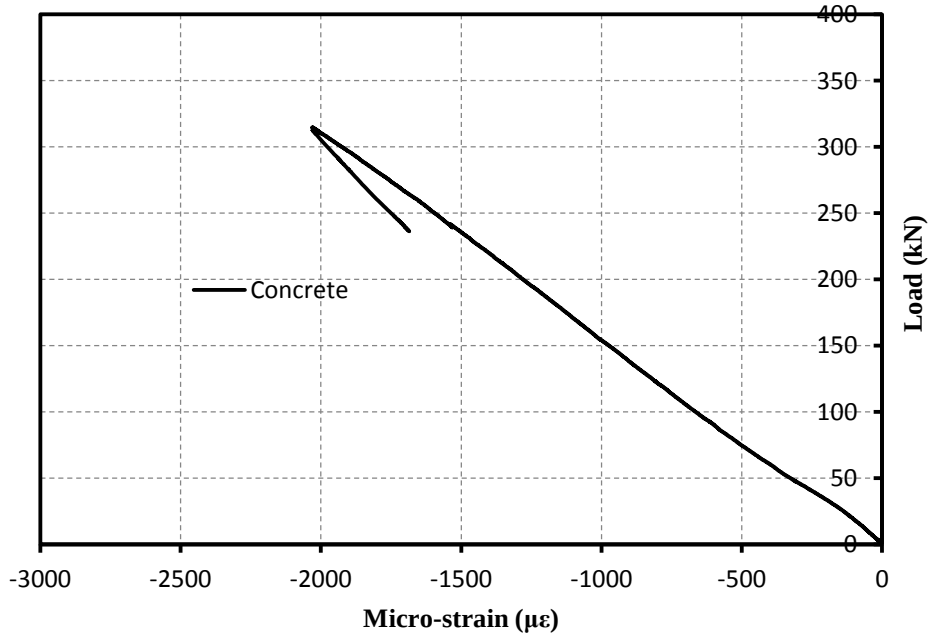


*Figure B.33 Concrete compression strain curve of the shear-span repaired beam with Mix M1 (SCC, 0%fibers)*

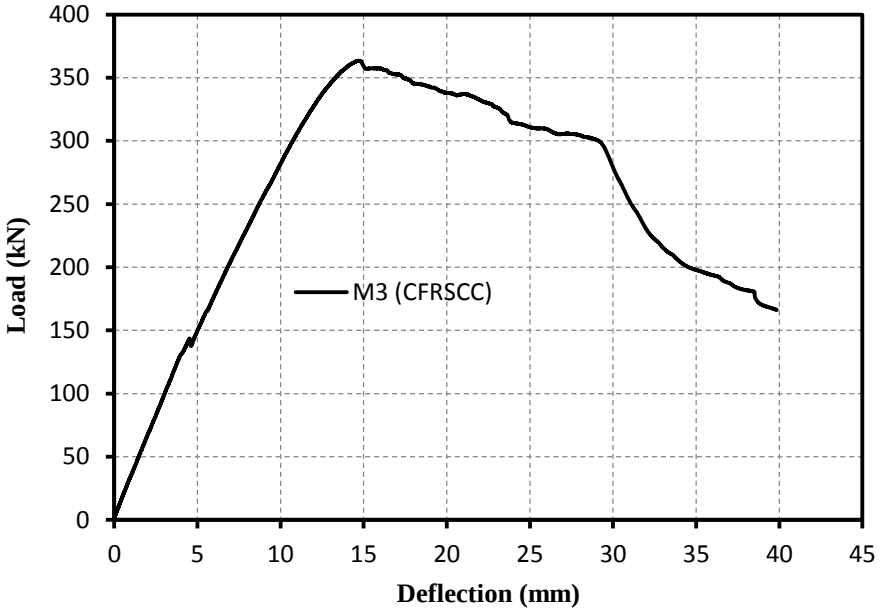


*Figure B.34 Shear load vs. deflection curve of the shear-span repaired beam with Mix M3 (CFRSCC, 0.50%fibers)*

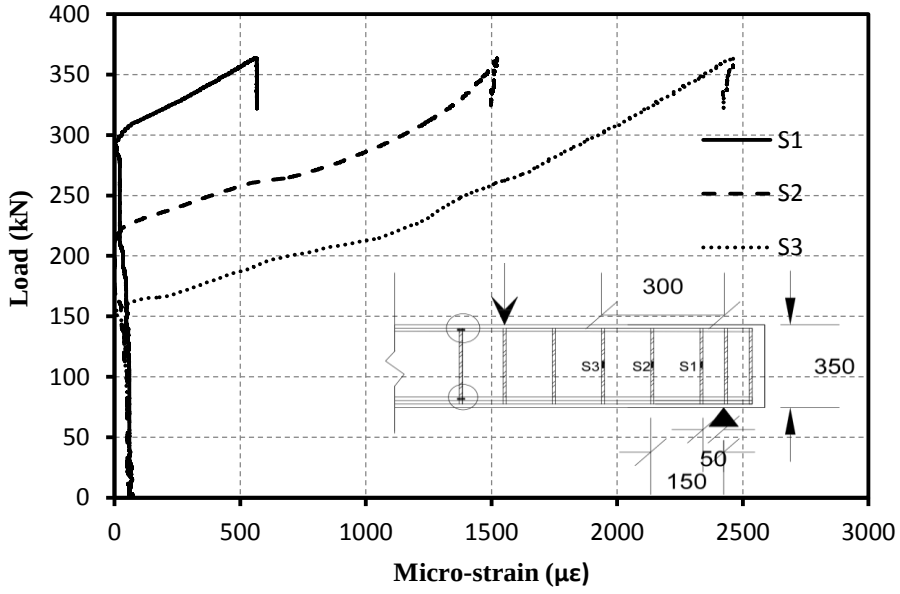


*Figure B.35 Strain curves on the stirrups of the shear-span repaired beam with Mix M3 (CFRSCC, 0.50%fibers)*

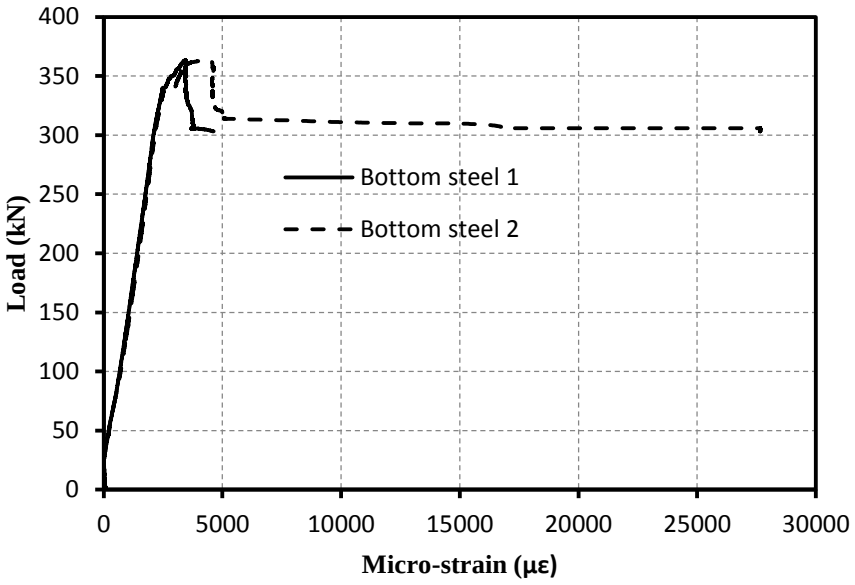


*Figure B.36 Bottom steel strain curves of the shear-span repaired beam with Mix M3 (CFRSCC, 0.50%fibers)*

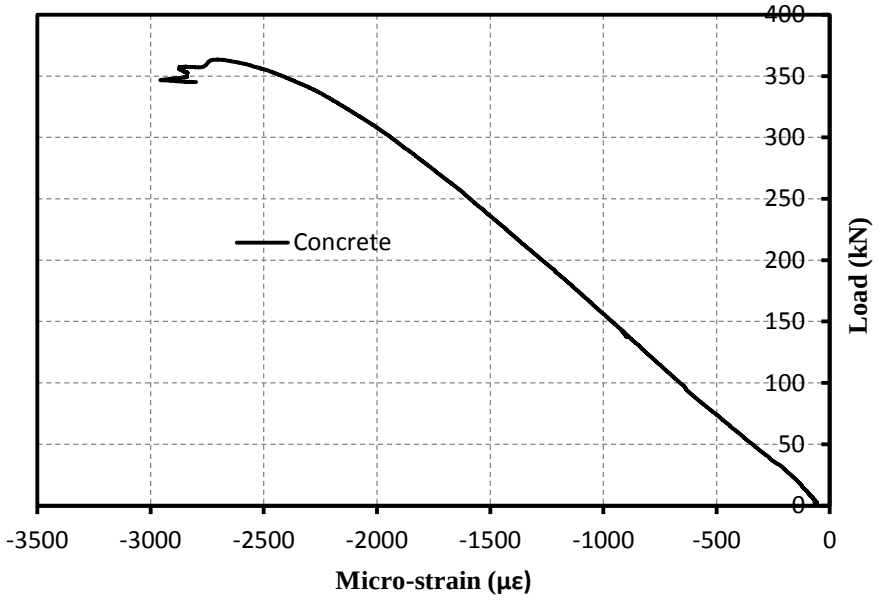


*Figure B.37 Concrete compression strain curve of the shear-span repaired beam with Mix M3 (CFRSCC, 0.50%fibers)*